When plate boundaries misalign

Distributing deformation at the terminations of continental transform faults

Megan Angharad Withers

MSci (Hons)

A thesis submitted for the degree of

Doctor of Philosophy

At Monash University in 2021

Faculty of Science

School of Earth, Atmosphere and Environment

Copyright notice

I certify that I have made all reasonable efforts to secure copyright permissions for third-party content included in this thesis and have not knowingly added copyright content to my work without the owner's permission.

Abstract

Continental transform faults transition to a new plate boundary type when strike-slip, transpression or transtension are no longer the most efficient way to accommodate plate motion. The northern termination of the Alpine Fault (New Zealand), the southern termination of the San Andreas Fault (California) and the western termination of the North Anatolian Fault (Turkey) are examples of plate boundary transitions where the continental transform fault is 'misaligned' with its connecting plate boundary. These examples show a consistent pattern of fault development across the transition zone between the misaligned plate boundary faults. Each transition zone comprises a number of evenly spaced, crustal scale faults oriented ~ 18° relative to the major transform fault. In this thesis, I use scaled strike-slip analogue experiments to investigate the development of these fault networks associated with transition zones. I show that these fault networks develop as crustal scale Riedel shears, where the basal boundary condition (i.e. the lower crust) deforms by distributed simple shear on a tectonic scale. I propose that such zones of distributed simple shear develop where the transition zone forms by propagation of the transform fault towards its connecting plate boundary. Fault networks developing over regions of distributed simple shear are shown to develop independently of the neighbouring transform fault. These faults can propagate laterally back towards the transform fault, creating an approaching and intersecting relationship with the transform fault. This geometry resembles that of branching splay faults, but such transitional fault networks do not result from propagation away from the primary fault. The results of the analogue experiments are compared in detail to the Marlborough Fault System, a fault network that forms the transition zone between the Alpine Fault and Hikurangi subduction zone in South Island, New Zealand. The experiments replicate the known sequential southward formation of each strike-slip fault in the system and indicate that each fault nucleates from a region of diffuse deformation, which develops into a single, continuous fault. I show that as each fault develops there is a rapid increase of incremental shear strain over that region, and hypothesise that this increase in shear strain may have contributed to the initiation of the 2016 Mw 7.8 Kaikoura earthquake, which occurred in a zone of diffuse faulting south of the present day of Marlborough Fault System that is hypothesised to be the location of an incipient fifth fault. Finally, analysis of existing structural and palaeomagnetic data from northeast South Island is used to propose a unifying hypothesis for the development of the Marlborough Fault System since 20 Ma, shortly after the initiation of the Alpine Fault. Here I propose that the 90° clockwise rotation of northeast South Island indicated by palaeomagnetic data between 20 Ma and 10 Ma occurred around a hinge that was generated and controlled by the anticlockwise rotation of the Hikurangi subduction zone. At 10 Ma, the bulk rotation ceased as distributed simple shear initiated between the Alpine Fault and the Hikurangi subduction zone, which caused the sequential southward development of the Marlborough Fault System.

Plain language summary

Continental transform faults develop where one tectonic plate slides past another and their role is to link plate motion between other plate boundaries. In some instances, the transform fault does not link directly to its connecting plate boundary. Where this occurs, there is no plate boundary to accommodate plate motion. This thesis investigates how plate motion is transferred across such regions by recreating plate boundary conditions in scaled laboratory experiments. Results show that a network of faults develop over these regions in a consistent pattern to accommodate plate motion, which has implications for better understanding earthquake initiation within these regions.

Declaration

This thesis is an original work of my research and contains no material which has been accepted for the award of any other degree or diploma at any university or equivalent institution and that, to the best of my knowledge and belief, this thesis contains no material previously published or written by another person, except where due reference is made in the text of the thesis.

Print Name: Megan Withers

Date: 17/12/2021

This thesis also includes four research chapters which have not been submitted for publication. In the case of chapters 2, 3, 4 and 5, my contribution to the work involved the following:

Thesis Chapter	Publication Title	Status	Nature and % of student contribution	Co-author name(s) Nature and % of Co-author's contribution*	Co-author(s), Monash student
2	The development of fault networks at termination of continental transform faults when their connecting plate boundary is 'misaligned'	Not submitted	90% Design, concept and method development, experiments, analysis, manuscript writing	1) Alexander Cruden, input into manuscript 6% 2) Mark Quigley, input into manuscript 4%	No No
3	To splay or not to splay? That is the question	Not submitted	85% Concept, experiments, analysis, manuscript writing	1) Lachlan Grose, 3D models, input into manuscript 9% 2) Alexander Cruden, manuscript writing 3% 3) Mark Quigley, manuscript writing 3%	No No No
4	Sandbox experiments explain the development of the Marlborough Fault System, New Zealand	Not submitted	90% Design, concept and method development, experiments, analysis and writing	1) Alexander Cruden, input into manuscript 4% 2) Mark Quigley, input into manuscript 4% 3) Mike Hall, 2% assistance in manuscript	No No No
5	A new interpretation for the structural development of northeast South Island, New Zealand, from 20 Ma to present	Not submitted	88% Design, fieldwork, analysis of existing literature and datasets, concept development, writing	1) Mark Quigley, input into manuscript 3% 2) Sandy Cruden, input into manuscript, fieldwork assistance 5% 3) Mike Hall, input into manuscript, fieldwork assistance 4%	No No No

Student name: Megan Withers

Date: 17/12/2021

I hereby certify that the above declaration correctly reflects the nature and extent of the student's and co-authors' contributions to this work. In instances where I am not the responsible author I have consulted with the responsible author to agree on the respective contributions of the authors.

Main Supervisor name: Alexander R Cruden

Date: 17/12/2021

Acknowledgements

First and foremost I would like to thank my main supervisor Sandy Cruden. Thank you for giving me the opportunity and free reign to develop this PhD project, and for your help, support and guidance over the last four years. Thanks also go to my other supervisors, Mark Quigley and Mike Hall, for your guidance, suggestions, and for sharing your expert knowledge on New Zealand.

Thanks go to the Monash Structural Group and to my milestone panel, Laurent, Roberto and Fabio, for support and feedback over the course of my PhD. Thanks also go to Nicola Litchfield and GNS Science for hosting myself and Mike, and allowing me to complete research using their facilities. Thanks go to Ulrich Riller, Jan Oliver Eisermann and Paul Göllner for being lovely hosts during my short visit to Universität Hamburg, although this part of my research was cut short, thanks so much for welcoming me and showing me around. To Anung, thanks for teaching me all there is to know about the analogue modelling in the geodynamics lab.

To my friends I have made over the course of my PhD. Thanks for keeping me smiling to the finish line. Jonas, Anung, Lynn, Sam and Bethan, thanks for being amazing friends and for the support you have given me at uni. To my old housemates Tara and Fernanda, thanks so much for choosing me as a housemate and for being great friends. To Robbo, Michelle, Jeff and Jane, thanks for welcoming me to Melbourne, and always being there for support. To Bayside Triathlon Club and in particular Christian, thanks for the runs, rides and training sessions and for making me feel so at home in Melbourne. To Briony, thanks for the mountain bike rides over the last few lockdowns. Thanks to Michelle and all the friendly faces on Townley Place, thanks for keeping me on the straight and narrow to submit my thesis.

I am forever thankful to those people who helped me when I became stuck overseas during the global pandemic, and for those who supported me upon returning to Australia. Those who wrote statements allowing me to gain an exemption to travel: Lachie, Laurent, Sandy, Bethan, Anung, Mum and Peter. Those at Monash who have supported and assisted me in returning and with issues since returning: Pete, Rob, Yuzhou. My friends and family who have been so supportive along the way. I quite simply would not be submitting my thesis without all this help and support, so thank you.

To my Australian family; Peter and Robyn, thank you so much for all your support, it means the world to me. To my family in Wales; Mum and Dad, thanks for always being so supportive, for always being there when I need you and thanks for always believing in me. To my brother Sam, hopefully this thesis finally convinces you that geology IS in fact, a real science. To Ayla, thanks for keeping Sam in check! To Gran and Grandad, thanks for all your love and for always believing in me.

Thanks to my PhD sidekick, my dog Cwtch, who has been by my side and kept me smiling over the last 1.5 years. And finally to Lachie, there are no words that amount to the support you have given to me, all I can say is thank you, always.

Table of Contents

Chapter 1

Introduction

1.1. Scope of thesis and research questions

Continental transform faults are strike-slip dominated plate boundary faults that cut through continental lithosphere and can accommodate hundreds of kilometres of displacement along their length, connecting convergent and/or divergent plate boundaries, or (in the case of a triple junction) other transform faults (Wilson, 1965; Woodcock and Daly, 1986; Sylvester, 1988; Legg et al., 2004; Norris and Toy, 2014; Şengör et al., 2019). Their name was given for their role in 'transforming' plate motion along their length, to a different kind of plate motion at their connecting plate boundary (Wilson, 1965). Hundreds of kilometres of strike-slip deformation must be accommodated across the plate boundary connection, where the plate motion 'transform' occurs (Wilson, 1965; Legg et al., 2004).

In some instances, rather than the transform fault 'transforming' plate motion directly to its connecting plate boundary, the continental transform fault can become 'misaligned' with its connecting plate boundary. Where a plate boundary misalignment occurs, plate motion can become distributed over a broad, intervening transition zone between the two major plate boundary faults (Mann et al., 1999; Legg et al., 2004; Wilson et al., 2004; Wannamaker et al., 2009; Eberhart-Phillips and Bannister, 2010). As with any plate boundary, these transition zones have a large risk of high-magnitude earthquakes, however unlike the major plate boundaries, how deformation localises and migrates across these transition zones remains poorly understood (Bilich et al., 2004; Wilson et al., 2004; Hamling et al., 2017). Understanding the formation of these broad intervening transition zones and large-scale strike-slip fault networks that develop within them is critical for seismic hazard analysis.

The unusually complex 2016 Mw 7.8 Kaikoura Earthquake is associated with the ongoing transfer of deformation across a 200 km wide transition zone in northeast South Island New Zealand, between the continental transform Alpine Fault and the Hikurangi subduction zone (Hamling et al., 2017). A series of four major strike-slip faults, termed the Marlborough Fault System (MFS), have developed to accommodate deformation across this transition zone (Bilich et al., 2004; Wilson et al., 2004; Rattenbury et al., 2006; Wallace et al., 2007, 2012). However, none of the ruptures from the Kaikoura Earthquake occurred along these major strike-slip faults (Berryman et al., 2018). The reason for the complexity of the Kaikoura earthquake remains highly debated. In order to understand the complexity of small-scale earthquake ruptures associated with it, a better understanding of the large-scale tectonic and structural geological evolution of the region is required.

There are numerous hypotheses for the development of the MFS (Little and Roberts, 1997; King, 2000; Townsend, 2001; Hall et al., 2004; Wilson et al., 2004; Wood and Stagpoole, 2007; Wannamaker et al., 2009; Lamb, 2011; Randall et al., 2011; Ghisetti, 2021). The most favoured hypothesis proposes sequential southward reactivation of a series of pre-existing crustal scale faults that bounded rigid crustal blocks (Hall et al., 2004; Lamb, 2011; Randall et al., 2011). Rodgers and Little (2006) and

Henrys et al. (2013) suggested that further data are needed to resolve the subsurface geometry of the major faults in the MFS.

The similarity of the MFS with fault patterns associated with other examples of plate boundary transition zones, such as the southern termination of the San Andreas Fault and the western termination of the North Anatolian Fault, suggests that the major MFS faults may have developed in a similar way to these other systems.

The following research questions in this thesis aim to answer the following knowledge gaps:

1. How and why do fault networks develop where plate boundary deformation becomes distributed over a transition zone between a continental transform fault and a connecting plate boundary?
2. Can the findings from Research Question 1 provide insight into the development of the MFS and the complexity of the Kaikoura earthquake?
3. How do the findings from Research Questions 1 and 2 compare with existing hypotheses for the development of the MFS and palaeomagetic and structural data from the region?

It is challenging to understand complex fault geometries that are observed in strike-slip (and transpressional/transtensional) systems from structural analysis of two-dimensional (2D) horizontal and vertical outcrops in the field. To overcome this problem, analogue laboratory experiments are frequently used to investigate fundamental deformation processes in such systems, and to test ideas about the development and evolution of structures in three dimensions (3D) through time (e.g., Dooley and Schreurs, 2012). Existing hypotheses for the development of the MFS, or other such transition zones, have yet to be investigated using 3D analogue modelling methods.

The internal 3D evolution of deformation within analogue models of simple shear is often inferred by changes in surface structures and topography and by using Digital Image Correlation (DIC) to analyse incremental and finite strain on the model surface (Adam et al., 2005; Schrank et al., 2008; Schrank and Cruden, 2010). This approach is similar to the study of horizontal outcrop and map patterns, except that the results show the evolution of structures and strain features through time. Vertical cross sections revealing the internal 3D geometry of simple shear experiments can only be observed at the end of each experiment, making it difficult to visualise the 3D structural evolution through time. To overcome this limitation, X-Ray Computed Tomography (XRCT) scanning can be used to analyse the 3D evolution of localised and distributed deformation in experimental strike-slip fault systems over time (e.g. Schreurs and Colletta, 1998; Schreurs, 2003; Fedorik et al., 2019).

In order to answer the research questions outlined above, a series of analogue experiments were designed to investigate the development of localised and distributed simple shear zones, and tectonic boundary conditions analogous to those acting on northeast South Island, New Zealand. These

experiments investigate and contribute to understanding the development of strike-slip fault networks in transitional plate boundary settings with specific focus on the MFS.

1.2. Thesis structure

This thesis has been prepared as four stand-alone research chapters that are intended for submission as refereed journal publications. These are bookended by an Introduction chapter (Chapter 1) and a Discussion chapter (Chapter 6), which summarises the main findings and makes suggestions for future work.

Chapter 2 - The generation of large scale strike-slip fault networks at the terminations of continental transform faults, where their connecting plate boundary is 'misaligned'

Megan Withers, Alexander Cruden, Mark Quigley. *Unpublished*

This research chapter introduces three example regions where plate boundary deformation becomes distributed over a transition zone between a continental transform fault and its connecting plate boundary: the northern termination of the Alpine Fault (the MFS), the southern termination of the San Andreas Fault, and the western termination of the North Anatolian Fault. We present the results of a series of strike-slip analogue experiments that compare the formation of faults in the upper crust where deformation of the lower crust remains localised on a shear zone (analogous to a transform fault) with faults that form in upper crust overlying a lower crust that deforms by distributed simple shear (analogous to the aforementioned transition zones). Fault development in the experiments is analysed using Digital Image Correlation (DIC).

Chapter 3 – To splay or not to splay? That is the question

Megan Withers, Lachlan Grose, Alexander Cruden, Mark Quigley. *Unpublished*

The surface geometry of fault networks associated with the propagating tips of strike-slip faults appears the same regardless of scale (including the terminations of transform faults). In this investigation we compare the formation and 3D geometry of large-scale (100 km wide) fault networks associated with transform transition zones to smaller-scale (10 km wide) fault networks associated with the tips of strike-slip faults that are not plate boundary faults. To do this, we repeat analogue experiments outlined in Chapter 2 and analyse the resulting 3D fault patterns using XRCT scanning. The results are compared to natural examples in the USA, Europe and New Zealand (MFS). We consider whether the resulting fault systems truly 'splay' from or propagate towards and abut their primary fault, and refine the definition for the term 'splay fault'.

Chapter 4 - Sandbox experiments explain the development of the Marlborough Fault System, New Zealand

Megan Withers, Alexander Cruden, Mark Quigley. *Unpublished*

We present a 'transition' analogue experiment that has boundary conditions analogous to the MFS of northeast South Island, New Zealand where the transform Alpine Fault is transitioning to the Hikurangi subduction zone. We use the modelling results to explain the sequential southward development of each of the major MFS faults, and to demonstrate how strike-slip simple shear is migrating and localising across the region. These results provide a potential explanation for the initiation and initial complexity of the 2016 Kaikoura earthquake ruptures.

Chapter 5 - A new interpretation for the structural development of northeast South Island, New Zealand, from 20 Ma to present

Megan Withers, Mark Quigley, Mike Hall, Alexander Cruden. *Unpublished*

In this research chapter we review current hypotheses for the tectonic development of northeast South Island, New Zealand, which are based on interpretations from palaeomagnetic and structural data. We analyse the existing palaeomagnetic and structural data and present an alternative interpretation for the tectonic development of northeast South Island from 20 Ma to present. This new interpretation satisfies the palaeomagnetic and structural data and combines results of analogue modelling data presented in Chapters 2, 3 and 4 with elements of existing hypotheses.

1.3. Background

The following sections provide critical background detail for this thesis. Where topics in this section are explained briefly, such as the geology of the MFS and hypotheses for its development, further detail can be found in Chapters 2-5, to avoid excessive repetition within the thesis.

1.3.1. Explanation of language used in this thesis

In this thesis, I refer to plate boundaries as being 'misaligned' in regions where plate boundary deformation has become distributed across transition zones. The term 'misaligned' reflects the physical positioning of the plate boundaries to generate such transition zones (Fig. 1.1). The misalignment is similar to a fault 'stepover', which creates restraining and releasing bends on <10 km scales (Section 1.3.2). However, plate boundary misalignment occurs on a much larger $\gtrsim$ 100 km scales. In this context, the term plate boundary misalignment should not be confused with the term 'misoriented', which is often used to reflect a change in stress orientation relative to a fault.

This thesis investigates the formation of faults in regions of localised and distributed simple shear. We recognise that the terms localised and distributed simple shear can be interpreted differently at different scales. For example, simple shear can be considered 'distributed' in the initial phases of development of a strike-slip fault, where a single, continuous strike-slip fault is yet to develop. In this thesis, we are

investigating localised and distributed simple shear at tectonic scales. I therefore refer to deformation over a plate boundary fault as 'localised' and deformation across a transition zone as 'distributed'.

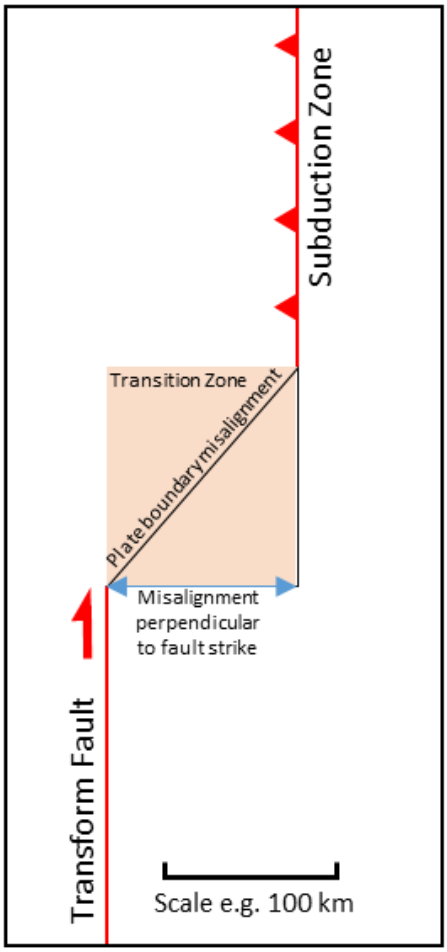

Figure 1.1. An example of a plate boundary misalignment as defined and referred to throughout this thesis. The 'misalignment' is the physical misalignment between the plate boundaries, which generates a plate boundary 'transition zone' between the two plate boundaries. This schematic figure is a simplified representation of the plate boundary misalignment between the transform Alpine Fault and the Hikurangi subduction zone in northeast South Island, New Zealand.

1.3.2. The formation of strike-slip faults

Strike-slip faults can form within all plate boundary and intraplate settings, for example to connect normal faults in rift settings and along mid ocean ridges, or to connect thrust faults in fold and thrust belts (Woodcock and Daly, 1986; Sylvester, 1988). They are characteristically long, relatively straight faults that are vertical or near vertical in cross section, and remain as narrow, localised zones of deformation at depth (Wilson, 1965; Cunningham and Mann, 2007; Qu, 2019).

Progressive simple shear refers to deformation where uniform shear strain occurs in a plane parallel direction and during this deformation, parallel planes remain parallel and at a constant spacing (Simpson and De Paor, 1993) (Fig. 1.2). Ramsay and Graham, (1970) demonstrate that the only constant volume strain regime that can occur in straight, parallel sided shear zones is simple shear. Hence, strike-slip faults are almost always a product of deformation by progressive simple shear (Ramsay and Graham, 1970; Simpson and De Paor, 1993; Qu, 2019). Exceptions to generation of strike-slip faults through simple shear can occur if there is structural inheritance within the shear zone (Ramsay and Graham,

1970), or as the result of conjugate faulting from pure shear (Sylvester, 1988). However large-scale strike-slip faults cannot be generated by progressive pure shear deformation (Sylvester, 1988; Qu, 2019). Therefore, this thesis focuses on the formation of strike-slip faults via progressive simple shear only.

The sequence of brittle faulting that leads to the development of a through-going strike-slip fault (Fig. 1.2) is an example of a scale independent (or invariant) process and has been well documented in strike-slip analogue experiments using Mohr-Coulomb materials such as clay and sand (e.g. Riedel, 1929; Tchalenko, 1970; Wilcox et al., 1973; Naylor et al., 1986). The stages of development of strike-slip faults illustrated by analogue models are consistent with field observations and earthquake rupture patterns (e.g. Naylor et al., 1986; Swanson, 2006; Rao et al., 2011; Hornblow et al., 2014).

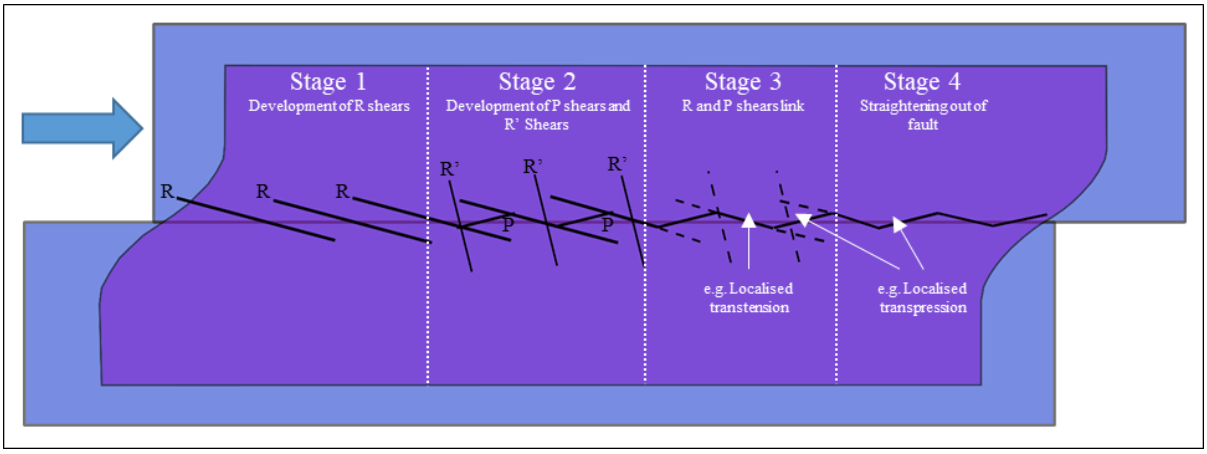

Figure 1.2. The development of a strike-slip faults over a region of localised simple shear. Adapted from Fossen (2010). Riedel (R) shears are the first structures to develop (Stage 1), followed by antithetic (R') shears and P shears (Stage 2). With increased displacement the R and P shears link to form a through-going faults (Stage 3), abandoning displacement on the outer edges of the shears (dashed lines in Stage 3). Over time these shears straighten out to form a well-established, approximately straight strike-slip fault (Stage 4). Location where anastomosing R and P shears remain may define localised regions of transpression and transtension, as labelled.

Named after Wolfgang Riedel for his 1929 clay layer analogue experiments (Riedel, 1929), strike-slip fault zones develop initially as an array of small, en-echelon shear fractures called Riedel shears (R shears) (Fig. 1.2). R shears are oriented 10 ° to 20 ° clockwise or anticlockwise (for dextral or sinistral faults respectively) relative to the shear direction. This acute angle is equal to half the angle of internal friction of the material. These shears are shown to be helical in 3D and link at depth (Naylor et al., 1986). With further deformation, a set of antithetic shear fractures, termed R' shears form, which are usually less well developed (Fig. 1.2). P shears can form to link R shears. These are synthetic and oriented symmetrically to the R shears with respect to the shear direction (Wilcox et al., 1973; Naylor et al., 1986; Sylvester, 1988; Fossen, 2010) (Fig.1.2). A set of antithetic P' shears can form as conjugate shear fractures to the P shears. P shears are much less commonly observed during the development of strike-slip fault zones than R shears (Naylor et al., 1986; Swanson, 2006).

After their formation, the R, R' and P shears link to create a through-going anastomosing fault zone (Naylor et al., 1986; Swanson, 2006) (Fig. 1.2). Over time this can straighten to form a well-established, approximately straight strike-slip fault. Locations where anastomosing segments remain, bounded by alternating R and P shears, may define alternating areas of localised convergence (transpression) and divergence (transtension) (Crowell, 1973; Christie-Blick and Biddle, 1985; Cunningham and Mann, 2007) (Fig. 1.2). These areas are defined by fault 'bends' and/or 'stepovers' (which often develop into fault bends following linkage of faults across the stepover) (Crowell, 1973; Wilcox et al., 1973). These fault bends occur at all scales (Tchalenko, 1970) and can be 10's km wide for crustal-scale strike-slip faults. Contractional bends are termed restraining bends and extensional bends are termed releasing bends (Christie-Blick and Biddle, 1985; Cunningham and Mann, 2007), and both are common in strike-slip fault systems (Cunningham and Mann, 2007).

Restraining bends are sites of shortening through a series of thrust faults and folds, which causes topographic uplift. Releasing bends form pull apart basins via a series of normal faults, and are topographic lows (Cunningham and Mann, 2007; Fossen, 2010) (Fig. 1.3). In cross section faults that develop across releasing and restraining bends link at depth into a single strike-slip fault (Fig 1.3B). Hence the cross section view of a restraining bend is often referred to as a positive flower structure, while a releasing bend is often termed a negative flower structure (Harding, 1985) (Fig.1.3B).

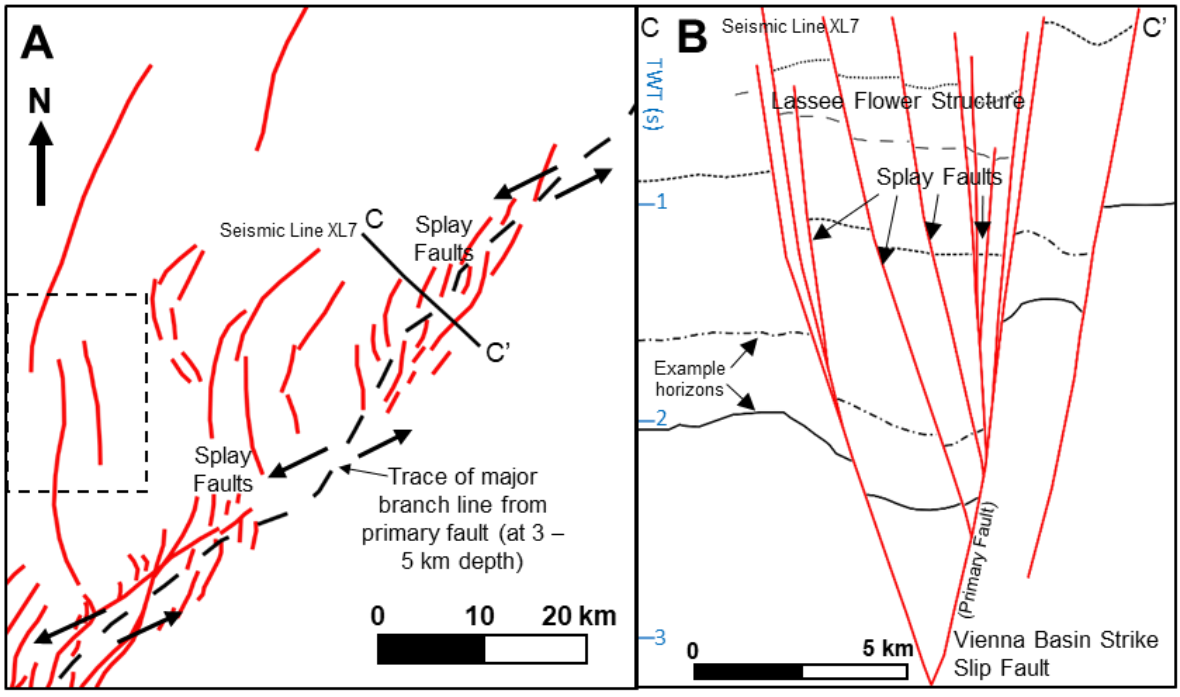

Figure 1.3. The Lassee fault segment of the Vienna Basin strike-slip fault. This a natural example of a releasing bend which has formed a transtensional rift from localised extension along the fault. The primary strike-slip fault is not present at the surface, its branching point at depth is dashed across the map **A.** Map view of the transtensional rift, line C – C' marks the cross section line in **B.** In cross section, this transtensional rift creates a negative flower structure. Adapted from Beidinger and Decker (2011), seismic line XL7.

Other features that may form during strike-slip faulting are tension gashes (or T shears). These form perpendicular to the maximum instantaneous strain (Fossen, 2010). Folds are also a common in strike-slip shear zones, and typically form prior to the development of faults. The axial traces of these folds are parallel to the maximum instantaneous stretching direction (Fossen, 2010).

1.3.3. Transpression and transtension in continental transform faults

As explained in Section 1.1, transform faults are large scale strike-slip faults that connect plate boundaries and are themselves plate boundaries. Continental transform faults, the focus of this thesis, propagate through continental lithosphere (Wilson, 1965; Woodcock and Daly, 1986; Legg et al., 2004; Norris and Toy, 2014; Şengör et al., 2019).

By definition transform faults form parallel to relative plate motion (Wilson, 1965). However, continental transform faults can also develop where plate motion is oblique, creating transpression or transtension along the plate boundary (Norris and Cooper, 1995; Dewey et al., 1998; Cunningham and Mann, 2007; Wu et al., 2012), although the dominant mode of deformation will still be strike-slip. The Alpine Fault, South Island, New Zealand is an example of a continental transform fault that is subject to tranpression (Norris and Cooper, 1995). Oblique relative motion between the Pacific and Australian plates causes an element of continent-continent collision, which is accommodated by reverse motion on the 60° east-dipping Alpine Fault. This has resulted in mountain building of the Southern Alps, despite the dominantly strike-slip nature of the Alpine Fault. Norris and Cooper (1995) document

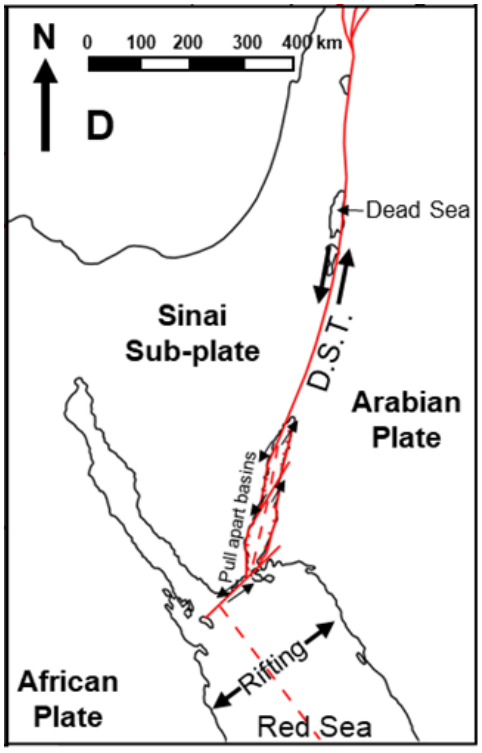

Figure 1.4. The Dead Sea Transform (D.S.T.) is subject to transtension. The extension element increases to the south where there are an increasing number of pull apart basins. This motion eventually becomes dominated by extension and there is a transition in plate boundary type to rifting within the Red Sea. Adapted from Segev et al. (2014).

segmentation along the surface trace of the Alpine Fault into a series of thrust dominated segments, connected by dextral strike-slip dominated segments.

The Dead Sea Transform (Fig. 1.4) is an example of an oblique sinistral strike-slip fault that is subject to transtension (Wu et al., 2012). The extensional element along this transtensional plate boundary is accommodated by a series of pull apart basins connected by elongate strike-slip faults, in a similar way to the releasing bends that develop in smaller scale strike-slip faults (Cunningham and Mann, 2007; Wu et al., 2012).

1.3.4. Propagating strike-slip faults and fault tip geometries

As they accommodate more strain, faults remain as narrow zones of deformation and grow in length by lateral propagation (e.g. Keller et al., 1999; Manighetti et al., 2001; Perrin et al., 2016). Understanding the processes and structures associated with lateral propagation is important because it increases the fault's ability to interact with other faults (Perrin et al., 2016). Propagating fault tips are associated with zones of additional fracturing, which are often referred to as 'tip damage zones' (Scholz et al., 1993; Mcgrath, 1995; Kim et al., 2004; Kim and Sanderson, 2006). Tip damage zones are absent at non-propagating fault tips (Perrin et al., 2016). Features associated with tip damage zones include wing cracks, horse tail splays, branching faults and antithetic faults (Kim and Sanderson, 2006). Wing cracks are tensile fractures associated with rapid decrease in displacement toward the fault tip and they are limited to smaller strike-slip faults (Kim et al., 2004; Fossen, 2010). Horse tail splays, branching splay faults and antithetic faults are commonplace in outcrop to map scale strike-slip faults (Kim et al., 2004) (Fig. 1.5).

Horse tail splays develop as an array of shear fractures at the fault tip (Fossen, 2010). Horsetail splays and branching faults are often grouped as synthetic splay faults because they 'spread out' from their primary fault at an acute angle (Brace and Bombolakis, 1963; Mcgrath, 1995; Fossen, 2010; Perrin et al., 2016), although more restrictive definitions have been proposed (Ando et al., 2009; Scholz et al., 2010). Perrin et al. (2016) show that typical length of a splay fault is ~ 30 % of the parent fault length, with a width that is ~ 10 % of its parent fault. Crustal-scale examples of splay faults are discussed in Chapter 3 of this thesis.

The array of faults that develop in the tip damage zone of a propagating strike-slip fault act to distribute the deformation of the primary strike-slip fault (Perrin et al., 2016). This reduces the energy expended by each fracture and slows propagation of the primary fault tip (Fossen, 2010).

The propagation of a strike-slip fault and its associated tip damage zone increases the likelihood of interactions with other faults, since faults often develop as networks, and strike-slip faults often develop as 'connectors' between other faults (Woodcock and Daly, 1986; Sylvester, 1988; Peacock et al., 2017). Peacock et al. (2017) characterise fault interactions by their geometry, kinematics, relative chronology,

displacement direction and strain in the interaction zone. A network of interacting faults can form within a single stress field (Peacock and Sanderson, 1999; Peacock et al., 2017) - faults associated with the tip damage zones of propagating strike-slip faults fall into this category.

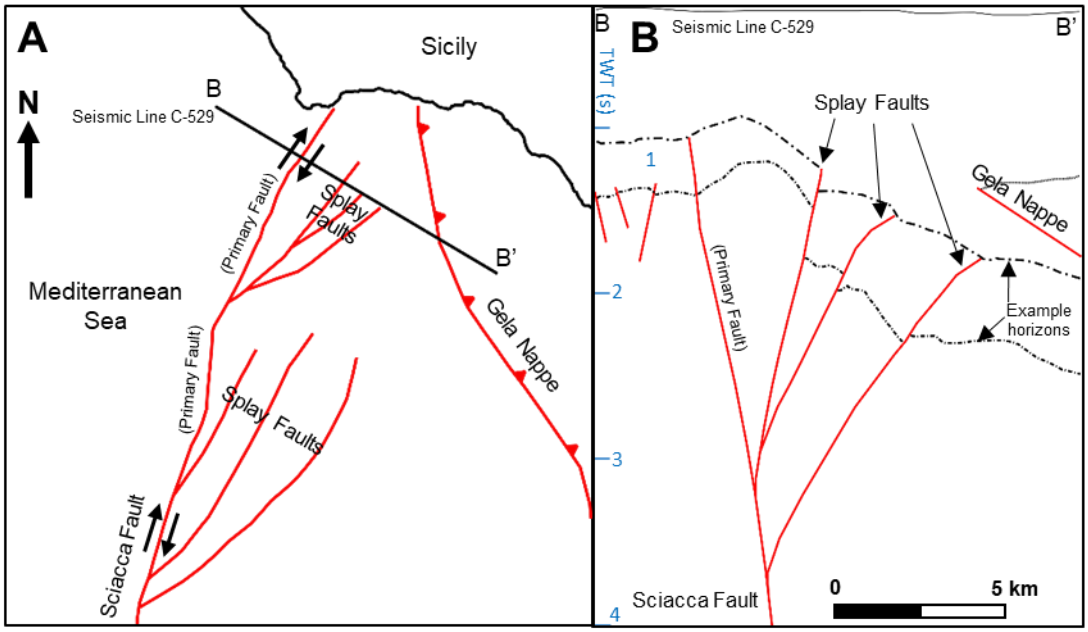

Figure 1.5. A series of branching faults associated with the fault tip of the Sciacca strike-slip fault off of the coast of Sicily. **A**. The branching faults in map view with location of cross section line B-B'. **B**. Cross section along B-B' showing branching faults that join at depth to create a positive flower structure. Adapted from Fedorik et al. 2019 and Fedorik et al. 2018. Seismic reflection profile C-529 and is available from www.videpi.com.

Sub-parallel arrays of evenly spaced strike-slip faults are common in nature. Large scale examples of such fault networks are associated with the terminations of transform faults, for example the Alpine Fault and the Marlborough Fault System and the southern termination of the San Andreas Fault. Yang et al., (2019) show that the fault spacing positively correlates with brittle layer thickness, viscous lower crust thickness, and the strength contrast between active faults and the surrounding undeformed rocks, while inversely correlating to lower crustal viscosity.

1.3.5. Introduction to the Marlborough Fault System

In north-eastern South Island, relative plate motion of the Alpine Fault becomes distributed across four large, active, oblique strike-slip faults, termed the Marlborough Fault System (MFS) (Fig 1.6). These faults accommodate relative plate motion across the 'transition zone' that has developed between the transform Alpine Fault and its 'connecting' plate boundary, the Hikurangi subduction zone (Barnes et al., 1998; Wallace et al., 2012). The dextral MFS faults strike sub-parallel to the Australian – Pacific relative plate motion vector (Wallace et al., 2012). The MFS is undergoing active deformation and is a high risk earthquake hazard zone in New Zealand (Berryman et al., 2018). There are many smaller

faults within the fault blocks bounded by the four main MFS faults. The southernmost faults accommodate most of the current displacement and the Hope Fault has the fastest slip rate in the region at 18 – 32 mm per year (Van Dissen and Yeats, 1991).

Interpretations of geophysical data indicate ongoing distributed, dextral shearing within the ductile lower crust across the transition zone between the Alpine Fault and Hikurangi subduction zone (Wilson et al., 2004; Wannamaker et al., 2009; Eberhart-Phillips and Bannister, 2010). This shear strain initiated between the Alpine Fault and the Hikurangi subduction zone at ~ 10 Ma and the MFS developed sequentially southward from 8 Ma to present (Browne, 1992; Little and Jones, 1998; Langridge and Berryman, 2005). A zone of diffuse faulting to the south of the MFS, which includes the Porters Pass to Amberley Fault Zone (PPAFZ), is located in the comparably low strain rate North Canterbury Tectonic Domain (NCD) and has been hypothesised to be developing into a fifth major fault in the MFS (Cowan et al., 1996) (Fig 1.6B).

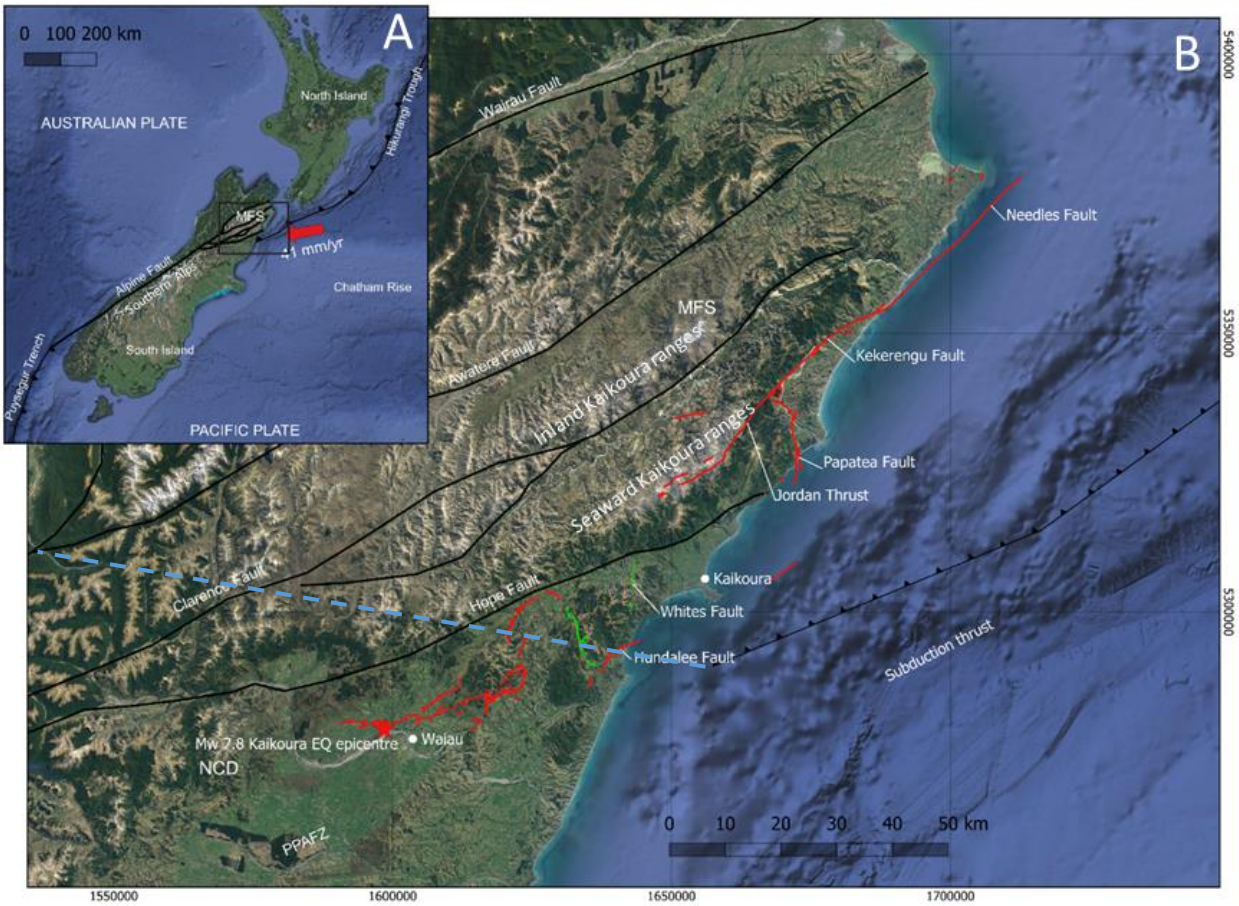

Figure 1.6. A. The tectonic setting of New Zealand, the box indicates the region shown in B. **B.** The major faults of the Marlborough Fault System (MFS). The main regions of transpression within the MFS, the Inland and Seaward Kaikoura Ranges are labelled. The location of the Porters Pass to Amberley Fault Zone (PPAFZ), within the North Canterbury Tectonic Domain (NCD, to the south of the MFS is shown. The star within the NCD indicates the epicentre for the 2016 Kaikoura earthquake. The ruptures shown in red are those which occurs on faults that had been identified and mapped prior to the earthquake. The ruptures in green occurred on faults which had not been identified prior to the earthquake. The blue dashed line indicates the hypothesised position of the subducted slab by Randall et al. (2011).

A number of hypotheses have been proposed for the development of the MFS, which are based on interpretation of existing structural and palaeomagnetic data in northeast South Island. These data are generally interpreted to suggest that the major faults within the MFS emerge or splay from the Alpine Fault, and that they developed by the sequential southward reactivation of pre-existing subduction-accretion faults that bound rigid crustal blocks in the basement rocks of the MFS (Little and Roberts, 1997; Hall et al., 2004; Lamb, 2011; Randall et al., 2011; Wallace et al., 2012). The inherited faults are hypothesised to have formed in a Cretaceous Gondwanan subduction zone, where the Torlesse composite terrain, which makes up the basement rock across the MFS, was deformed in an subduction-accretionary complex (MacKinnon, 1983; Reay and Pye, 1993; Bassett and Orlowski, 2004; Rattenbury et al., 2006; Willis, 2017). Palaeomagnetic and structural data provide evidence for ~ 100 ° clockwise rotation of the central MFS between 20 Ma and 10 Ma, with an extra ~ 30 ° clockwise rotation constrained to the northeast edge of the system since 10 Ma. Rotation is generally inferred to have been accommodated by either; 1) Vertical axis rotation of the rigid crustal blocks bounded by the inherited subduction-accretion faults (Hall et al., 2004), known as the 'Floating Block' model; 2) Rotation about a crustal scale hinge in the manner of a 'flexed telephone book' (Little and Roberts, 1997); or 3) A combination of these two models (Lamb, 2011; Randall et al., 2011).

Some interpretations for the development of the MFS do not explain palaeomagneric evidence for rotation within the system, or limit the rotations to North Island only (King, 2000; Wood and Stagpoole, 2007; Ghisetti, 2021). More recent work has suggested that the MFS formed by propagation of faults that nucleated some distance away from the Alpine Fault, back towards it, creating complex connections between the MFS faults and the Alpine Fault (Ghisetti, 2021; Vermeer et al., 2021).

1.3.6. Transpression in the Marlborough Fault System

The MFS is not limited to strike-slip deformation as there is a significant element of transpression within the system that has caused the uplift of the Seaward and Inward Kaikoura ranges (Fig.1.6B), which are bounded by the Hope Fault and Jordan Thrust, and Clarence Fault respectively. The ranges are located at the eastern edge of the transition zone and are underlain by the subducted Pacific Plate. This location corresponds to a change in strike of MFS faults from ~ 070° in the SW to ~055° in the NE (Lamb, 1988), which is oblique to the plate motion vector and therefore a more favourable orientation to generate compression and uplift (Van Dissen and Yeats, 1991; Little and Jones, 1998; Nicol and Van Dissen, 2002; Collett et al., 2019). Wellman (1979) estimated the rate of uplift in the Seaward and Inward Kaikoura ranges to be 5 – 10 mm/yr. Van Dissen and Yeats (1991) used the decrease in horizontal slip rate from the western section of the Hope Fault on to the Jordan Thrust to calculate a more refined uplift rate of 7 – 10 mm/yr for the Seaward Kaikoura ranges. Collett et al., (2019) used fission track measurements to suggest that exhumation has been occurring since 25 Ma, and therefore topographic relief in the region was present before the initiation of dextral displacement on the MFS

faults. They suggest that the MFS faults were once thrust faults that accommodated this exhumation. Baker and Seward (1996) calculated an average uplift rate of 0.2 mm/yr since exhumation commenced. Wellman (1979) and Lamb and Bibby (1989) calculated that the rate of uplift increased substantially during the Quaternary. Eberhart-Phillips and Bannister (2010) suggested that uplift of the Kaikoura ranges is occurring due to the dextral translation of thick continental crust along the MFS fault into a zone that cannot accommodate such thick crust due to the presence of the shallow subducting slab. Willis (2017) modelled compression in the overlying plate and the subsequent uplift of the Seaward and Inland Kaikoura ranges as being caused by congestion of the Hikurangi subduction zone by oceanic lithosphere of the adjacent, buoyant Hikurangi Plateau. It should be noted that, while the Seaward and Inland Kaikoura ranges are undergoing active uplift, the bulk of the MFS is oriented optimally for pure strike-slip faulting in within the contemporary strain field (Khajavi et al., 2018) and the majority of the transition zone in the MFS appears to be actively eroding. Khajavi et al., (2018) determined the mean H:V ratio of the Hope Fault to be ~ 33:1.

While we acknowledge that elements of transpression or transtension can be present within transition zones, investigating their effects are not within the scope of this thesis, which focuses on the dominant strike-slip motion only. The addition of transpression or transtension within transition zones is discussed as future work in Section 6.2.2.

1.3.7. Boundary conditions of the MFS: the Alpine Fault

The dextral offset of basement terranes across the Alpine Fault is 460 km, indicating that since its initiation at ~ 25 Ma it has accommodated just over half of the ~ 800 km strike-slip displacement estimated to have occurred across New Zealand since 45 Ma (Stock and Molnar, 1987; Sutherland, 1995; Little and Jones, 1998; Hall et al., 2004). A more recent investigation by Lamb et al. (2016) proposed that prior to the initiation the Alpine Fault as a dextral strike-slip fault, there was > 225 km of sinistral displacement across Zealandia, which the Alpine Fault subsequently reversed. Lamb et al. (2016) therefore argue that the Alpine Fault has a cumulative offset of around 700 km, accommodating close to the entire strike-slip displacement of New Zealand across central South Island. Following its initiation, the Alpine Fault propagated northeast towards the Hikurangi subduction zone (Wilson et al., 2004; Randall et al., 2011; Wallace et al., 2012; Lamb et al., 2016).

As mentioned in Section 1.3.3., the Alpine Fault is an example of a transpressional continental transform fault (Norris and Cooper, 1995). The reverse, east-over-west component of displacement on the Alpine Fault has resulted in exhumation of Pacific Plate rocks over Australian Plate rocks, which formed the Southern Alps mountain range (Fig. 1.6A). Uplift rates of 8 mm/yr have been determined from GPS measurements, while geologically determined uplift rates are up to 11 mm/yr (Adams, 1980; Beavan et al., 2004; Little et al., 2005).

This thesis analyses large-scale strike-slip tectonic processes. When considering the Alpine Fault on a tectonic scale, the fault trace is remarkably straight and localises plate motion. At the kilometre scale, the surface trace of the Alpine Fault is split into smaller 'zig-zag' segments, which switch between thrust dominated and strike-slip dominated segments depending on their orientation (Norris and Cooper, 1995). The thrust dominated segments are oblique to the plate motion vector and thus accommodate transpression through ramp like uplift. The highest part of the Southern Alps is constrained by a fault segment oriented 30° to the plate motion vector. (Yeats and Berryman, 1987; Van Dissen and Yeats, 1991).

1.3.8. Boundary conditions of the MFS: the Hikurangi subduction zone

The offshore Hikurangi subduction zone is parallel to the coastline of North Island, terminating at the Kaikoura canyon adjacent to the northern edge of the Chatham Rise, which is a ridge of continental crust that ranges in thickness from 23 – 26 km (Lewis and Pettinga, 1993; Barnes, 1994; Eberhart - Phillips and Reyners, 1997; Little and Roberts, 1997; Boiret et al., 2014) (Fig 1.6)

The convergence rate associated with the Hikurangi subduction margin decreases dramatically southwards from 60 mm/yr in the north to 20 mm/yr at the Cook Strait and is very low off north-eastern South Island (Barnes et al., 1998; Wallace et al., 2012). Willis, (2017) attributes the slowing in convergence rate to subduction of the buoyant Hikurangi Plateau causing lock up or congestion of the subduction zone, and the subsequent termination of subduction due to the presence of the continental Chatham Rise. This southward decrease in subduction rate causes a transfer of stress from the subduction interface onto the upper plate in the Cook Strait and MFS, as the plate boundary transitions to upper plate strike-slip faulting (Wallace et al., 2004, 2005, 2012; Randall et al., 2011). Using GPS velocities and active fault slip data, Wallace et al., (2012) determined that east-trending strike-slip faults such as the Boo Boo Fault in the Cook Strait are key features that transfer stress from the Hikurangi subduction thrust to strike-slip motion in South Island. Subduction also becomes increasingly oblique to the Hikurangi margin from north to south and at its termination the Pacific Plate is migrating southwest at 41mm/yr, parallel to the strikes of active faults of the MFS (Wallace et al., 2012). It is proposed that this component of plate motion is causing the south-westward migration of both the Chatham Rise and the Hikurangi subduction zone (Barnes et al., 1998; Wallace et al., 2012). The location of the subducting slab edge under north-eastern South Island is widely debated, but its likely location is the junction between the Awatere and Alpine faults (Randall et al., 2011; Wallace et al., 2012) (Fig. 1.6B).

The lithosphere located over the subducting slab in North Island, adjacent to the Hikurangi margin, are undergoing rapid clockwise rotation of 4°/Myr relative to the Pacific Plate (Randall et al., 2011; Wallace et al., 2012; Willis, 2017). Wallace et al. (2012) propose that the rotation is the likely cause of the rapid southward decrease in convergence rate along the Hikurangi subduction zone. Further south, where the

plate boundary transitions to the Alpine Fault (and the subducting slab is no longer present), vertical axis rotations of the lithosphere are negligible. Randall et al. (2011) and Willis (2017) propose that the presence (or lack there-of) of the subducting slab determines the change from rotating to non-rotating domains.

1.3.9. The Kaikoura earthquake

At 00:02 on 14th November 2016 NZDT, a Mw 7.8 earthquake shook northeast South Island. The ruptures began 60 km southwest of the town of Kaikoura, and propagated northeast towards the town, continuing for 200 km. Shaking in Kaikoura lasted for two minutes and the town was cut off from all land routes due to landslides from the earthquakes. The highest energy release from the earthquake was in the northern part of the rupture, over one minute after the earthquake had started. The Kaikoura earthquake is now recognised to be the most structurally complex earthquake recorded in modern history (Hamling et al., 2017; Berryman et al., 2018).

Given the amount of deformation within the MFS, it is surprising that the epicentre of the 2016 Kaikoura earthquake occurred 20 km south of the Hope Fault in the PPAFZ (Nicol et al., 2018) (Fig 1.6B) . The surface ruptures associated with the earthquake propagated both northwards and eastwards into the MFS. However, surface rupture propagation was localised on smaller faults within the MFS, largely bypassing the Hope Fault (Berryman et al., 2018). The rupture initiated on the Humps Fault in the NCD at a depth of 14 km and propagated northward for almost 200 km, forming 21 faults with a wide range of orientations and displacement kinematics, creating a complex rupture pattern (Hamling et al., 2017; Litchfield et al., 2018; Nicol et al., 2018). There were twelve major surface ruptures and two of the faults that ruptured had not previously been mapped (Hamling et al., 2017; Shi et al., 2017; Berryman et al., 2018) (Fig. 1.6B). Prior to the 2016 Kaikoura earthquake it was believed that a gap of >5 km between two pre-existing faults would prevent a rupture occurring along one of the faults to jump over to the adjacent fault (Wesnousky, 2006). However, Hamling et al. (2017) report that ruptures that formed during the 2016 Kaikoura earthquake propagated between individual fault segments with gaps of up to 15 km.

The reason for the complexity of the Kaikoura earthquake remains highly debated (Hamling et al., 2017; Ulrich et al., 2019). Lamb et al. (2018) proposed that earthquake initiation and the complex rupture propagation pattern, including the ruptures that 'jump' from fault to fault, can be explained by locking and stress loading on the subduction megathrust. However, Ulrich et al. (2019) propose that movement on the subduction megathrust is not favoured by the regional stress orientation required to generate the rupture pattern of the 2016 Kaikoura earthquake. Instead, they favour dynamic rupturing of weak fault zones due to the regional stress field generated by distributed shear between the Alpine Fault and Hikurangi subduction zone. They also propose that the large depth of the subduction interface below the crustal fault network impedes its ability to trigger earthquakes like the 2016 Kaikoura event.

Despite the complexity of the 2016 Kaikoura earthquake, some aspects confirmed the interpretations of previous studies (Berryman et al., 2018; Kearse et al., 2018; Little et al., 2018). Although the earthquake epicentre was located outside the MFS, the ruptures propagated north-eastwards into the high strain MFS as expected, and the largest amount of the energy that was released occurred on the Kekerengu Fault within the MFS, associated with dextral slip of up to 12 m. The location of the ruptures follows tectonic block boundaries proposed by Wallace et al. (2012) in their 'new tectonic block model'. In this new model, Wallace et al. (2012) include additional fault blocks: the Pegasus block, Kekerengu block and the Needles block and the Kaikoura ruptures occurred on the boundaries of these newly proposed fault blocks. The south-western edge of the of the newly proposed Pegasus block is defined by a more diffuse zone of faulting in the PPAFZ. This tectonic block boundary is where the earthquake epicentre occurred, along with the ruptures in the NCD.

1.3.10. Structural inheritance and fault network formation

Plate boundaries continuously evolve through time and fault systems eventually become extinct due to reconfigurations of plate boundaries, leaving behind inherited planar zones of weakness. The presence of pre-existing weaknesses in older rocks can lead to structural inheritance that may accommodate deformation under modern plate boundary conditions (Molnar et al., 2017; Samsu et al., 2019). Tectonic structures can be reactivated even if they are not perfectly oriented relative to the current plate boundary conditions (Vallage et al., 2018). For example, Vallage et al., (2018) identify earthquake ruptures that formed during the M_w 7.7, 2013 Balochistan earthquake in Pakistan switched between pre-existing structures and secondary branches, concluding that pre-existing structures, as well as regional stress and dynamic rupture stress controlled the earthquake propagation path. This highlights the importance of understanding pre-existing structures in modern-day plate boundaries.

1.3.11. Analogue modelling of strike-slip faulting

Laboratory analogue modelling, or experimental tectonics, refers to the study of tectonic processes by means of scaled models (Ramberg, 1967; Ranalli, 2001; Schellart and Strak, 2016) and has become a fundamental tool for testing 3D tectonic and geodynamic hypotheses. Natural strike-slip fault systems, observed in the field and through geophysical data sets, only allow for observation of one snapshot in time of the evolutionary sequence of the fault system, and detailed knowledge of their 3D geometries is lacking (Dooley and Schreurs, 2012; Reber et al., 2020). Analogue modelling of strike-slip faults systems can help to provide a detailed 2D and 3D picture of the development of such fault systems over time. The modelling process involves simplifying and scaling down the geometry, kinematics and dynamics of the fundamental boundary conditions of natural strike-slip fault systems, so that geological processes can be studied in a laboratory over hours to days (Hubbert, 1937; Ramberg, 1967; Schellart and Strak, 2016). Specific parameters can be varied within the experiments in order to assess their

relevance to the geological process or example being studied (e.g., Dooley and Schreurs, 2012; Hatem et al., 2017; Fedorik et al., 2019).

Numerous analogue experiments on strike-slip faulting have been conducted (Dooley and Schreurs, 2012 and references therein). As mentioned in Section 1.3.2., the fault sequence that leads to the development of a single continuous strike-slip fault was first documented through analogue experiments (Riedel, 1929). Typical analogue experiments involve a strike-slip shear apparatus (a.k.a. a 'sandbox') (Schrank et al., 2008) (Fig 1.7), where the moveable half of a box slides past a fixed half, creating a strike-slip deformation boundary condition at the base of the box. Adaptations to the classic 'sandbox' are made to simulate the simplified boundary conditions of more complex natural processes or natural examples, including transpression and transtension, releasing and restraining bends, fault tip damage zones and fault development with the influence of structural inheritance (e.g. Casas et al., 2001; Dooley and Schreurs, 2012; Wu et al., 2012; Hatem et al., 2017; Sun et al., 2018; Toeneboehn et al., 2018; Fedorik et al., 2019; Cooke et al., 2020).

Analogue modelling materials are chosen so that their properties (e.g., density, brittle strength, viscosity, etc.) scale to those of rocks in nature. Scaling factors are defined as functions of length, time, stress, strain and strain rate in order to satisfy geometric, kinematic, dynamic and rheological similarity criteria (Hubbert, 1937; Ramberg, 1967; Weijermars and Schmeling, 1986; Poirier, 1988; Schellart and Strak, 2016; Reber et al., 2020). Analogue materials used to simulate the brittle upper crust must capture localised failure as well as processes that contribute to deformation prior to failure (Reber et al., 2020). Commonly used upper crustal analogues include clays and granular materials. Quartz sand is a granular material that is most favoured due to its relative ease of use, dynamic scalability and its brittle, Mohr Coulomb behaviour that is similar to that of upper crustal rocks in nature (e.g. Byerlee, 1978; Davy and Cobbold, 1991; Schellart, 2000; Reber et al., 2020). The shape, roughness, size, and mineralogy of grains, together with their degree of compaction can affect the angle of internal friction and cohesion of a granular material during deformation, which in turn effects the size of the shear zone that develops (e.g. Schreurs et al., 2006; Klinkmüller et al., 2016; Reber et al., 2020). Sieving sand (as opposed to pouring) increases the bulk density and degree of compaction of the sandpack (e.g. Lohrmann et al., 2003; Panien et al., 2006; Maillot, 2013; Reber et al., 2020), making the sand more strain hardening, and increasing the width of the shear zone which develops.

Analogue modelling materials that simulate flow in the lower crust should be viscous, conserve volume during deformation and, ideally, be sensitive to temperature and strain rate (Dooley and Schreurs, 2012; Reber et al., 2020). Furthermore, the lower crustal analogue must mimic the behaviour of the natural lower crust at the strain rate chosen for the experiment (Reber et al., 2020). A common lower crustal analogue chosen for use in strike-slip analogue model experiments is Newtonian viscous polydimethylsiloxane (PDMS) (e.g. Weijermars, 1986; Klinkmüller, 2011; Dooley and Schreurs, 2012).

The presence of a ductile lower crustal layer can be expected to result in more diffuse deformation in the brittle upper crust, with the spacing of shear zones being a function of the brittle-ductile strength ratio (Schueller and Davy, 2008; Riller et al., 2012).

Analogue models were traditionally analysed in surface view and or sectioned vertically at different locations during repeat experiments to analyse structures in cross section (Dooley and Schreurs, 2012). Analogue materials such as clays, talc, baking flour or other such materials with high cohesion values were originally popular, as the development of structures within these materials is easily observed with the naked eye. The popularity of coarser grained granular materials has increased significantly over the last few decades with the introduction of non-destructive methods for analysing 2D and 3D geometries within analogue models. 2D methods include Digital Image Correlation (DIC), also referred to as Particle Imaging Velocimetry (PIV) (e.g. Adam et al., 2005, 2013; Schrank et al., 2008; Schrank and Cruden, 2010; Boutelier, 2016; Molnar et al., 2017, 2018; Toeneboehn et al., 2018; Boutelier et al., 2019; Samsu et al., 2021). Structural geometries in 3D can be analysed using X-ray Computer-Tomography (XRCT Scanning) techniques (e.g. Mandl, 1988; Schreurs, 1994, 2003; Schreurs and Colletta, 1998; Ueta et al., 2000; Dooley and Schreurs, 2012; Fedorik et al., 2019).

1.4. Methods Development

Our analogue experiments are conducted in a 40 cm x 20 cm x 4 cm dextral strike-slip shear apparatus (aka 'the sandbox') at Monash University's Geodynamics laboratory, which is based on the 'analogue shear zone' apparatus of Schrank et al. (2008) and Schrank and Cruden (2010) (Fig. 1.7). The sandbox consists of a fixed and a mobile half, separated by a vertical, freely slipping, velocity discontinuity. The mobile half is pushed by a linear actuator at a velocity specified by the user, allowing one side of the box to move horizontally relative to the other side, generating strike-slip motion. The sandbox is capable of strike-slip motion only.

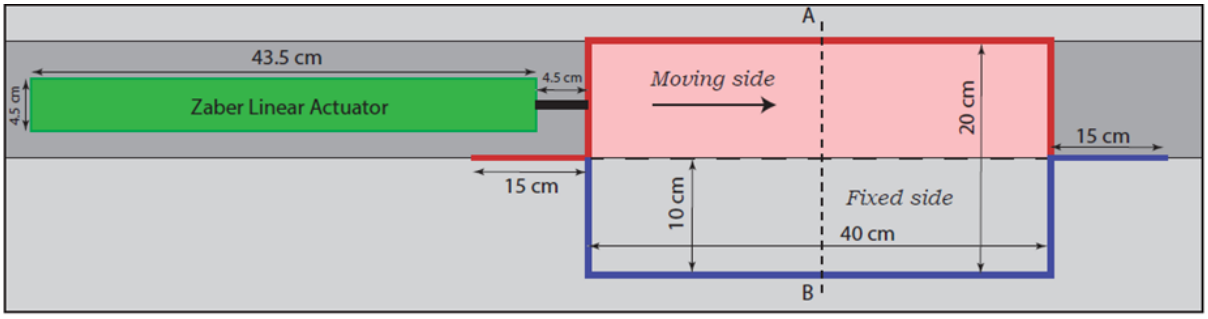

Figure 1.7. Schematic diagram of the analogue modelling apparatus aka 'the sandbox' used to conduct experiments for this investigation.

1.4.1. Preliminary experiment design

The preliminary design of experiments for investigating the development of fault networks at the termination of continental transform faults were motivated by existing hypotheses for the development of the MFS, which invoke reactivation of pre-existing weaknesses (Little and Roberts, 1997; Hall et al., 2004; Randall et al., 2011). The resulting analogue experimental setups are shown Fig. 1.8.

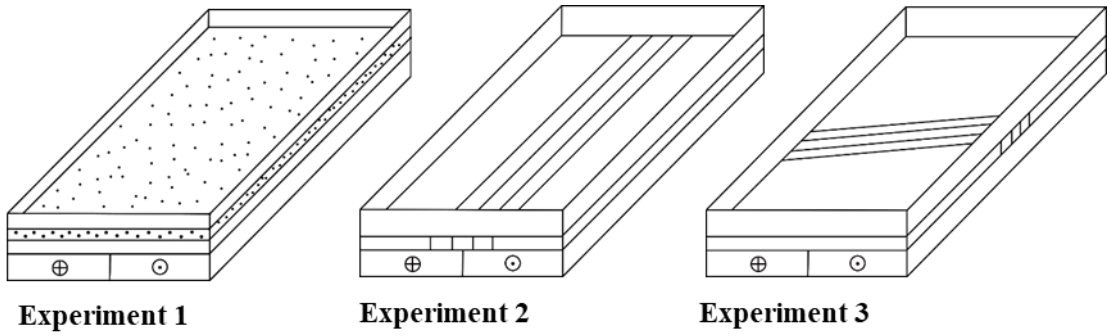

Figure 1.8. Experiment design for initial analogue models. Experiment design 1: Control experiment, homogeneous strong ductile lower crust with brittle upper crust. Experiment design 2: Strong, ductile lower crust with anisotropies parallel to plate motion – testing the 'flexed telephone book' model proposed by Little and Roberts (1997). Experiment design 3: Anisotropies rotated 080° to plate motion to investigate rotation of whole fault blocks – testing the 'floating block' model proposed by Hall et al. (2004). Experiments 2 and 3 are illustrated with no 'upper crust' material to show the orientation of lower crust anisotropies, 'upper crust' material will be placed over the 'lower crust' during these experiments.

Experiment 1 was a control experiment, containing no pre-existing weaknesses. Experiments 2 and 3 contained pre-existing weaknesses in the model lower crust and investigate the 'flexed telephone book' (Little and Roberts, 1997) and 'floating block' (Hall et al., 2004) end-member hypotheses for the MFS, respectively. The 'flexed telephone book' model involves reactivation of pre-existing weaknesses that are parallel to plate motion, while the 'floating block' model involves a ~ 100 ° clockwise rotation of rigid crustal blocks bounded by pre-existing weaknesses.

1.4.2. Materials and scaling

All experiments comprised analogue materials for a homogeneous strong ductile lower and a brittle upper crust, with the four major 'proto' faults of the MFS inserted as pre-existing weak layers in the lower crust. The materials chosen and the method for creating pre-existing heterogeneities in the ductile lower crust follow those used by Samsu et al. (2019). The mixtures and ratios are shown in Table 1.1 with comparison to their natural prototype density (the density for the upper crust is from Mielke et al., (2016)).

Materials	Weight (%)		
	Upper Crust	**Strong Lower Crust**	**Anisotropy Lower Crust**
Sand	60	-	-
Envirospheres	40	-	-
PDMS	-	63	100
Plasticine	-	33	-
Glass Bubbles	-	4	-
Model density (kg/m^3)	929	980	980
Prototype density (kg/m^3)	2560	2700	2700
Model viscosity (Pa s)	-	$2.9x10^5$	$4x10^4$
Prototype viscosity (Pa s)	-	$1.5x10^{22}$	$2x10^{21}$

Table 1.1. Materials and material ratios used to create the analogue mixtures for the upper crust, strong lower crust and lower crust anisotropies.

The upper crustal analogue consisted of a homogeneous, 60:40 ratio mixture of quartz sand and hollow ceramic Envirosphere® BLF). The strong lower crustal analogue consisted of a 63:33:4 PDMS, plasticine, glass bubbles mixture. The vertical weak layers in the lower crustal analogue, representing the pre-existing heterogeneities comprised pure PDMS. Rheology measurements of the ductile materials (Fig. 1.9) show the pure PDMS (the analogue heterogeneity) is essentially Newtonian with a

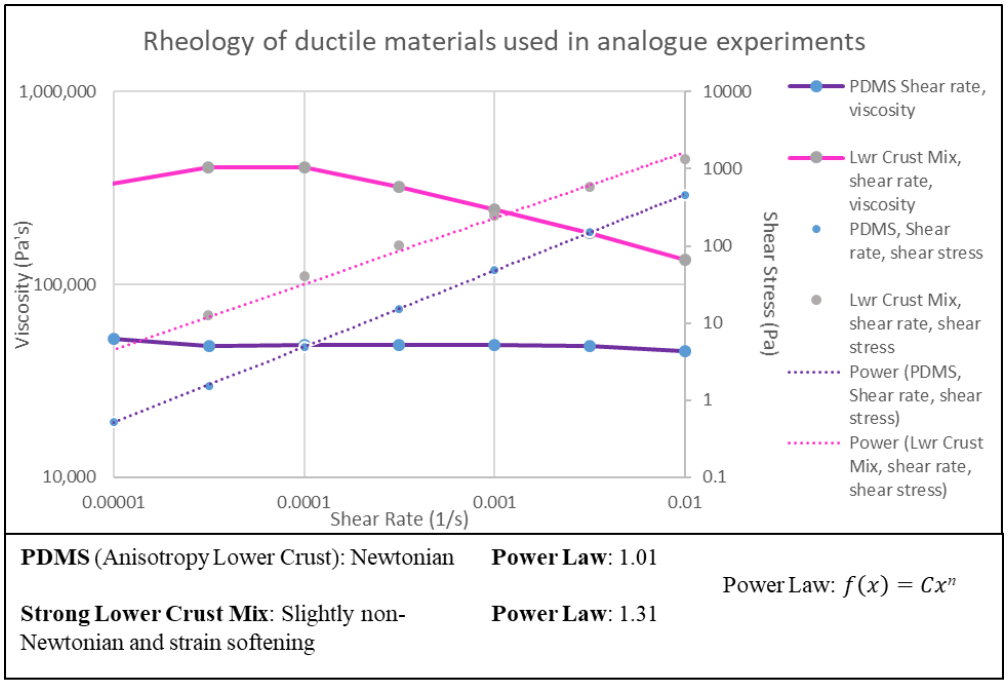

Figure 1.9. Rheology of ductile, lower crustal analogue materials used in the initial analogue experiments

power law of 1.01. The strong lower crustal analogue is slightly non-Newtonian and strain softening with a power law of 1.31 (Fig. 1.9).

The scaling parameters are provided in Table 1.2. The length scaling factor in the experiments was $1x10^{-6}$, Therefore 1 km in nature = 0.1 cm in the model. The analogue lower crust was 1.3 cm thick representing a 13 km thick lower crust in nature. The upper crustal analogue was 1.2 cm thick, representing a 12 km thick upper crust in nature (cf., Wannamaker et al., 2009). The model lower crustal anisotropies were 1 cm thick with 1 cm gap of strong lower crust between them. This 1 cm thickness represents a 10 km zone of weakness in the lower crust, similar to the widening weak zones beneath the major faults of the MFS inferred from electrical resistivity data (viz., Wannamaker et al., 2009). The central points of each zone of weakness were therefore 2 cm apart, representing 20 km in nature, approximately equal to the spacing of MFS faults in the upper crust.

		Thickness		Density		Viscosity		
		Model (mm)	Nature (km)	Model (kg/m^3)	Nature (kg/m^3)	Model (Pa s)	Nature (Pa s)	Material
Upper crust	Brittle	12	12	928.19	2560	-	-	Sand+ESPH
Weak lower crust	Ductile	13	13	980	2700	4×10^4	2×10^{21}	PDMS
Strong lower crust	Ductile	13	13	980	2700	2.9×10^5	1.5×10^{22}	PDMS+WPL+K1
Scaling factors: model/prototype		$L^* = 1 \times 10^{-6}$		$\rho^* = 0.363$		$\eta^* = 2 \times 10^{-17}$		
Time scaling factor		$t^* = \eta^*/(\rho^* \cdot g^* \cdot L^*)$		$t^* = 5.51 \times 10^{-11}$		1 h in model ≈ 2 Myrs in nature		
Velocity scaling factor		$v^* = l^*/t^*$		$v^* = 1.81 \times 10^4$		40 mm/h in model ≈ 20 mm/yr in nature		
Gravity scaling factor		$g^* = g_m/g_p = 1$						

Table 1.2. Scaling parameters for the initial analogue model experiments. Abbreviations: ESPH, Envirospheres®; PDMS, polydimethylsiloxane; WPL, White plasticine; K1, hollow glass microspheres.

Using the scaling factors in Table 1.2, the time scaling factor was calculated to be 5.51×10^{-11} (i.e. 1 hour in the model = 2.07 Myrs in nature) and the velocity scaling factor was 1.81×10^4 (i.e. 40 mm/h in model ≈ 20 mm/yr in nature). The model was displaced by 15 cm over 9.65 hours, representing 150 km in nature (an approximation of the 140 km displacement of the Wairau Fault (Little and Jones, 1998)), over 20 Ma (the approximate timeframe over which the Alpine Fault has been well established).

1.4.3. Results of preliminary experiments

The results of Experiments 1 - 3 are visualised using incremental shear strain maps determined from Digital Image Correlation (DIC) (Fig. 1.10). (DIC is explained in detail in Chapter 2). Incremental shear strain is the 'instantaneous' shear strain calculated from the velocity field determined from the change in location of clusters of particles between two images of the model surface. Here we use the instantaneous XY shear strain on the model surface, where X is parallel to the shear direction and Y is horizontal and perpendicular to X (Ramsay and Graham, 1970; Ramsay, 1980; Schrank et al., 2008).

Control Experiment 1, with no lower crustal anisotropies, developed Riedel shears after 1 hour of displacement (Fig. 1.10A). After 4 hours of displacement a continuous 2 cm wide shear zone had

formed along the sandbox, above the basal velocity discontinuity (Fig. 1.10B). In Experiment 2, with shear direction-parallel lower crustal weak zones, 'linking' faults formed between the two central anisotropies after one hour of displacement (Fig 1.10C) with orientations consistent with the Riedel shears in Experiment 1 (Fig 1.10A). After 4 hours of displacement, deformation was concentrated over the two central anisotropies and outer anisotropies did not accommodate any displacement (i.e., they were not reactivated) (Fig 1.10D). Analysis of the lower crust after removing the granular upper crustal layer after the experiment had finished (Fig. 1.11) showed deformation in the lower crustal analogue

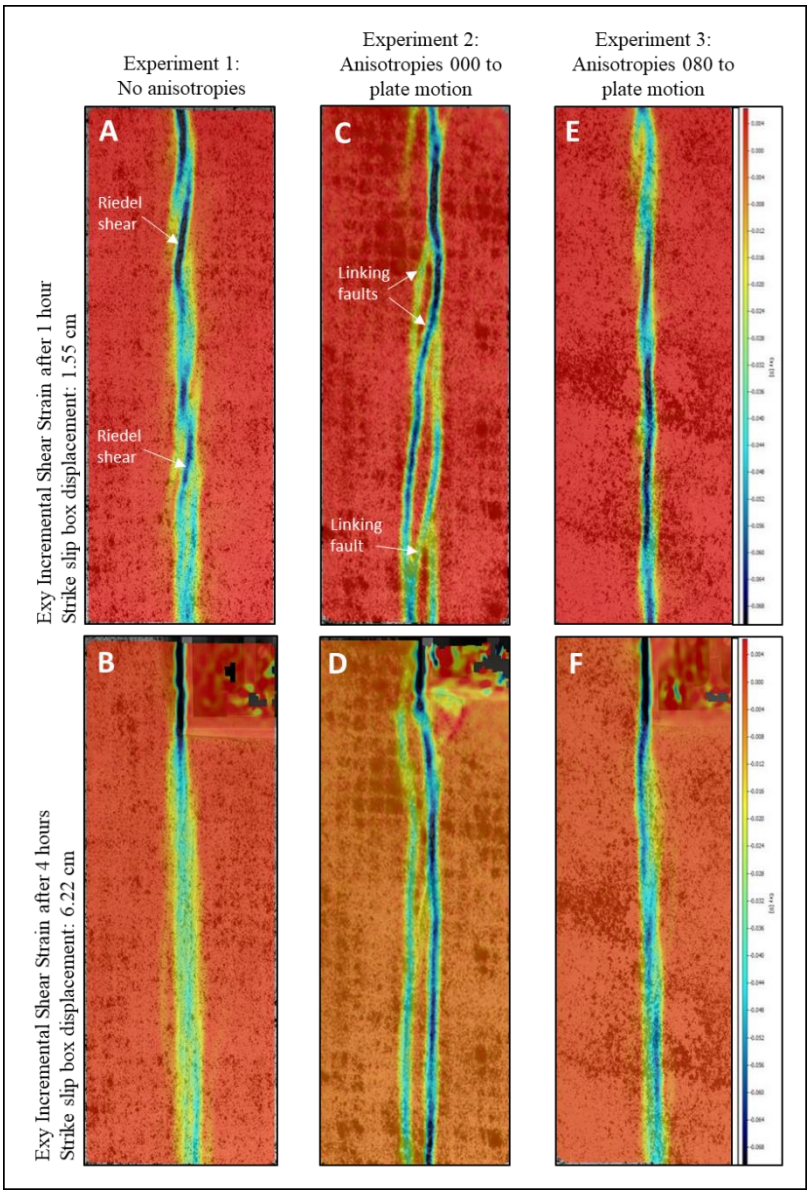

Figure 1.10. Exy incremental shear strain maps determined from DIC, showing results of Experiments 1, 2 and 3 after one and four hours of dextral strike-slip motion in the analogue shear box. Colour indicates amount of shear strain occurring at that moment in time, blue is high and red is low. Experiment 1 shows Riedel shears (A) developing into a continuous, 3 cm wide shear zone (B). Experiment 2 shows linking faults developing in the upper crust, joining the central two anisotropies (C), before deformation becomes concentrated on the central two anisotropies (D). Experiment 3 appears similar to experiment 1, showing that the anisotropies at 080 degrees do not influence fault development in this model (E) and (F).

was limited to the two central anisotropies, therefore the linking faults between them were limited to the upper crustal analogue. Experiment 3, with obliquely oriented lower crustal anisotropies, had very similar outcomes to Experiment 1. This indicates that the presence of 080° oriented anisotropies does not influence upper crustal fault development, and that these anisotropies did not rotate with increased displacement of the sandbox (Fig 1.10E,F).

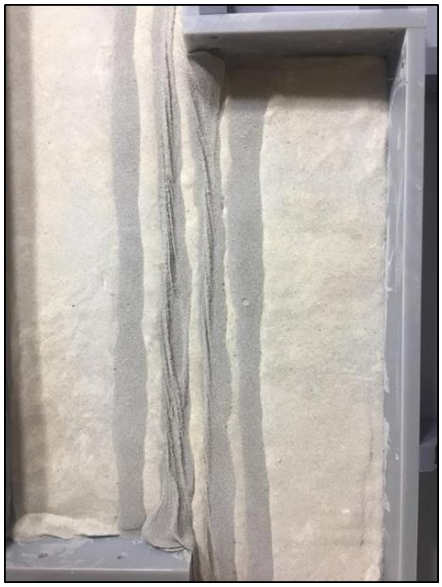

Figure 1.11. Photograph of the lower crustal analogue at the end of Experiment 2 (anisotropies parallel to strike-slip motion) after 15 cm of dextral displacement over 9.65 hours (and after removal of the upper crustal analogue). Distinct shearing can be seen in the central two anisotropies, corresponding with the upper crustal faulting in Fig. 1.8D. There is no evidence of the 'linking' faults, shown in Fig. 1.8C in the analogue lower crustal, suggesting that these 'linking' faults were limited to the brittle upper crustal analogue.

1.4.4. Discussion of preliminary experimental results

Experiment 2 revealed the most interesting results in terms of potential analogues with the MFS, in which 'linking' faults that are limited to the analogue upper crust developed between the two central anisotropies (Fig. 1.10C, Fig 1.11). Fig. 1.12 illustrates how the linking faults that formed in Experiment 2 are not oriented in such a way to be analogous to faults in the MFS basement rocks that appear to 'link' the major MFS faults (Fig. 12A,B). However, if the scaling for Experiment 2 is disregarded, and we consider the westernmost anisotropy in the experiment to represent the Alpine Fault and the easternmost one to represent the Hikurangi subduction zone (Fig. 12C), the linking faults that connect the two anisotropies have the same relative orientation as the MFS faults. However, unlike the MFS these faults did not develop sequentially southward.

My interpretation of the upper crustal linking faults in Experiment 2 is that they are the result of distributed deformation in the strong lower crust between the two central anisotropies. The formation of the MFS faults in the upper crust over a region of lower crust deforming by distributed simple shear is consistent with interpretations from geophysical data (Wilson et al., 2004; Wannamaker et al., 2009; Eberhart-Phillips and Bannister, 2010) (Section 1.3.5).

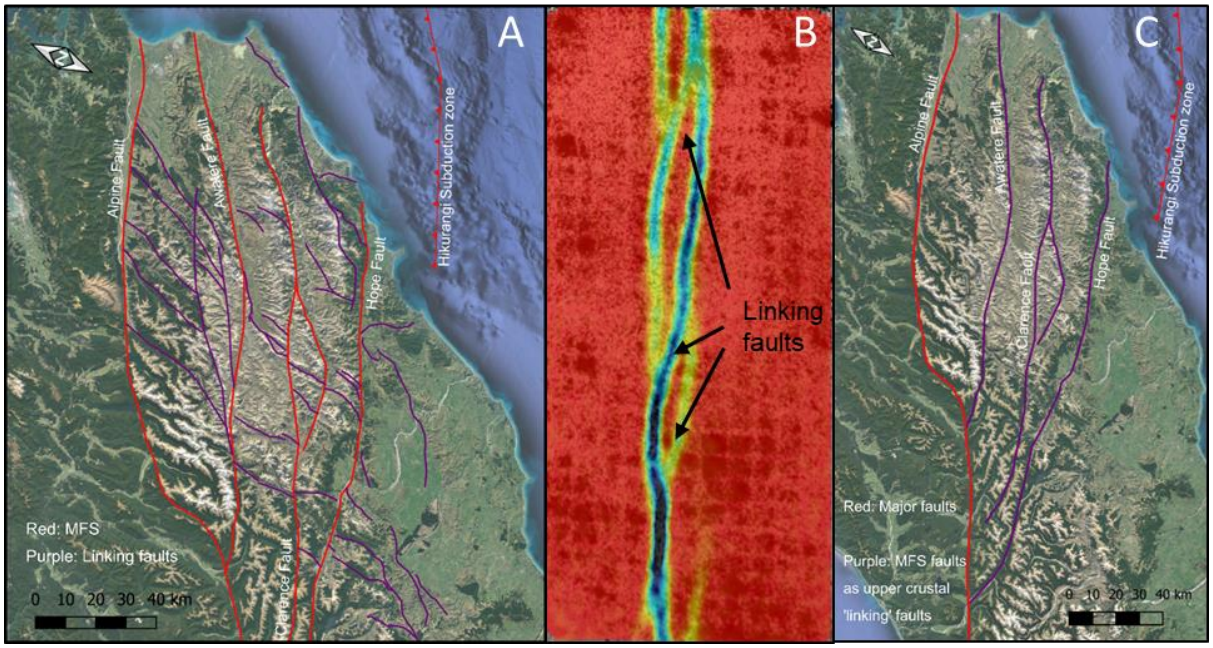

Figure 1.12. Comparison between Experiment 2 and the Marlborough Fault System (MFS). **A**. shows the MFS as the four parallel anisotropies (Red) and the faults between them (purple) within the basement rocks as linking faults. (The MFS is rotated for comparison with B). **B.** Experiment 2 (anisotropies parallel to strike-slip motion) after 1 hour of displacement with linking faults labelled. **C.** The major plate boundary faults are shown in red and can be considered to be 'subparallel' anisotropies. The MFS faults (purple) are considered to be 'linking' faults. (Rotated for comparison with B). The linking faults in (A) are at a different orientation to those in (B).

The presence of a ductile lower crustal layer can be expected to result in more diffuse deformation in the brittle upper crust, with the spacing of shear zones being a function of the brittle-ductile strength ratio (Schueller and Davy, 2008; Riller et al., 2012). However, results of these preliminary experiments show that the zone of deformation in the shear box remains relatively concentrated over the central basal discontinuity. When scaled to the MFS, the zone of deformation in the shear box is equivalent to 30 km at its widest, which is narrower than the 100 km wide zone of distributed simple shear across the MFS.

Unlike the shear box, upper crustal deformation in the MFS is not governed by velocity discontinuity in the lower crust. Instead, the major faults constraining the deformation are on the outer edges of the zone of deformation, namely the Alpine/Wairau Fault and the Hikurangi subduction zone (Fig. 1.13A). The findings from these preliminary analogue experiments demonstrate the need for an alternative approach for creating distributed simple shear in the analogue sandbox that diminishes or removes entirely the effect of the central basal velocity discontinuity.

In order to create distributed upper crustal deformation over wider area, we modified the sandbox by taping a piece of four-way stretchable material to its base (e.g. Fig. 1.13B), explained in detail in Chapters 2, 3 and 4. This material deformed in a manner analogous to the lower crust beneath the brittle upper crust of the MFS, and its presence annulled the effects of the central discontinuity.

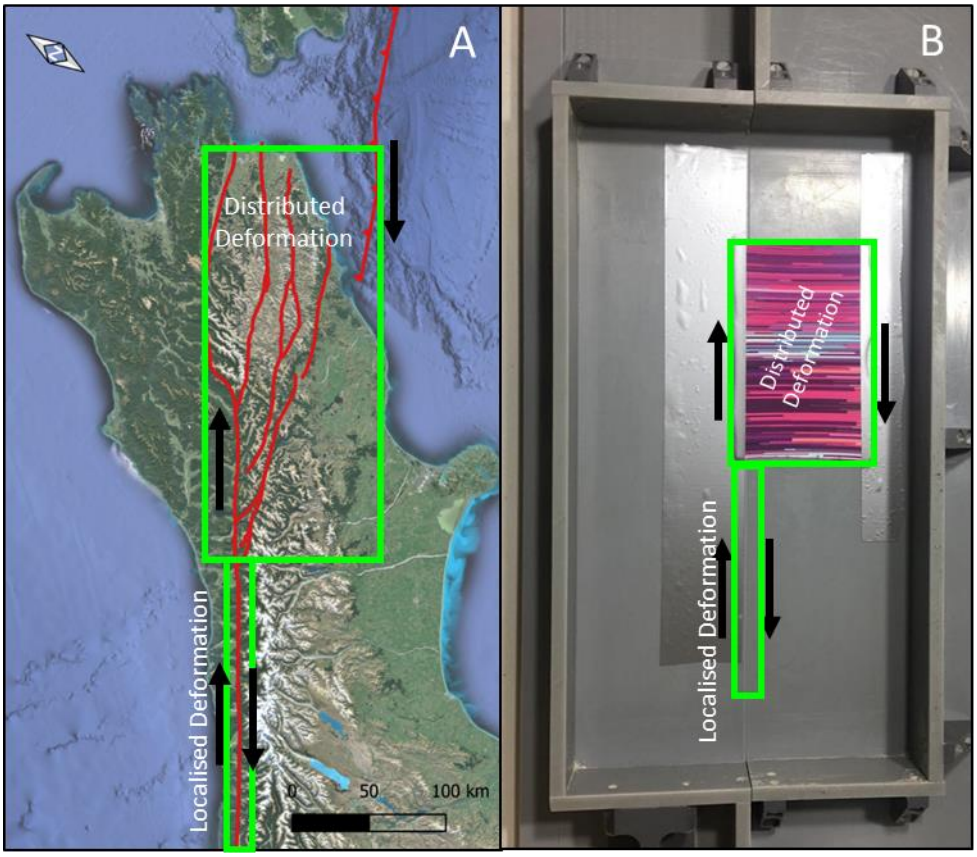

Figure 1.13. Modification of the sandbox to simulate the simplified, distributed simple shear basal boundary conditions of a transition zone. **A.** The simplified basal boundary conditions of NE South Island in which deformation that is localised on the continental transform Alpine Fault becomes distributed across the transition zone to the Hikurangi subduction zone. **B.** An example of the modified sandbox replicating the basal boundary conditions of NE South Island, the central velocity discontinuity at the base of the box simulates localised simple shear, the stretchable material (pink) simulates distributed simple shear.

The analogue experiments presented in the Chapters 2,3 and 4 of this thesis use this stretchable fabric approach to create a distributed simple shear boundary condition at the base of the upper crust that is analogous to the large-scale distributed deformation occurring in lower crust. The development of structures within these regions of upper crustal distributed deformation are analysed and compared to structures that develop over regions of localised simple shear, where the influence of the central basal velocity discontinuity remains. These experiments use an upper crustal analogue only and do not explicitly attempt to simulate deformation in the lower crust and or upper mantle. Test experiments found that a viscous lower crustal analogue could not be used in conjunction with the stretchable material because the substances typically used for this purpose (e.g., PDMS silicones) saturated the fabric and became 'stuck' to both it and the underlying base of the box. Test experiments with the stretchable material and only upper crustal granular material analogues showed remarkable consistency with previous analogue experiments investigating distributed simple shear within a specialised analogue apparatus that permitted the use of a lower crustal analogue (Schreurs, 2003). From these preliminary

tests, we concluded that presence of the stretchable material alone acts as a suitable proxy for lower crustal distributed simple shear, in which strain is transferred into the upper crust in the same manner. The design of a "next generation" strike-slip shear box apparatus that will allow both localised and distributed deformation with the presence of a ductile lower crustal analogue is discussed in Chapter 6, Section 6.2.1.

Chapter 2

The development of fault networks at the termination of continental transform faults when their connecting plate boundary is ‘misaligned’

Abstract

Here we use scaled laboratory experiments to investigate the development of fault systems in plate boundary transition zones, where defined continental transform faults (e.g., Alpine Fault, New Zealand; North Anatolian Fault, Turkey; San Andreas Fault, USA) are observed in nature to branch on to multiple subsidiary faults where changes in the geology, fault geometry and /or kinematics of the plate boundary are observed. We show that large-scale, transition zone fault networks comprise crustal-scale Riedel shears that develop sequentially outwards and away from the parent transform fault. Such fault networks form within brittle upper crust that overlies a ductile lower crust that deforms by large scale distributed simple shear. We argue that large-scale distributed deformation of the lower crust occurs when continental transform faults are 'misaligned' with their connecting plate boundaries. This misalignment may occur: (1) where a transform fault does not directly connect with a convergent or divergent plate boundary, as in the northern termination of the Alpine fault and the western termination of the North Anatolian fault. (2) Where a significant bend in the transform fault occurs in the plate boundary transition zone, as in the southern termination of the San Andreas Fault. The development of such plate boundary misalignments appears to occur when the plate boundary transition zone develops from propagation of the transform fault towards its 'connecting' plate boundary.

2.1. Introduction

Continental transform faults are major strike-slip faults that cut through the continental lithosphere and connect convergent and/or divergent plate boundary faults (Wilson, 1965; Woodcock and Daly, 1986; Legg et al., 2004; Norris and Toy, 2014; Şengör et al., 2019). As such, these transform faults can accommodate hundreds of kilometres of strike-slip deformation (e.g., Wilson, 1965). Examples of major continental transform faults are the San Andreas Fault (California), the Alpine Fault (South Island, New Zealand), the Dead Sea Transform (Lebanon, Israel, Jorden, Syria) and the North Anatolian Fault (Turkey) (Fig. 2.1).

Major continental transform faults rarely record pure strike-slip deformation and instead are usually subject to varying degrees of transpression or transtension (Schreurs and Colletta, 1998), although the dominant mode of deformation is strike-slip. The transpressional or transtensional elements commonly play a role in the termination of continental transform faults and their connection to other plate boundary types (Mann, 2007). Transpression often occurs along a continental transform faults when they connect with convergent plate boundary faults, and transtension tends to occur when the transform faults connect with divergent plate boundaries. For example, the transpressional Alpine Fault connects with the Puseygur subduction zone in the south and the Hikurangi subduction zone in the north (Furlong and Kamp, 2009) (Fig. 2.1A(1)), and the transtensional Dead Sea Transform connects to a divergent plate boundary in the Red Sea (Lazar et al., 2012; Wu et al., 2012; Segev et al., 2014) (Fig. 2.1D.).

Where continental transform faults terminate and 'connect' with another plate boundary type, hundreds of kilometres of strike slip deformation must be accommodated across a plate boundary transition (Wilson, 1965; Legg et al., 2004). In some instances, this transition is 'seamless' and continuous, where the deformation remains localised to the plate boundary fault as the type of plate boundary changes (when considering the plate boundaries on a tectonic scale). For example, the southern end of the transpressional Alpine Fault transitions to subduction of the Australian plate beneath the Pacific plate where the crust of the Australian plate transitions from continental to oceanic remains as a continuous fault throughout the transition (Sutherland et al., 2000; Shuck et al., 2021) (Fig. 2.1A(1)). Another example of a 'seamless' transition is the southern termination of the transtensional Dead Sea transform, where an increasing number and size of pull apart basins transition to sea floor spreading in the Red Sea (Wu et al., 2012) (Fig. 2.1D.).

However, there are other examples where the transition from a continental transform fault to a new plate boundary type is more complicated. These examples occur where the transform fault appears 'misaligned' with its connecting plate boundary fault. In these instances, deformation becomes distributed over a broad, intervening transition zone between the major plate boundary faults (Legg et al., 2004; Wilson et al., 2004; Wannamaker et al., 2009; Eberhart-Phillips and Bannister, 2010). A

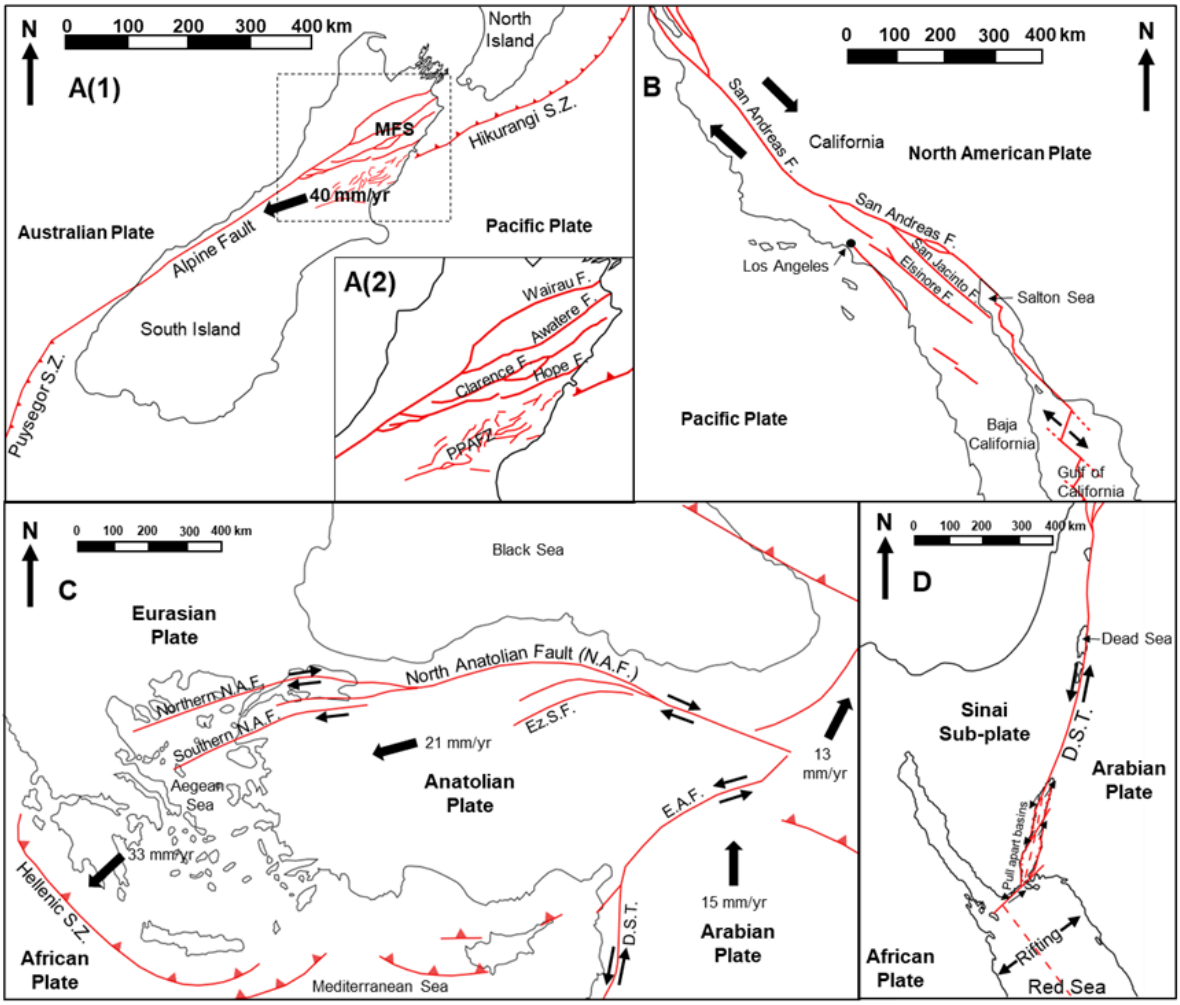

Figure 2.1. Four fault maps showing examples of continental transform faults from across the globe, and their termination and transition to a new plate boundary type. **A(1).** The oblique dextral Alpine Fault in South Island, New Zealand. To the south its termination and transition to subduction along the Puysegor subduction zone. To the north the transition to subduction along the Hikurangi subduction zone with accommodation of deformation through the Marlborough Fault System (MFS). **A(2)**, a more in depth look at the faults of the MFS. PPAFZ = Porters Pass to Amberley Fault Zone. Fault geometries in A1 and A2 © GNS Science 2016. **B.** The San Andreas fault (California) and its southern termination in the Salton Sea and transition to sea floor spreading in the Gulf of California. Fault geometry adapted from Legg et al. (2004) **C.** The North Anatolian Fault (N.A.F.) has propagated progressively westward from its eastern termination against the East Anatolian Fault (E.A.F.). At its western termination it branches in its mid section: Ez.S.F. = Ezinepazar-Sungurlu Fault, and at its western termination into northern and southern branches. Fault geometry adapted from Sunal and Korhan Erturaç (2012) **D.** The Dead Sea Transform (D.S.T.), its southern termination with pull apart basins that transition to rifting in the Red Sea (which transitions to sea floor spreading further south). Fault geometry adapted from Segev et al. (2014).

number of major crustal scale faults develop in these transition zones. Examples are the northern termination of the Alpine Fault (Fig. 2.1A(1),A(2)), the southern termination of the San Andreas Fault (Fig. 2.1B) and the western termination of the North Anatolian Fault (Fig. 2.1C). In this investigation, we refer to the plate boundaries as being 'misaligned' in regions where plate boundary deformation has become distributed across these transition zones. The term 'misaligned' reflects the physical positioning of the plate boundaries to generate these transition zones, as discussed in section 2.5. As with all plate boundaries, these transition zones have a large risk of high magnitude earthquakes, but unlike other

major plate boundary types, how deformation localises and migrates across them remains poorly understood (Bilich et al., 2004; Wilson et al., 2004; Hamling et al., 2017).

Here, we simulate the boundary conditions of these broad transition zones using scaled laboratory experiments (a.k.a. analogue models) in order to determine the how faults develop across such transition zones and therefore how deformation localises and migrates in the upper crust. In particular, our experiment design is motivated by the boundary conditions of the transition zone in northeast South Island, New Zealand, between the Alpine Fault and the Hikurangi subduction zone (Fig. 2.1). This is because there are multiple interpretations of geophysical data across the transition zone, which provide additional constraints for experiment design (Wilson et al., 2004; Wannamaker et al., 2009; Eberhart-Phillips and Bannister, 2010). Geophysical data indicates that deformation in the ductile lower crust beneath the transition zone is distributed between the two plate boundary faults, whereas deformation in the lower crust away from the transition zone is localised in large shear zones beneath the plate boundary faults themselves.

2.2. Geological background of case studies

2.2.1. Alpine Fault and Marlborough Fault System

The Marlborough Fault System (MFS) comprises four major northeast-southwest striking dextral strike slip faults that have developed within the ~ 100 km x 200 km transition zone between the dextral transpressive Alpine fault and the Hikurangi subduction zone (Fig. 2.1A(1)) (Wallace et al., 2007, 2012). These faults are considered to have developed sequentially southward from 6 Ma to present day (Little and Roberts, 1997; Hall et al., 2004; Lamb, 2011; Randall et al., 2011) and their strike is sub parallel to the oblique convergent plate motion vector between the Pacific and Australian plates (Wallace et al., 2012). South of the MFS is the Porters Pass to Amberley Fault Zone (PPAFZ), a zone of diffuse faulting with a relatively low strain rate (Fig. 2.1A(2)). The PPAFZ is a hypothesised location for an incipient fifth fault in the MFS (Cowan et al., 1996).

The Alpine fault accommodates the bulk of the ~ 40 mm/yr oblique convergence across central South Island in present day (Altamimi et al., 2012; Beavan et al., 2016). In northeast South Island, this plate motion is distributed across the faults of the MFS. The Wairau, Awatere and Clarence faults (Fig. 2.1A)) record slip rates of 4 – 8 mm/yr, while the Hope fault has a slip rate between 18 – 30 mm/yr (Van Dissen and Yeats, 1991; Litchfield et al., 2014).

2.2.2. Southern termination of the San Andreas Fault

The San Andreas Fault (SAF) extends northwest-southeast for 1200 km across California, USA, forming the plate boundary between the American and Pacific Plates (Fig. 2.1B). The SAF translates plate motion dextrally, connecting the Cascadia subduction zone in the north and sea floor spreading in

the Gulf of California in the south. The relative motion between the Pacific and North American plates is estimated to be 50 mm/yr (DeMets et al., 2010). The SAF itself accommodates between 20 – 35 mm/yr of this motion along its length (Norris and Toy, 2014). This rate significantly decreases at the 'Big Bend', where presently, the San Jacinto fault splits from the San Andreas Fault (Fig. 2.1B). To the south of the Big Bend, the slip rate of the San Jacinto fault is approximately equal to the SAF (Lindsey and Fialko, 2013). To the west of the San Jacinto fault are the Elsinore and Newport Inglewood Rose Canyon (NIRC) faults. These faults are equally spaced at ~ 30 km from each other (Scholz et al., 2010), and the net slip decreases sequentially westward across them. The San Jacinto fault has a net slip of 20 km (Kendrick et al., 2002), the Elsinore fault 12 km (Magistrale and Rockwell, 1996) and the NIRC fault 4 km (Mills and Fisc, 1991). The San Jacinto fault developed at 1.5 Ma, at the same time the Big Bend formed in the San Andreas fault system (Morton and Matti, 1993; Bennett et al., 2004). The Elsinore fault is slightly younger, having developed at ~ 1.2 Ma (Dorsey et al., 2012).

2.2.3. Western termination of the North Anatolian Fault

The North Anatolian Fault (NAF) is an east-west trending, 1200 km long dextral strike-slip fault that forms the plate boundary between the Anatolian and Eurasian plates (Şengör et al., 2005; Sunal and Korhan Erturaç, 2012; Norris and Toy, 2014) (Fig. 2.1C.). The NAF developed between 13 – 11 Ma in the east and propagated to the west, while accommodating lateral westward extrusion of the Anatolian plate away from the collision zone between the Arabian and Eurasian plates, reaching its current western termination in the Sea of Marmara at 200 Ka (Provost et al., 2003; Şengör et al., 2005; Norris and Toy, 2014). The western termination of the NAF occurs northeast of the Hellenic subduction zone, which bounds the Anatolian plate to the south and west (i.e., they do not connect) (Fig. 2.1C). The shear zone associated with the North Anatolian Fault is narrow in the east, forming a localised, crustal scale weakness that accommodates the bulk of the plate motion. Slip rates are calculated at 22 to 24 mm/yr with an average total displacement of 75 – 85 km (Provost et al., 2003; Şengör et al., 2005; Hubert-Ferrari et al., 2009; Sunal and Korhan Erturaç, 2012; Norris and Toy, 2014). The shear zone becomes progressively wider towards the west, where the fault is younger. At the sea of Marmara, the fault splits into multiple strands, the two main structures being the Northern NAF and the Southern NAF, creating similar fault pattern to those observed in the MFS and the southern termination of the SAF.

2.3. Methods

It can be challenging to understand how strike-slip, transpressional or transtensional fault systems develop through time from field data alone. By recreating such deformation systems in simplified, scaled-down analogue models, we can test hypotheses for and analyse the development of geological structures in three dimensions (3D) and through time in a controlled laboratory environment (Dooley and Schreurs, 2012).

In this investigation, we design and run a series of analogue experiments to investigate and compare the formation of geological structures in regions of localised simple shear and regions where simple shear becomes distributed over a much larger area, as well as the transition between the two. The region of localised simple shear is analogous to a transform fault (Norris and Toy, 2014). Regions of distributed simple shear aim to simulate transition zones at the termination of transform faults where the adjoining plate boundary does not directly connect with the transform fault (Wilson et al., 2004), as illustrated by the case studies outlines above.

2.3.1. Laboratory apparatus

We conduct a series of experiments using a 40 cm x 20 cm x 4 cm strike-slip shear apparatus (Fig. 2.2) (a.k.a. 'sandbox' or analogue shear zone) (Schrank et al., 2008).

The sandbox consists of two halves, one that remains fixed and another which is mobile. The mobile half is pushed (dextral motion) or pulled (sinistral motion) by a linear actuator at a velocity specified

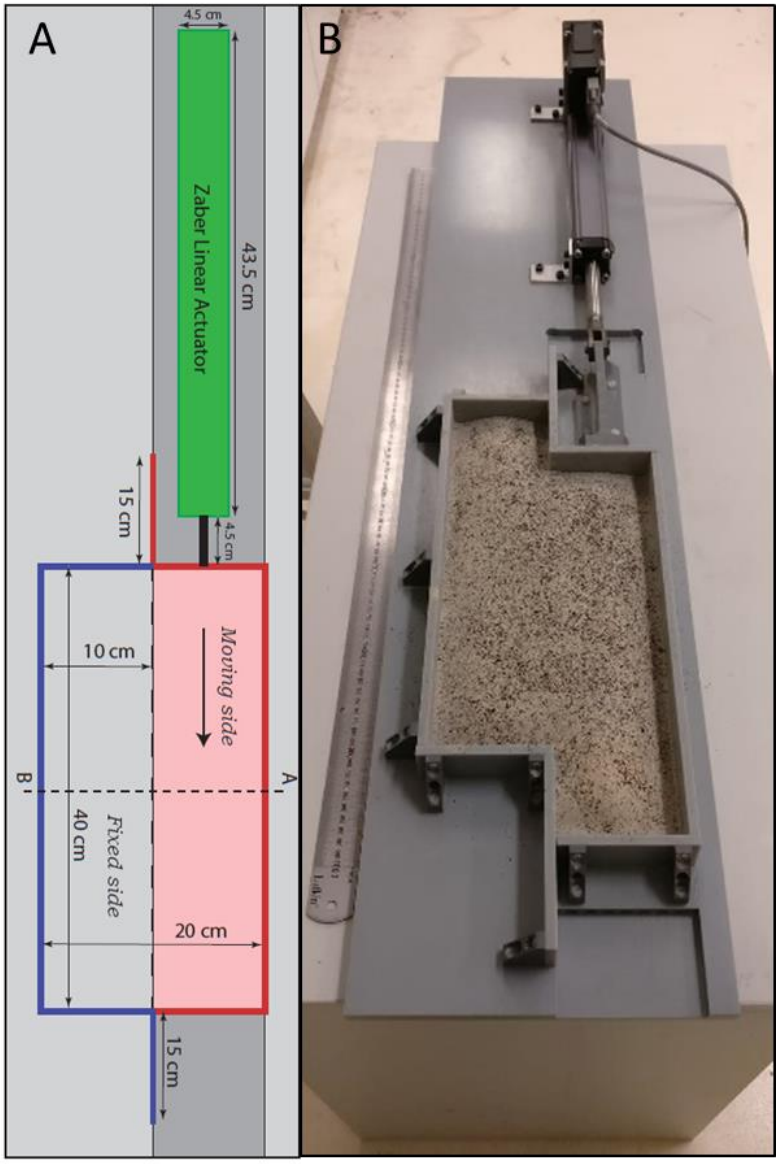

Figure 2.2. Analogue modelling apparatus aka 'the sandbox' used to conduct experiments for this investigation. **A**. Schematic diagram of the Sandbox. **B**. Photograph of the sandbox after the moving side has pushed 6 cm by the linear actuator.

by the user, allowing one side of the box to move horizontally relative to the other side, generating strike-slip motion. This motion creates a central velocity discontinuity along the base of the sandbox. This sandbox is only capable of strike-slip motion so our experiments are limited to strike-slip settings, rather than transpression or transtension. The limitation to strike-slip motion differs from the natural examples, which show elements of transpression and transtension. However, in each case study, the dominant mode of deformation is strike-slip, hence these faults are considered transform faults. Our analogue models are therefore representative of this dominant strike-slip component.

2.3.2. Materials

The sandbox is filled with a 2.5 cm thick homogeneous granular material. Our granular material has a density of 960 kg/m^3 and consists of a mixture of dry quartz sand (60%) and hollow ceramic microspheres (Envirospheres® 40%) (Molnar et al., 2017; Samsu et al., 2021). Both the quartz sand and the ceramic Envirospheres® have homogenous grain size distributions. Using a Hubbert-type shear box, Molnar et al. (2017) determined that this mixture has an angle of internal friction angle < 38° and a cohesion value of ~9 Pa respectively, making it an appropriate analogue for modelling the brittle, Mohr Coulomb behaviour of upper crustal rocks (Byerlee, 1978; Davy and Cobbold, 1991; Schellart, 2000). The material is sieved into the sandbox from a height of 10 cm, and once in place is not manipulated in any way to avoid localised compaction of grains.

2.3.3. Basal boundary conditions

Deformation of the granular material is determined by the boundary condition at the base of the box. Without modification, deformation in the granular material becomes localised over the central basal discontinuity, analogous to a transform fault.

The presence of a ductile lower crustal analogue layer can be expected to result in more diffuse deformation in the brittle upper crust, with the spacing of shear zones being a function of the brittle-ductile strength ratio (Riller et al., 2012). However, test experiments showed that the addition of a lower crustal analogue in the sandbox, without any other modifications, was not sufficient to distribute deformation across the ~ 100 km scale that is occurring in the transition zones, and deformation within the lower crustal analogue remained concentrated over the central discontinuity. The test experiments (Chapter 1) demonstrated the need for a modification to the sandbox to create a basal boundary condition that deformed by large scale distributed deformation and 'annulled' the effects of the central discontinuity, in order to be most analogous to the basal boundary conditions of a 'transition zone'. To achieve this basal boundary condition, we tape a rectangular piece of thin, four-way stretchable elastic fabric to the base of the sandbox using vinyl tape (Fig. 2.3). The material is taped over the central discontinuity in each experiment (Fig. 2.3). Test experiments with the stretchable material and upper crustal analogue showed remarkable consistency with previous analogue experiments investigating distributed simple shear in a specialised analogue box where a lower crustal analogue was used

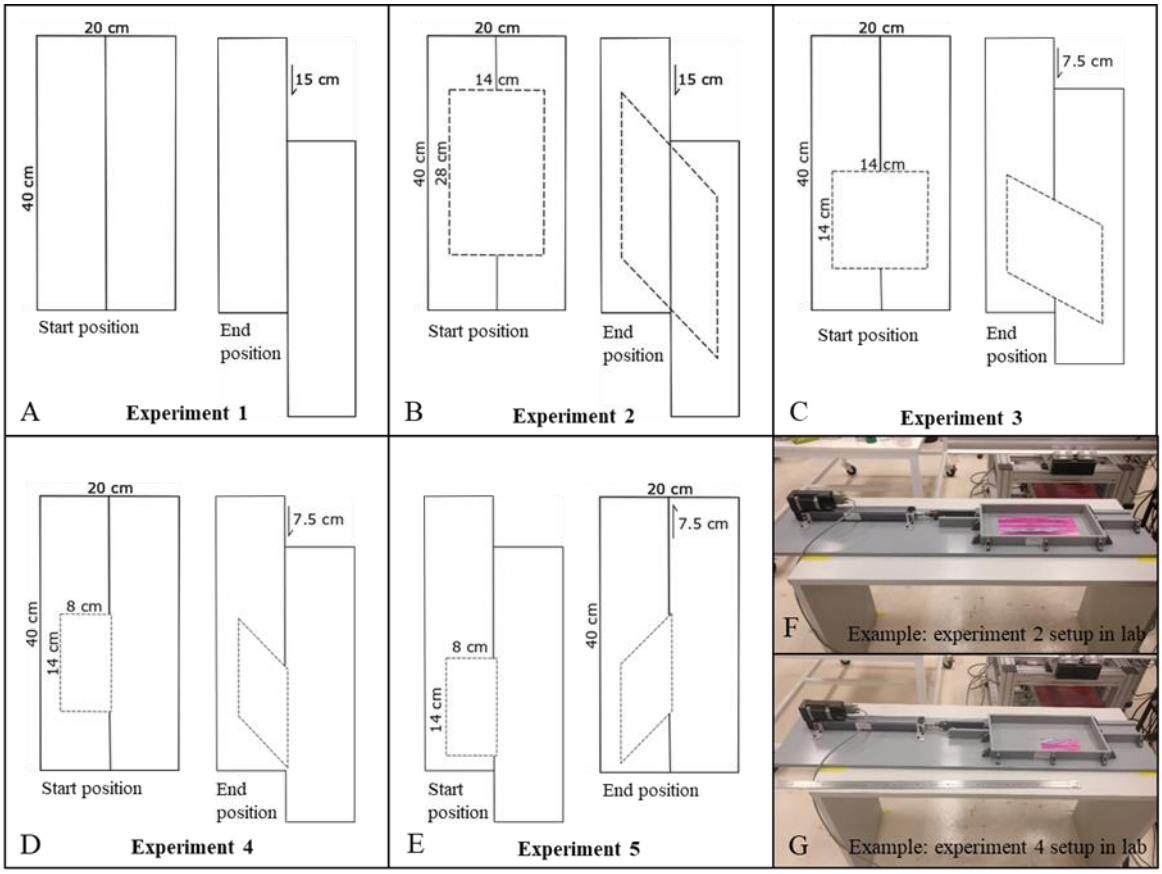

Figure 2.3. The basal boundary conditions of the 'sandbox' for each experiment run in this investigation. **A – E** show schematic diagrams of the starting and finishing position of each experiment. The dashed line shows the position of the stretchable material taped to the base of the sandbox in each experiment. **A:** Experiment 1, Localised simple shear experiment, sandbox is unmodified. **B:** Experiment 2, Distributed simple shear experiment, stretchable material taped across the base of the sandbox. **C:** Experiment 3, the stretchable material is taped across half of the sandbox, so half deforms by localised and half by distributed simple shear. **D**: Experiment 4, the stretchable material is taped so that distributed simple shear occurs on one side of the localised shear zone, analogous to the boundary conditions of the Alpine Fault and MFS. **E:** Experiment 5, a replica of experiment 4 except the box is pulled sinistrally by the linear actuator. **F:** A photograph of the experimental setup of the basal boundary conditions for Experiment 2 (B). **G:** A photograph of the experimental setup of the basal boundary conditions for experiment 4 (D).

(Schreurs, 2003). When the sandbox is deformed, the effects of the central discontinuity are annulled where the stretchable material is taped, and so deformation along the central discontinuity becomes distributed across the stretchable material. The stretchable material creates the boundary condition analogous to the lower crust deforming by large scale distributed deformation, without the need for a ductile lower crustal analogue material. Granular material sieved into the sandbox above the stretchable material is then subjected to the effects of a distributed simple shear basal boundary condition, which we consider to be analogous to the 'transition' zones in the case studies summarised above. The size and location of the stretchable material can be varied to define several different basal boundary conditions as described in section 2.3.4.

2.3.4. Experiments

The five setups used in the series of experiments reported here are illustrated in Figure 3 and characterised in Table 1. Experiment 1 (Fig. 3A) was designed to characterise the development of a localised simple shear zone, and so involved no modification to the sandbox. Experiment 2 (Fig. 3B and F) was designed to investigate the development of a distributed simple shear zone. Distributed shear was generated by taping a 14 cm x 28 cm piece of four-way stretchable fabric across the base of the box prior to adding the granular material. Experiment 3 (Fig. 3C) was designed to model adjacent localised and distributed simple shear zones. A 14 cm x 14 cm piece of four-way stretchable fabric was taped over the base of one half of the box, while retaining the central discontinuity at the base of the other half. Experiment 4 (Fig. 3.D and G) tested the development of both localised and distributed shear zones in which the distributed shear zone occurs only on one side of the localised shear zone (approximating the boundary conditions of the Alpine fault and MFS). A 7 cm x 14 cm piece of four-way stretchable fabric was taped over the base of the box in the position shown in Figs. 3D and G. Experiment 5 repeated Experiment 4 except the motion was sinistral, as shown in Fig. 3. E.

Experiment	**Basal Boundary Condition**	**Stretchable Fabric/Size (cm)**	**Displacement Direction**	**Velocity (mm/hr)**	**Displacement (mm)**	**Tectonic Setting**
1	Localised	No	Dextral	150	150	Transform fault
2	Distributed	Yes / 14 x 28	Dextral	150	150	Transition zone
3	Transition	Yes / 14 x 14	Dextral	150	75	Transform fault with adjacent transition zone
4	Transition	Yes / 7 x 14	Dextral	150	75	Transition zone to one side of transform fault
5	Transition	Yes / 7 x 14	Sinistral	150	75	Transition zone to one side of transform fault

Table 2.1. Details of the 5 analogue experiments conducted for this investigation. Where the term 'transition' is used in the column Basal Boundary Condition, it implies a region of localised and distributed deformation within the same experiment

Each experiment was deformed at a constant velocity of 150 mm/hr. Experiments 1 and 2 were displaced dextrally by 150 mm over 60 minutes. Experiment 3 and 4 were displaced dextrally by 75 mm in 30 minutes and Experiment 5 was deformed sinistrally by 75 mm in 30 minutes. The shorter displacements in these experiments were imposed by how far the basal fabric could stretch with these setups. This did not affect the outcomes of the investigation because mature fault systems developed in each experiment after 30 mm of sandbox displacement. Each experiment was repeated a minimum of three times to ensure reliable, repeatable results.

2.3.5. Experimental Analysis

A Nikon 7500 digital camera captured top view images of the experiment surface at fixed 30 second intervals during deformation of the sandbox. We use Digital Image Correlation (DIC) analyse the 2D deformation in the experiments (Adam et al., 2005). The displacement field is computed by cross correlation of the particle pattern on the surface of the experiment between successive images, which distort and translate in each successive image due to ongoing displacement of the sandbox over the course of the experiment. To aid the DIC algorithm we randomly distribute coffee grains onto the surface of each experiment to provide a high contrast, random pattern suitable for feature tracking. The calculation of the displacement field is explained in detail by Adam et al., (2005). The calculated incremental displacement vector is used as the basis for calculation of further values including incremental and cumulative shear strain (E_{xy}) (Schrank et al., 2008; Riller et al., 2012; Boutelier and Cruden, 2013; Molnar et al., 2017, 2018; Samsu et al., 2021). Incremental shear strain is the calculated 'instantaneous' strain from the tracked change in particle location between two images along an XY axis where X is parallel to the direction of shear strain (Ramsay and Graham, 1970; Ramsay, 1980; Schrank et al., 2008). The cumulative shear stain being the sum of the incremental shear strain. Our results are presented as incremental shear strain maps of the surface of the sandbox models.

2.3.6. Scaling

Since our experiments focus on modelling brittle behaviour of the upper crust, we need to scale for stress, such that the stress scale factor $\Sigma = P\lambda$, where P is the density scale factor and λ is the length scale factor (Schellart, 2000; Cruden et al., 2006). Taking the density of the granular material in the laboratory ρ_m = 960 kg/m^3, to represent upper crust with a density ρ_p 2650 kg/m^3 (Molnar et al., 2017) gives $P = \rho_m / \rho_p = 0.36$, where subscripts m and p denote the model and natural prototype, respectively. Assuming, for convenience that a 2.5 cm thick sand layer (l_m) represents a 25 km thick brittle crust (l_p) in nature gives $\lambda = l_m/l_p = 1 \times 10^{-6}$ and $\Sigma = 3.6 \times 10^{-7}$. This means that brittle rocks with values of cohesion ~50 MPa must be modelled by granular materials with cohesion values ~ 50×10^{-7} = 5 Pa, which is matched closely by our sand + Envirospheres® mixtures.

With the length scale factor above, the 7 cm x 14 cm piece of stretchable material at the base of the sandbox in Experiments 4 and 5 represent a 70 km x 140 km area of distributed deformation in the lower crust in nature. A displacement of 7.5 cm in the sandbox is equivalent to 75 km in nature. This area and net displacement are comparable to the MFS. The results presented only show displacement to 3 cm, as this is the point where a mature fault system has developed for each experiment, so there is little change to the developed fault system after this point. Since the Mohr Coulomb rheology of granular material is rate independent, we do not strictly need to consider time for scaling the deformation rates in our experiments (McClay, 1990; Fedorik et al., 2019).

2.4. Results

2.4.1. Experiment 1: Localised deformation experiment

Figure 2.4A1 shows that no discrete structures formed during the initial stages of deformation (< 2.5 mm displacement), but a 35 mm wide zone of outwardly decreasing incremental shear strain developed over the central discontinuity. Riedel shears became visible after 4 mm displacement of the sandbox (Fig. 2.4A2). These structures have a maximum orientation of 18° clockwise relative to the displacement direction of the sandbox, with a spacing of 90 mm measured parallel to the central discontinuity and a perpendicular spacing of around 35 mm. At > 5 mm displacement, P shears formed that link the Riedel shears and by 10 mm displacement (Fig. 2.4.A3), the Riedel shears were mostly abandoned with deformation almost entirely centred on a single fault located over the central discontinuity. This single fault accommodated the deformation for the remainder of the experiment, although relic popup structures remained (Fig. 2.4A3 – A7), preserved from stage when the Riedel shears were abandoned in favour of the central through-going fault.

2.4.2. Experiment 2: Distributed deformation experiment

Discrete geological structures took longer to form in Experiment 2 compared to Experiment 1. During the initial stages of deformation, up to 2.5 mm displacement (Fig 2.4B1), incremental shear strain is accommodated in a broad 40 mm wide zone over the centre of the box, which is slightly wider than Experiment 1 (Fig 2.4.A1) but with lower values of incremental shear strain. With increased displacement (Fig. 2.4B2 and B3), this zone of incremental shear strain broadens across the width of stretchable material at the base of the box. After ~15 mm displacement two main sets of linear structures began to form (Figure 2.4B4). The dominant structure is a set of equally spaced faults oriented 18° clockwise relative to the displacement direction of the sandbox, with a perpendicular spacing ranging between 10 mm and 20 mm, averaging around 17 mm. The orientation of these structures is consistent with them being conjugate Riedel shears. When the spacing between two faults becomes greater than 20 mm, a smaller, parallel fault develops in-between them (Fig. 2.4B7). A second set of equally spaced linear structures is oriented around 80 ° relative to the displacement direction of the sandbox, with a perpendicular spacing of around 10 mm. The orientation of these structures is consistent with them being antithetic Riedel shears.

2.4.3. Experiments 3 and 4: Dextral transition experiments

The area of localised deformation above the basal discontinuity in both Experiments 3 and 4 developed in the same manner as Experiment 1 (Fig. 2.4C1,2 and D1,2). By the time that Riedel shears developed in the zone of localised simple shear in both experiments (~5 mm displacement), no structures were present in the area of distributed simple shear above the stretchable material. Instead, outwards decreasing, diffuse incremental shear strain is observed over the region (Fig. 2.4C1 and D2).

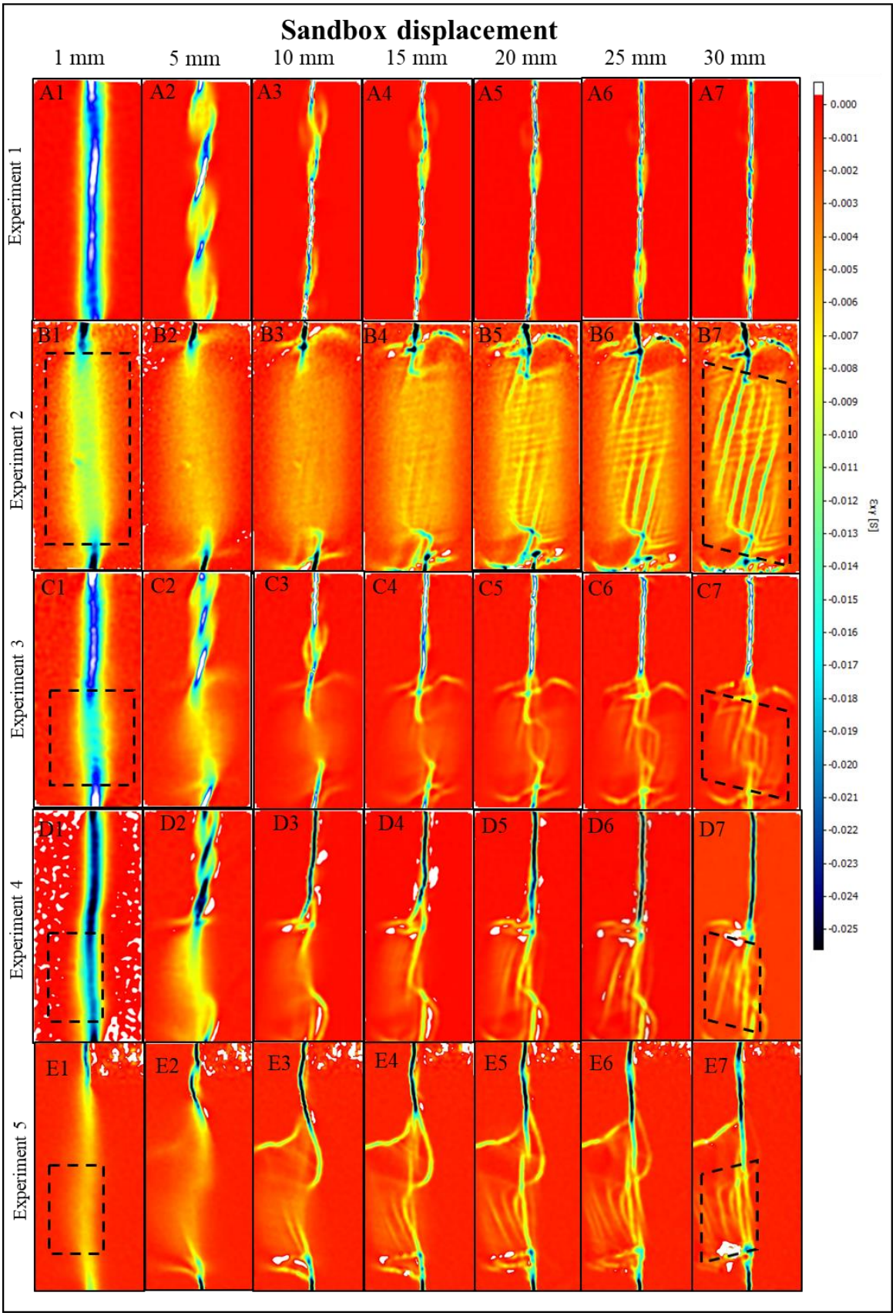

Figure 2.4. Exy incremental shear strain maps at 5 mm displacement intervals (from 0 mm to 30 mm) of the surface of each analogue model experiment, determined by PIV. The dashed line indicates the position of the stretchable material taped to the base of experiments 2 – 5 at 0 mm and at 30 mm. Each incremental shear strain map is given a label for reference in the results section.

By 10 mm of displacement in both experiments, a single fault had formed above the central discontinuity in the localised simple shear region.

Major faults began to develop in the region of distributed simple shear after ~15 mm of displacement in both experiments. These faults are consistent with those formed in Experiment 2 with an orientation ~18 ° clockwise relative to the displacement direction of the sandbox and a perpendicular spacing of ~20 mm. In both experiments, the first faults in the regions of diffuse simple shear formed over the centre of the sandbox. With increased displacement, more faults developed sequentially away from the centre of the box, outwards towards the edges of the stretchable material. The faults that formed closer to the centre of the box eventually linked and connected with the major fault over the region of localised simple shear. However, faults developed in the region of distributed deformation but further away from the centre of the box did not connect with the earlier formed faults closer to the centre of the box.

2.4.4. Experiment 5: Sinistral transition experiment

The faults that formed in this experiment (Fig. 2.4E1-7) developed in the same manner as Experiment 4. The fault in the zone of localised deformation formed first, followed by the faults in the region of distributed deformation. The faults in the region of distributed deformation once again nucleated within a region of diffuse strain, developing sequentially outwards from the centre of the box towards the edge of the stretchable material. As in the previously described experiments, these faults are oriented 18° relative to the sinistral displacement direction of the sandbox but with the opposite polarity.

2.4.5. Experimental artefacts and limitations

A number of artefacts developed at the ends of each experiment due to the geometry of the vertical side boundaries and corners of the sandbox (Fig. 2.2). For example, in Experiment 2 regions of extension and compression are present at either end of the box, becoming more pronounced with increasing displacement (Fig. 2.4B). Although unwanted, these boundary effects are outside the region of interest in the central region of the sandbox and therefore do not have a strong influence on the experimental results.

Other artefacts are related to the stretchable material used to create the distributed simple shear basal boundary condition. Pop-up structures and pull apart basins formed above the untaped edges of the stretchable material (perpendicular to the central discontinuity) (Fig. 2.5). As with the artefacts related to the vertical side walls and corners, these features have no equivalent in nature. For this reason, we were careful to restrict our observations and analyses to the regions above the central part of the stretchable material, which are not obviously influenced by edge effects.

The experimental setup is also limited by the elasticity of the stretchable material, which cannot deform indefinitely. This effect is avoided by limiting the displacement of the experiments that involve smaller pieces of stretchable material.

2.5. Discussion

2.5.1. Fault development in regions of localised deformation

Experimental results showed firstly the development of conjugate Riedel shears, followed by the development of P Shears, which linked the Riedel shears to form a single, continuous fault that localised over the central discontinuity at the base of the sandbox. The development of structures in regions of localised deformation are consistent with many similar analogue modelling and field studies on the evolution of strike-slip faults (Riedel, 1929; Tchalenko, 1970; Wilcox et al., 1973; Naylor et al., 1986; Schrank et al., 2008; Schrank and Cruden, 2010; Dooley and Schreurs, 2012). The single faults that developed above the basal discontinuity in Experiment 1, and in the localised regions of simple shear in Experiments 3, 4 and 5 (Fig. 2.4), accommodated the bulk of the deformation within these regions. These faults are analogous to the Alpine, San Andreas (to the north of the big bend) and North Anatolian transform faults (Fig. 2.5, 2.6).

2.5.2. Fault development in regions of distributed deformation

In regions that were overlying a basal boundary condition of distributed deformation, the upper crustal analogue developed a sub-parallel array of approximately equally spaced faults. These faults were oriented ~ 18° relative to the central discontinuity, consistent with the orientation of Riedel shears that developed over the region of localised deformation. We therefore refer to these faults in the region of distributed deformation as Riedel shears. In experiment 2, antithetic Riedel shears also develop. The development of faults in this pattern is consistent with similar analogue modelling studies (Schreurs, 2003).

The faults that formed over the regions of distributed simple shear (Fig. 2.4, Experiments 2, 3, 4, 5), are similar to the fault patterns observed at the northern termination of the Alpine Fault (the MFS) (Fig. 2.1A), the southern termination of the San Andreas fault (Fig. 2.1B) and the western termination of the North Anatolian Fault (Fig. 2.1C). These fault systems are oriented close to ~ 18° relative to their transform fault. These equally spaced arrays of faults localise and constrain deformation of the brittle upper crust over a basal boundary condition simulating large scale distributed deformation of the lower crust.

The southern San Andreas fault system is younger than the MFS, beginning its development at 1.5 Ma compared to 6 Ma in the MFS (Morton and Matti, 1993; Bennett et al., 2004; Wallace et al., 2012). The MFS can therefore be considered to be a more evolved system, similar to Experiment 4 at 30 mm displacement (Fig. 2.4D7). In comparison to the MFS, the southern San Andreas Fault pattern is similar to Experiment 4 at 20 mm displacement (Fig. 2.4D5). The western termination of the NAF fault is even

younger, having developed over the last 200 Kyrs (Şengör et al., 2005), showing similarities to Experiment 4 at 15 mm displacement (Fig. 2.4D4).

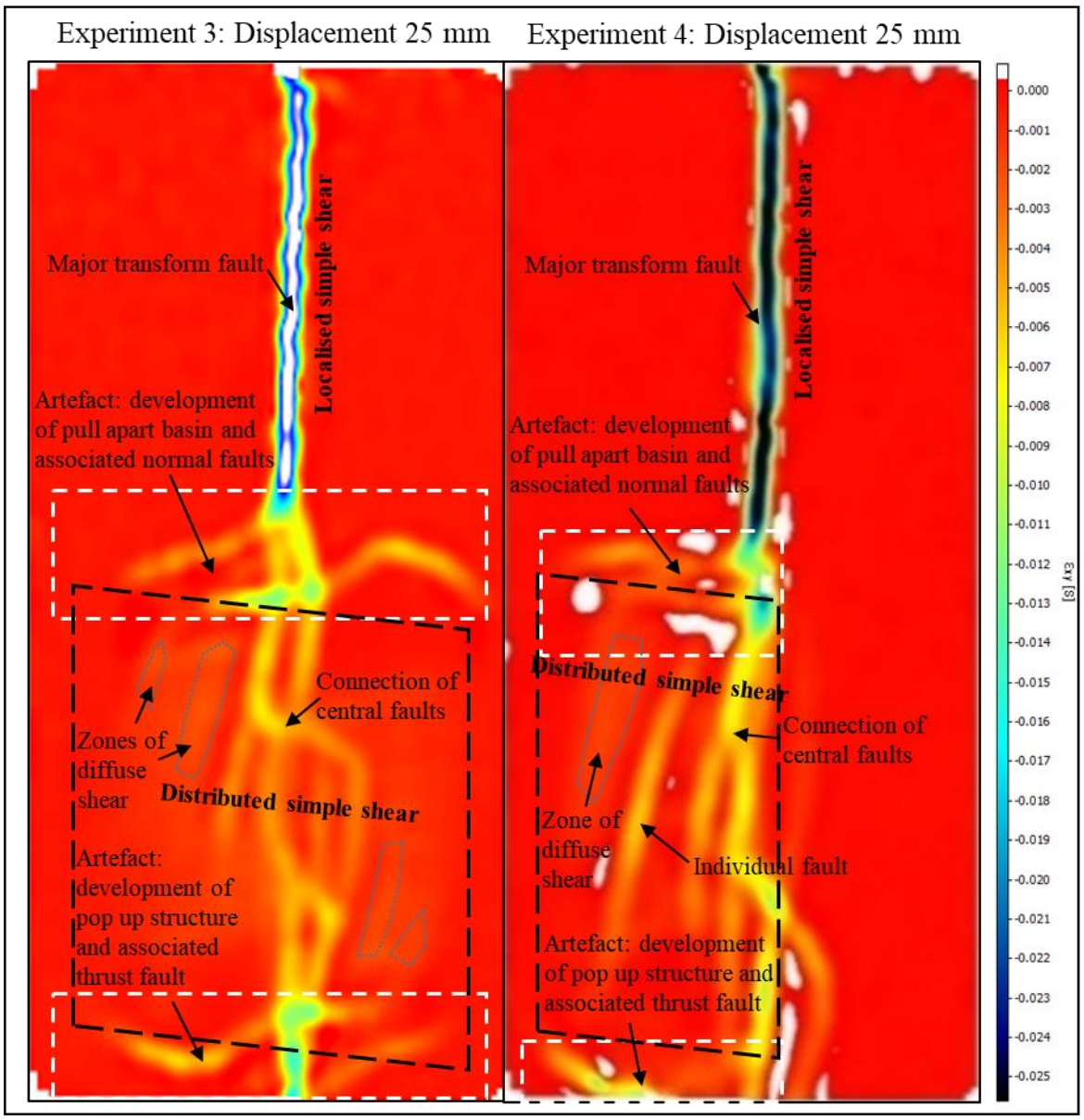

Figure 2.5. Analysis of developing faults in **A**: Experiment 3 at 25 mm displacement (Figure 4.C6). **B**: Experiment 4 at 25 mm displacement (Figure 4.D6). Each image consists of a incremental shear strain map determined by PIV. The white dashed boxes represent areas where artefacts are present in the analogue model. The black dashed boxes show the location of the stretchable material and region of distributed simple shear. The blue dotted ovals show regions of diffuse shear that are localising to form faults.

2.5.3. Fault development at transitions between localised and distributed simple shear

Where localised deformation transitions to distributed simple shear in Experiments 3, 4 and 5, the faults in the centre of the sandbox develop first and then connect to the major transform fault in the region of localised deformation (Fig. 2.4C,D,E). Starting as a zone of diffuse deformation (Fig. 2.5), faults in the

region of distributed simple shear nucleate sequentially outwards. The faults in the area of distributed shear strain therefore develop independently and are not splays from the major transform fault in the region of localised deformation (Fig.2.5). These faults exhibit significant slip rate reductions towards the major analogue transform fault. The early forming central faults in the regions of distributed simple shear link to the main transform fault (Fig.2.5), and they accommodate much more displacement than the younger faults that develop subsequently. The displacement on these faults also decreases with age, so the youngest, peripheral faults record the least displacement. The connection of the central faults occurs by a series of cross-faults, which suggest participation of smaller linkage faults in allowing these spaced, major faults to 'communicate' and collectively accommodate distributed shear.

These experimental results are consistent with the fault patterns and the proposed development of faults in the natural examples (Fig. 2.1A,B,C). Both the Wairau Fault in the MFS (Fig. 2.1A) and the southern segment of the San Andreas Fault (south of the Big Bend) (Fig. 2.1B) formed later, and accommodate less displacement than the main transform fault they join up with (Morton and Matti, 1993; Bennett et al., 2004; Wallace et al., 2012).

The MFS developed sequentially southward across the region between the Alpine fault and Hikurangi subduction zone. The San Jacinto, Elsinore and NIRC faults associated with the southern San Andreas developed sequentially westward, away from the major transform fault (Dorsey et al., 2012). Displacement across each of these fault systems also decreases (on average) with age, consistent with fault development in Experiments 3 and 4 (Fig. 2.4).

In the MFS (Fig. 2.1A), the Wairau fault is a continuation of the Alpine fault and the Awatere fault to the south appears to either splay from or join the Alpine fault. Both faults formed around 6 Ma (Wallace et al., 2012). Bennett et al. (2004) found that the southern San Andreas and San Jacinto faults developed at 1.5 Ma at the same time as the 'Big Bend' formed on the San Andreas Fault. This is similar to the formation of the initial faults within the regions of distributed simple shear in the transition experiments (Fig 2.4, Experiments 3 and 4).

The connection of the Clarence and Hope faults in the MFS with the Alpine/Wairau fault is poorly constrained and slip rate is shown to decrease towards the Alpine Fault. The Hope fault has been recently shown to have propagated from the centre of the Marlborough region between the Alpine fault and Hikurangi subduction zone, back towards the Alpine fault (Vermeer et al., 2021). In the southern San Andreas, the San Jacinto fault does not directly connect with the San Andreas Fault SAF. Scholz et al. (2010) also showed that the San Jacinto fault developed at a distance away from the SAF and propagated back towards it, similar to the proposed development of the Hope fault in the MFS. The Elsinore and NIRC faults also formed sequentially and further away from the San Andreas Fault and do not connect with it. The sequential nucleation of faults in this manner starting with an initially

diffuse region of deformation at a distance from the main fault branches, is consistent with the results of Experiments 3 and 4 (Fig. 2.5).

The ages of the northern and southern branches of the NAF are currently unknown but the NAF had only propagated to the Sea of Marmara by 200 Ka (Provost et al., 2003; Şengör et al., 2005; Norris and Toy, 2014), so these branches of the NAF must be relatively young. The consistency of the development of the MFS and faults associated with the southern termination of the San Andreas Fault with the analogue modelling results, suggest that the northern NAF and the southern NAF would have developed coeval with one another. Consistent with the development of the Wairau and Awatere Faults in the MFS and the southern San Andreas and San Jacinto faults in California, in each case these are the first two faults to develop in the transition zone.

2.5.4. What causes deformation to become distributed?

Although the fault pattern evolution in Experiments 3 and 4 (Figs. 2.4 and 2.5) helps to explain key features of the MFS, southern SAF and western NAF, similar fault patterns do not occur at the terminations and plate boundary transitions of all continental transform faults. In many examples, such as the southern Alpine Fault and the southern Dead Sea Transform (Figure 2.1 A, D), the transition between plate boundary types is localised and continuous. In these examples, the plate boundaries directly connect and deformation of the lower crust remains localised within the plate boundary. Here we discuss the possible causes of distributed deformation at plate boundary transitions.

How zones of distributed deformation develop where continental transform faults transition to a new plate boundary type, appears to depend on the tectonic history of the transform fault itself. Where the transition between the transform fault and the connecting plate boundary remains localised on a continuous plate boundary fault, the tectonic development of the adjoining plate boundaries is coeval (Sutherland et al., 2000; Shuck et al., 2021). Conversely, the northern Alpine Fault, southern SAF and western NAF all evolved independently from their 'connecting' plate boundary. In each case, the transition zone between the continental transform fault and its connecting plate boundary developed by propagation of the transform fault towards the connecting plate boundary, resulting in a 'misalignment' of the plate boundaries and the generation of a region of distributed deformation.

In New Zealand, the Alpine Fault propagated northeast while the Hikurangi subduction zone migrated southwest, leading to a transition zone of distributed deformation marked by the MFS (Fig. 2.6A.) (Wilson et al., 2004; Randall et al., 2011; Wallace et al., 2012; Lamb et al., 2016).

The San Andreas Fault began to develop at 28 Ma, propagating southwards to accommodate plate motion where a spreading ridge had entered a subduction zone and halted subduction (Mckenzie and Morgan, 1969; Dickinson and Snyder, 1979a, 1979b). This southward propagation resulted in the

development of the Big Bend (Bennett et al., 2004) and the associated misalignment was sufficient to cause distributed deformation (Fig. 2.6B.)

In Turkey, the NAF formed in response to the westward escape of the Anatolian plate in response to the collision between the Arabian and Eurasian plates. The fault is propagating westward towards the Hellenic subduction zone but is yet to connect with it, causing deformation to become distributed towards the fault tip (Provost et al., 2003; Şengör et al., 2005; Norris and Toy, 2014). The fault is only 200 Ka its western end where it reaches the Sea of Marmara (Şengör et al., 2005). (Fig. 2.6C).

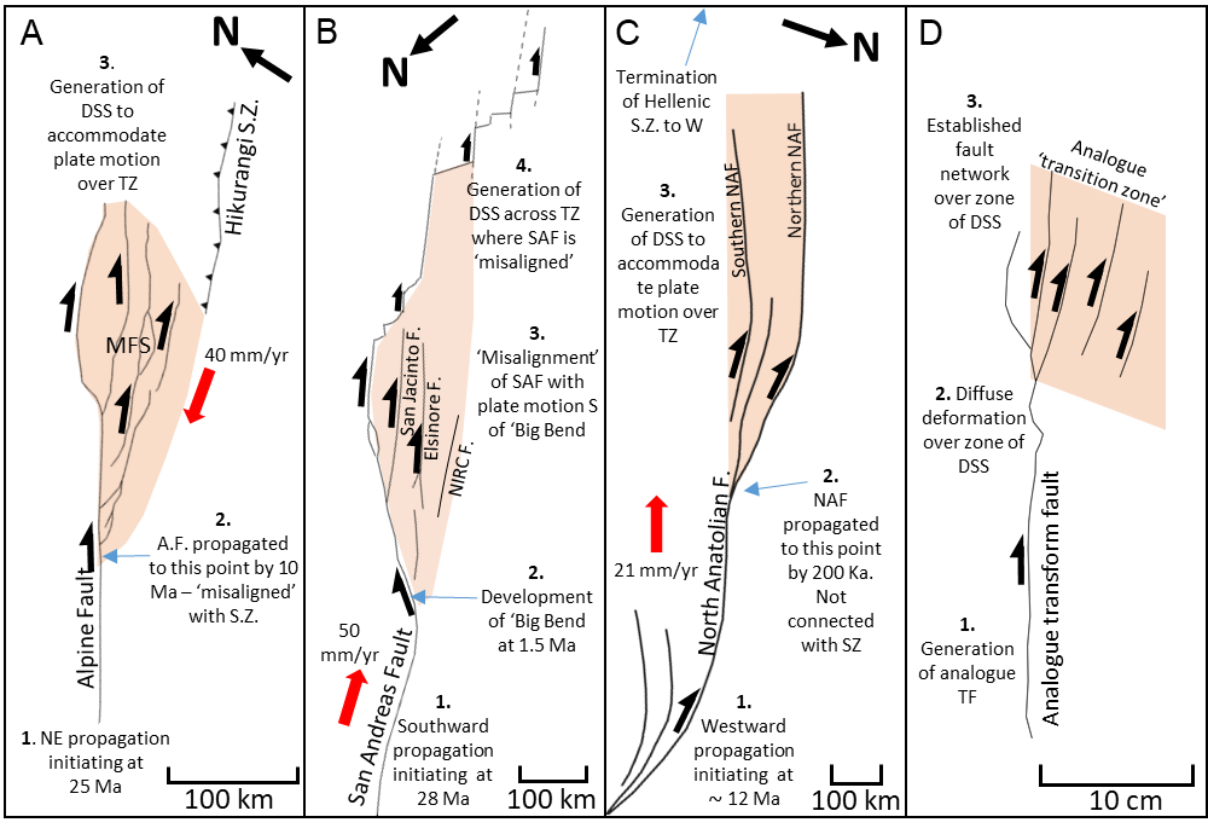

Figure 2.6. Fault outlines of the case studies compared to the fault outline of experiment 4 at 30 mm displacement (Figure 2.4 D7). The case studies have been rotated for comparison with the analogue experiment. The region of proposed distributed shear is highlighted in orange each for each example. Red arrows indicate direction of plate motion. DSS = Distributed Simple Shear. TZ = Transition Zone. SZ = Subduction Zone. TF = Transform Fault **A.** The northern termination of the Alpine Fault and the Marlborough Fault System (MFS). **B**. The southern termination of the San Andreas Fault (SAF). **C**. The western termination of the North Anatolian Fault (NAF). **D**. Analogue model (Experiment 4 at 30 mm displacement).

Conclusion

The fault patterns that develop in the analogue experiments presented here (Fig. 2.4) are consistent with those observed in nature in the MFS (the northern termination of the Alpine fault), the southern termination of the SAF, and the western termination of the NAF (Fig. 2.6).

The experiments suggest that fault patterns in transition zone settings develop during deformation of brittle upper crust overlying ductile lower crust undergoing distributed simple shear. The resulting fault pattern forms as a series of equally spaced, crustal-scale Riedel shear faults that develop sequentially away from the major transform fault, outwards across the region of distributed deformation. These faults occur away from the major transform fault, and nucleate within a zone of initially diffuse deformation (Fig. 2.5). Once formed these faults propagate back towards the major transform fault and for the most part do not connect with it, except for the first formed fault in the region of distributed deformation that eventually becomes a continuation of the major transform.

Distributed simple shear deformation of the lower crust can occur when transitions between continental transform faults and adjoining plate boundaries become misaligned. We propose that this is likely to occur when the two plate boundaries develop at different times, and where the transition zone develops as a continental transform fault propagates towards its connecting plate boundary. We propose that such zones of distributed deformation essentially represent 'young' plate boundary transitions, and with time the associated crustal scale Riedel shear faults may be abandoned to form a continuous transition from one plate boundary to another.

Chapter 3

To splay or not to splay? That is the question

Abstract

Splay faults are usually assumed to be secondary faults that have propagated away from a primary fault. Here we present the results of a series of analogue modelling experiments investigating the evolution of strike-slip fault systems that have branching surface fault geometries, which resemble those of splay faults. We find that where the basal boundary condition remains localised, branching fault networks develop by propagation away from a primary fault. Whereas if the basal boundary condition becomes distributed, faults develop as sub parallel, equally spaced arrays that can approach and intersect a larger primary fault, creating an abutting relationship. Although the surface geometries resemble branching splay fault systems, the evolution of fault networks over regions of distributed simple shear is not consistent with how splay faults are normally assumed to develop. We therefore suggest that the application of the splay fault concept should be made with caution when interpreting branching fault systems and that consideration of scale is an important factor when making such interpretations. To highlight this importance, we construct a three-dimensional (3D) model of the Marlborough Fault System, New Zealand, using LoopStructural, which requires interpretation of the intersection relationships of the 'branching' faults within the fault system.

3.1. Introduction

Geologists use the term ‘splay fault’ to refer to a secondary fault that branches from a primary fault at an acute angle, and with the same sense of shear as the primary fault (Brace and Bombolakis, 1963; Mcgrath, 1995; Fossen, 2010; Scholz et al., 2010; Perrin et al., 2016). The definition of the verb to ‘splay’ is ‘to cause to spread outward’ (Merriam-Webster, n.d.). Therefore it is also normally assumed that the secondary splay fault propagated away, or emerged from the primary fault (Peacock et al., 2017). This assumed mode of splay fault development has implications for geological interpretations, including the construction of cross sections and three-dimensional (3D) models (Bond et al., 2007b; Grose et al., 2020, 2021), which involve integrating observations, experience and knowledge.

In this paper we use X-Ray Computed Tomography (XRCT) to image the geometry of strike-slip faults in analogue model experiments as a proxy for the 3D evolution of fault networks that develop in regions of localised and distributed simple shear. We use these results to show that knowledge of how branching fault map patterns evolve is important for generating accurate 3D interpretations of strike-slip fault systems. We propose that the definition of the term ‘splay fault’ should not only include its geometry but also specifics of faulting kinematics, and description of spatial-temporal association of these fault(s) to their parent fault.

3.2. Background

Strike-slip splay faults typically occur close to the tip of a primary fault, as well as at releasing and restraining bends, forming as branching faults or horsetail splays that act to spread displacement over a wider area (Brace and Bombolakis, 1963; Mcgrath, 1995; Legg et al., 2004; Cunningham and Mann, 2007; Mann, 2007; Fossen, 2010; Perrin et al., 2016). Strike-slip splay faults occur from micro- to tectonic scales (Perrin et al., 2016).

Figure 3.1 illustrates four examples of strike-slip dominated fault systems that are often cited as examples of splay faults (Browne, 1992; Ando et al., 2009; Scholz et al., 2010; Norris and Toy, 2014; Fedorik et al., 2019). The San Andreas Fault and the Alpine Fault are examples of trans-lithospheric, continental transform faults (Figs. 3.1A, B.) that accommodate hundreds of kilometres of relative plate motion (Wilson, 1965; Woodcock and Daly, 1986; Legg et al., 2004; Norris and Toy, 2014; Şengör et al., 2019). The southern San Andreas Fault System (SAFS) and the Marlborough Fault System (MFS) are occur at the terminations of their respective transform faults, where they distribute deformation across ~ 100 km wide areas (Wilson et al., 2004; Wannamaker et al., 2009; Eberhart-Phillips and Bannister, 2010; Scholz et al., 2010). The Sciacca fault is an example of a smaller-scale strike-slip fault where branching faults associated with its termination distribute deformation over a ~ 10 km wide area (Fedorik et al., 2018, 2019). Figure 3.1D shows a series of faults collectively called the Lassee fault

segment, a transtensional rift section associated with a releasing bend of the Vienna Basin strike-slip fault (Beidinger and Decker, 2011). The Lassee fault segment distributes deformation over a ~ 10 km area and there is no surface expression of the primary strike-slip fault across this transtensional rift.

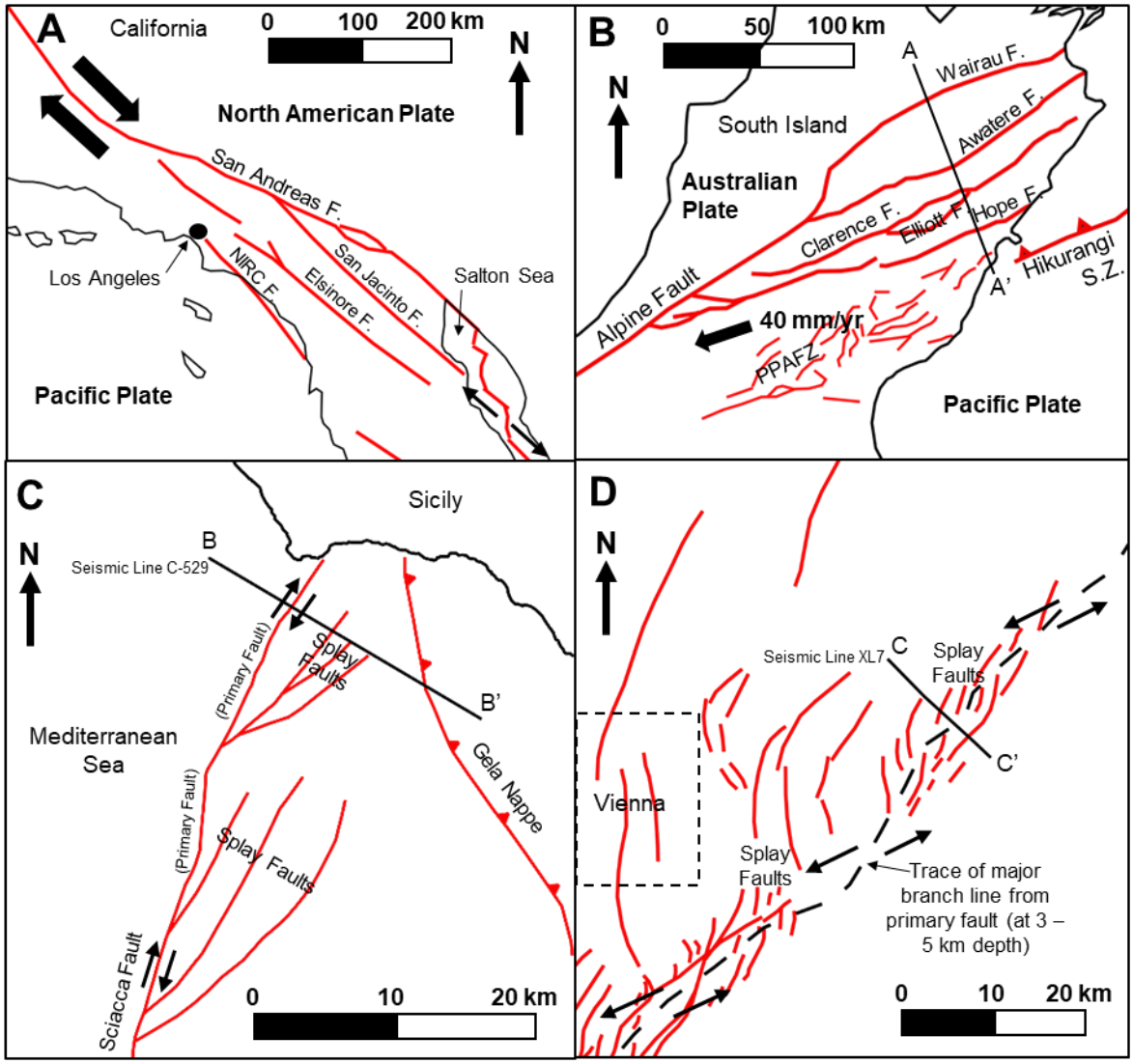

Figure 3.1. Fault networks with 'splay' fault geometries. **A.** Dextral strike-slip faults associated with the termination of the San Andreas Faults, referred to as the southern San Andreas Fault System (SAFS) in this paper. Adapted from Legg et al. (2004). NIRC F. = Newport Inglewood Rose Canyon Fault. **B.** The Marlborough Fault System (MFS), a series of dextral strike-slip faults that have developed at the termination of the Alpine Fault to transfer plate motion to the Hikurangi subduction zone (Fault traces © GNS Science 2016). PPAFZ = Porters Pass to Amberley Fault Zone. **C.** A series of faults associated with the termination of the Sciacca strike-slip faults off of the coast of Sicily. Adapted from Fedorik et al. (2019) and Fedorik et al. (2018). Seismic line of which interpretation is based is reflection profile C-529 and is available from www.videpi.com. **D.** The Lassee fault segment of the Vienna Basin strike-slip fault. This segment is a transtensional rift from localised transtension along the fault. The primary strike-slip fault is not present at the surface, its branching point at depth is dashed across the map. Adapted from Beidinger and Decker (2011), seismic line XL7. The lines of cross sections in B, C and D are shown in Figure 3.2.

The terminations of the San Andreas, Alpine and Sciacca faults have similar geometries in map view (Figs. 3.1A, B, C). Each fault system contains secondary faults that are approximately equally spaced and connect, or appear to connect, to the primary fault at an acute angle and with the same sense of

shear as the primary fault. These fault patterns match the typical branching pattern of splay faults associated with the tips of propagating strike-slip faults (Scholz et al., 1993; Mcgrath, 1995; Kim et al., 2004; Kim and Sanderson, 2006). However, despite their map view similarities, geophysical data shows that the MFS appears quite different in cross section to faults associated with the termination of the Sciacca Fault (Fig. 3.2A, B). The MFS faults are vertical to sub-vertical and are confined to the upper crust (Wannamaker et al., 2009; Eberhart-Phillips and Bannister, 2010), indicating that ductile deformation in the lower crust is distributed across a ~ 100 km wide area. In contrast, secondary faults associated with the termination of Sciacca fault coalesce at ~ 10 km depth (Fedorik et al., 2019), defining a positive flower structure in cross section. Deformation therefore becomes localised within a single, narrow fault zone at depth.

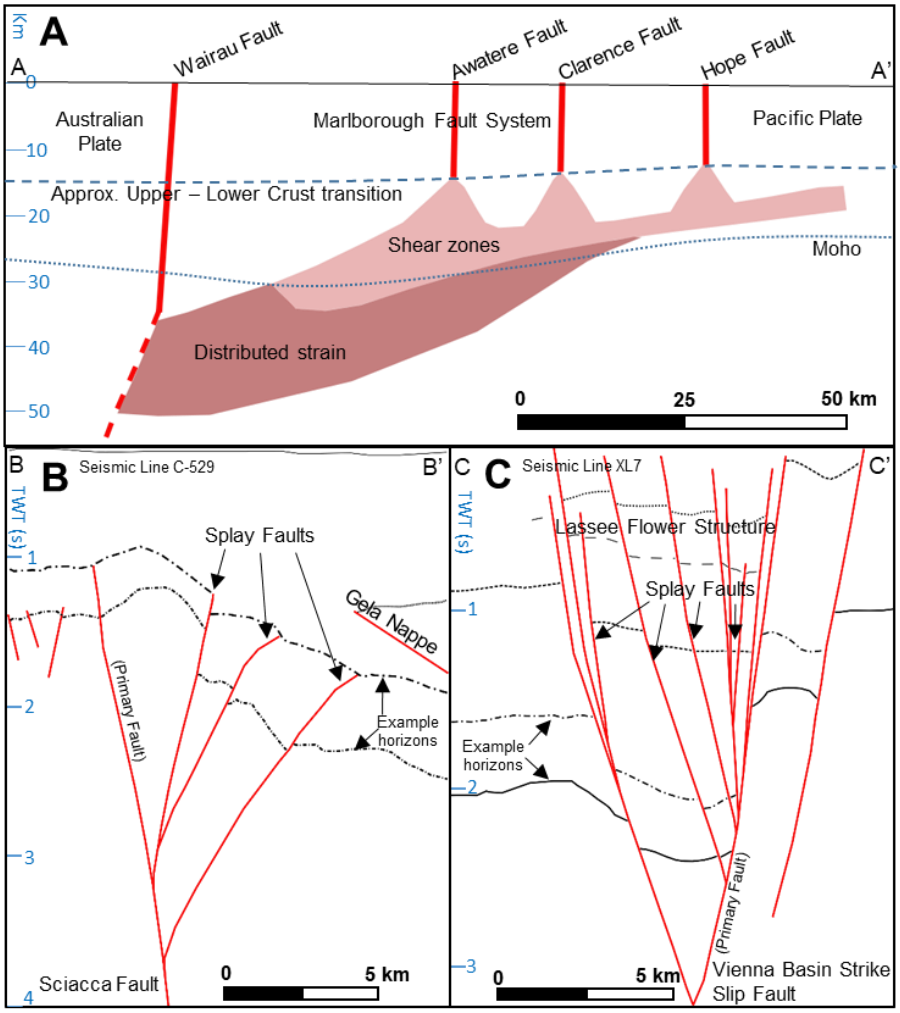

Figure 3.2. A. Cross section of the Marlborough Fault system along line A-A' (Fig. 3.1B.). Cross section modified from interpretations of seismic data by Eberhart-Phillips and Bannister (2010), with the Upper-Lower Crust Transition and Moho inferred from Wannamaker et al. (2009). The MFS faults propagate vertically to the lower crust transition. **B.** Cross section of the fault network associated with the termination of the Sciacca Fault, along line B-B' (Fig. 3.1C.). Adapted from Fedorik et al. 2019. Seismic reflection profile C-529 is available from www.videpi.com. The cross section shows a positive flower structure, with faults coalescing at depth. **C.** Cross section of the Lassee segment of the Vienna Basin strike slip fault, along line C-C' (Fig. 3.1D.). Adapted from the interpretations of seismic line XL7 from Beidinger and Decker (2011). Showing the negative flower structure generated from the transtensional rift, faults are shown to join at a branching point at depth.

Branching fault patterns observed in map view are often compared and assumed to be self-similar over a wide range of length scales (Norris and Toy, 2014; Fedorik et al., 2019). Peacock et al. (2017) demonstrate that approaching and intersecting faults can have similar patterns to splay faults as defined above. In their refined definition, Ando et al. (2009) and Scholz et al. (2010) consider such intersecting faults, as well as faults that do not connect with their primary fault to be splay faults. Their refined definition of a splay fault is based on the southern SAFS, which they compare to the MFS.

Although the Lassee Fault segment shows no surface expression of a primary strike-slip fault, the faults are interpreted to connect at depth to define a negative flower structure (Harding, 1985; Cunningham and Mann, 2007). Seismic studies confirm this interpretation and show that these secondary faults connect to primary displacement zone at ~ 10 km depth (Beidinger and Decker, 2011) (Fig. 3.2C). The Lassee segment faults therefore fit both cross sectional and map pattern definitions of splay faults. Similar to the termination of the Sciacca fault, deformation that is distributed over a 10 km wide area at the surface becomes localised at depth onto a single fault.

Chapter 2 in this thesis found that fault networks formed in experiments with boundary conditions that are analogous to the southern SAFS and the MFS can develop from distributed simple shear in the lower crust, consistent with previous interpretations of geophysical data (Wilson et al., 2004; Wannamaker et al., 2009; Eberhart-Phillips and Bannister, 2010). These results indicated that such faults localise a distance away from their associated primary transform fault in the centre of a region of distributed deformation, and that they propagate outwards towards the primary fault, often terminating prior to connecting with it. This result is consistent with the propagation of the San Jacinto fault outlined by Scholz et al. (2010) (which led to their definition of the term splay fault), and the Hope Fault by Vermeer et al., (2021). However, the development of the experimental fault systems was not analysed in cross section.

3.3. Methods

We conducted XRCT scans of simple shear analogue experiments to investigate the 3D evolution of fault networks over regions of localised and distributed simple shear. The experiment apparatus consisted of a 20 cm x 40 cm x 4 cm simple shear ‘sandbox’, comprising two halves separated by a central discontinuity. Simple shear deformation conditions are generated when a linear actuator pushes the movable half of the box relative to the fixed half (Schrank et al., 2008) (Fig. 3.3). The box was filled with a 2.5 cm homogeneous mixture of 60 % quartz sand and 40 % ceramic Envirospheres® as used and characterised by Samsu et al. (2021), which deforms as a granular Mohr-Coulomb material and acts as a suitable analogue for the brittle upper crust (Byerlee, 1978; Davy and Cobbold, 1991; Schellart, 2000). The analogue model apparatus and materials are described in detail in Chapter 2 of this thesis.

In order to analyse and compare the 3D evolution of fault networks that develop across upscaled ~ 100 km and ~ 10 km regions, we carried out three simple shear analogue experiments in an X-Ray Computed Tomography (XRCT) scanner, which provided images taken at regular displacement intervals during the experiment.

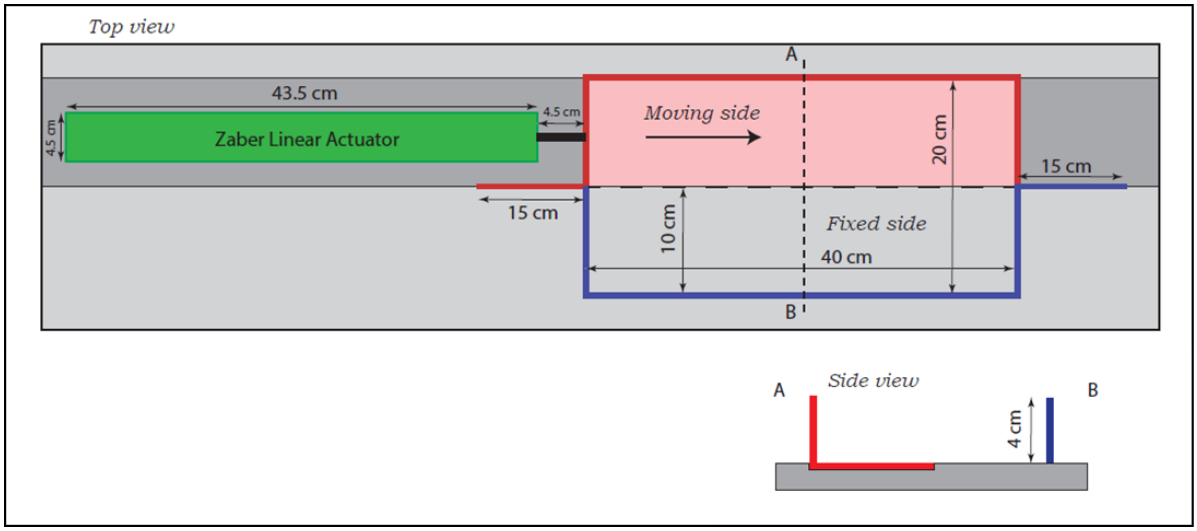

Figure 3.3. The analogue shear apparatus a.k.a 'The Sandbox'. The moveable half of the box is pushed past the fixed half of the box at a constant velocity.

Experiments 1, 2 and 3 in this chapter are repeats of Experiments 1, 2 and 4 in Chapter 2 of this thesis. The sandbox was modified by taping a piece of four-way stretchable elastic fabric that deforms by distributed deformation at the base of the box (Fig. 3.4) and the granular material above it undergoes distributed simple shear.

The analogue experiments conducted in the XRCT scanner are as follows:

Experiment 1. No modification to the sandbox, so deformation in the sand occurs by localised simple shear over the discontinuity at the base of the box (Fig. 3.4A).
Experiment 2. A 28 cm x 14 cm piece of four-way stretchable elastic fabric is taped in a central position to the base of the box (Fig. 3.4B).
Experiment 3. A 14 cm x 7 cm piece of stretchable material is taped to the base of the box in a position analogous to the MFS and the southern SAF, as explained in Chapter 2 (Fig. 3.4C). Half the box remains unmodified and the sand deforms by localised simple shear, while the sand over the stretchable material undergoes localised simple shear.

XRCT scans of Experiments 1 and 2 were conducted at 10 mm intervals over 100 mm of displacement of the box. After 40 mm displacement a well-established fault system had developed in each experiment (Fig. 3.5) and there was little change after this point. XRCT scans of Experiment 3 were conducted at 5 mm displacement intervals until 30 mm displacement, which was the limit of the stretch that could be sustained by the smaller piece of fabric. In all three experiments, XRCT scans were generated after

each displacement interval when the box was stopped prior to the next interval and scan. This allowed for higher fidelity images as the box was stationary. This start stop motion had no noticeable effect on the experiments because the granular upper crustal analogue is rate independent (McClay, 1990; Fedorik et al., 2019).

The XRCT scanner generates cross sectional slices of the experiment that show relative changes in density of the granular material within the box (e.g. Mandl, 1988; Schreurs, 1994, 2003; Schreurs and

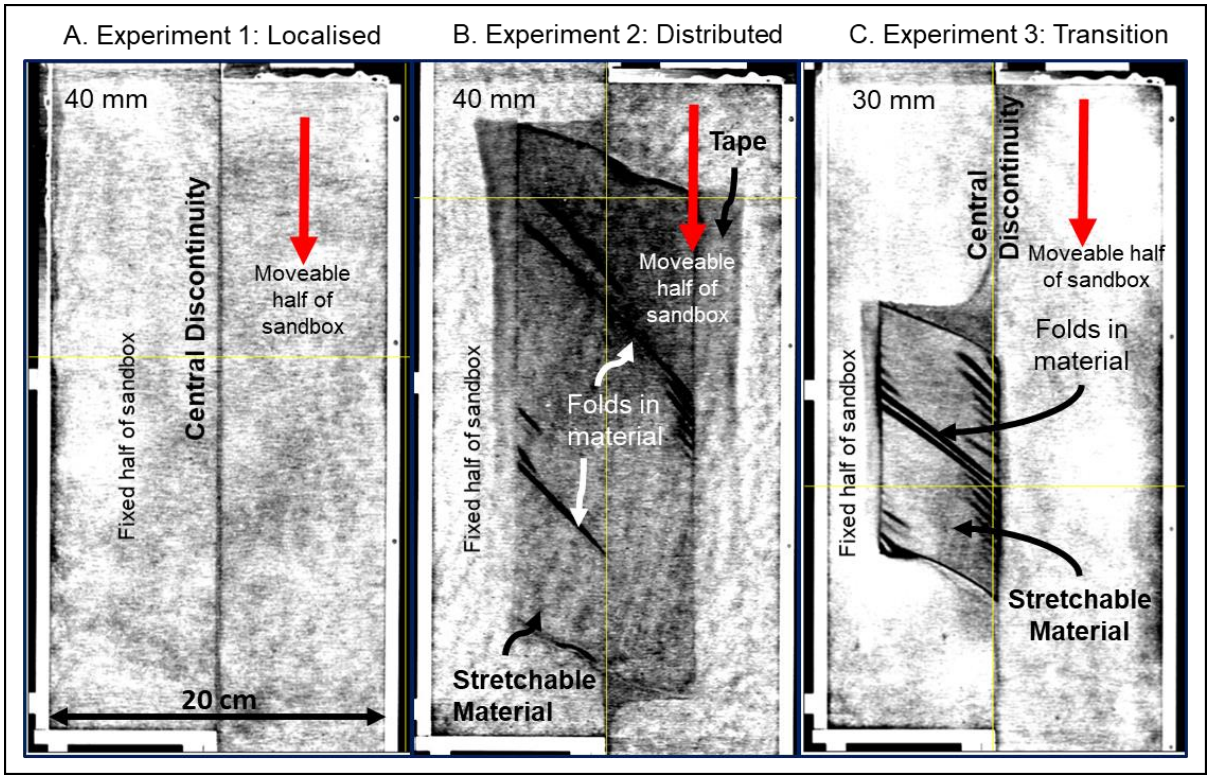

Figure 3.4. CT Scans in plan view (XZ slice) showing the basal boundary conditions of each analogue experiment at the final displacement interval shown in Figures 3.5 and 3.6. The central discontinuity and stretchable material can be clearly identified. Folds in the stretchable material which contributed to some boundary effects in the upper crustal analogue are labelled. The fixed half and moving half of the sandbox are labelled. **A.** Experiment 1: No modifications to the sandbox. **B.** Experiment 2: 14 cm x 28 c, stretchable material taped across box. **C.** Experiment 3: Smaller piece 7 cm x 14 cm stretchable fabric taped to base of box.

Colletta, 1998; Ueta et al., 2000; Dooley and Schreurs, 2012; Fedorik et al., 2019). Paler tones in the grey level XRCT scans correspond to areas of higher density while darker tones identify areas of lower density. In our experiments, the density of the granular material is an indication of relative degrees of dilation (less dense - dark tones) or compaction (more dense – paler tones). Faults, which are characterised by relative dilation, therefore appear as dark lines within the CT scan slices.

3.4. Results

Faults that developed in Experiments 1, 2 and 3 have surface patterns that are consistent with those described in Chapter 2 of this thesis. The sequence of faulting that leads to the formation of a well-established strike-slip fault over the region of localised simple shear is consistent with other classic

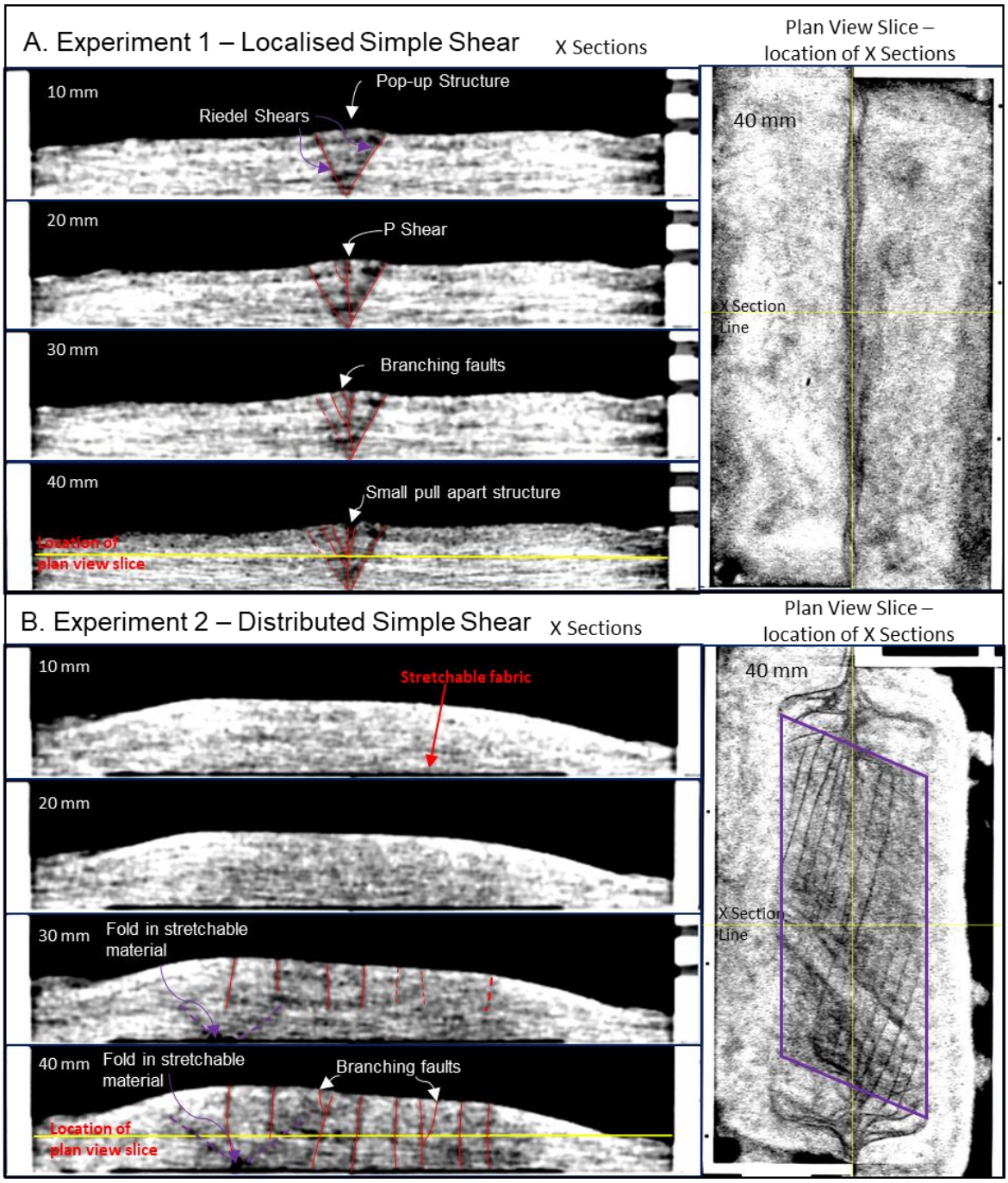

Figure 3.5. CT Scans of analogue experiments, with cross sections from 10 mm to 40 mm displacement of the sandbox, with a plan view slice at 40 mm showing the locations of the cross sections. **A**. Results from experiment 1: localised simple shear experiment with no modifications to the sandbox. Developing faults form by branching and coalesce at depth, over the central discontinuity at the base of the box. **B.** Results Experiment 2: Distributed simple shear. Stretchable material is taped to the base of the box, location shown by the purple box. The sand is subject to the effects of distributed simple shear as a basal boundary condition over the stretchable material is taped. Faults that develop in the sand propagate as individual faults to the base of the sandbox. Some of these individual faults show branching splay faults. (Original figures, without interpretations are shown in Appendix B).

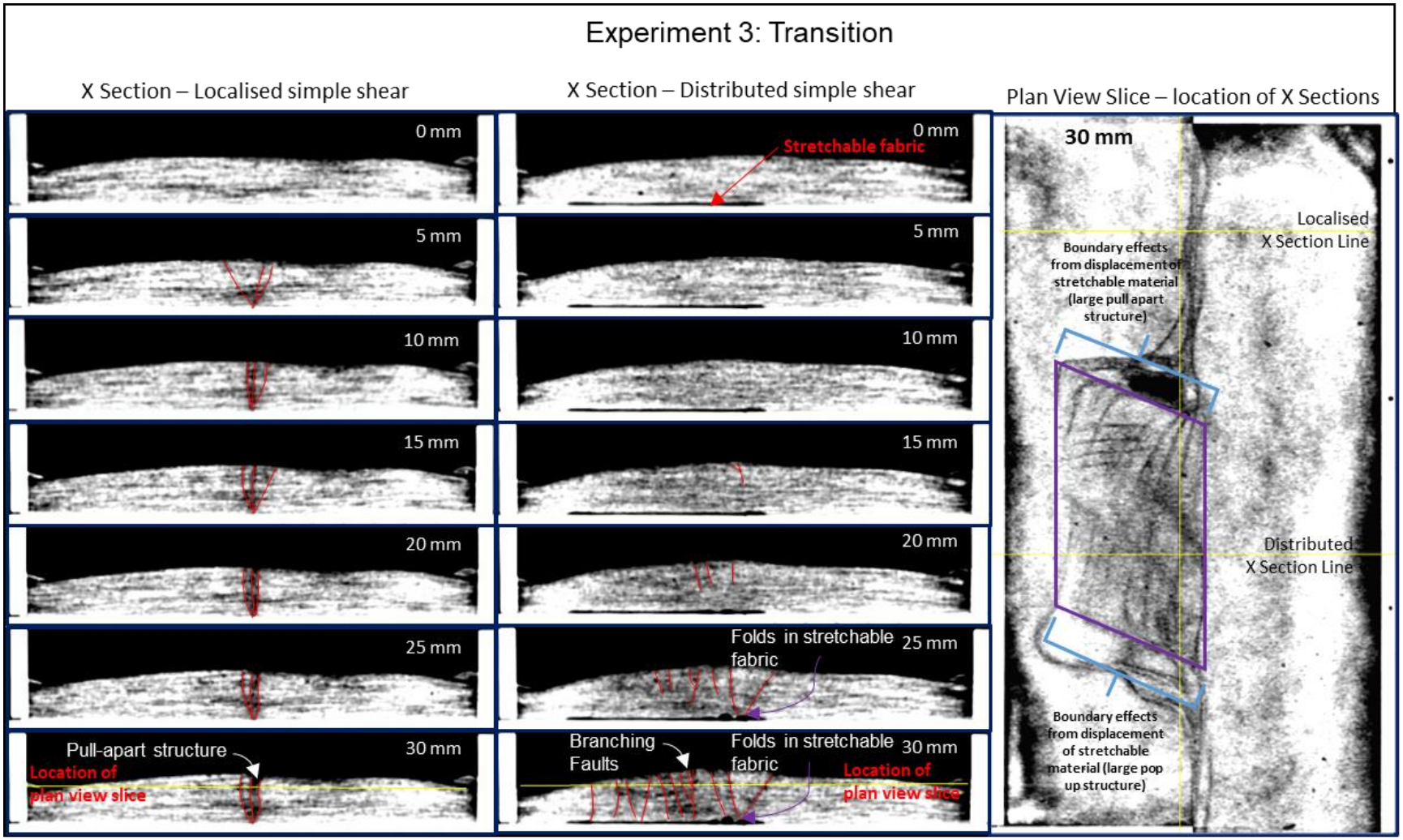

Figure 3.6. Results from Experiment 3, the transition experiment. Stretchable material is taped to the base of the box in the location of the purple box, the sand overlying this region is subject to the effects of distributed simple shear as a basal boundary condition. The rest of the box remains unmodified so deforms by localised simple shear over the central discontinuity at the base of the sandbox. Cross sections show displacement from 0 mm to 30 mm. The location of these cross sections is detailed in the plan view slice. The plan view slice shows the sandbox at 30 mm displacement. (Original figures, without interpretations are shown in Appendix B).

strike-slip analogue experiments (e.g. Riedel, 1929; Tchalenko, 1970; Wilcox et al., 1973; Naylor et al., 1986). Riedel shears that developed over the region of localised simple shear in Experiments 1 and 3 (Figs. 3.5A, 3.6) have helical geometries in 3D and they propagate from the central discontinuity at the base of the box. With increased deformation, P shears developed that are more centred over the central discontinuity and eventually link the Riedel shears to form a through-going, continuous fault. Small pop-up and pull-apart structures are present between the abandoned Riedel shears and P shears (Figs. 3.5A, 3.6). These developed from localised regions of transpression and transtension associated with the slight sinuosity of the linking faults.

Faults that developed over the region of distributed simple shear (Figs. 3.5B, 3.6) are vertical to sub-vertical and equally spaced. These faults do not connect at depth, and propagate individually from the surface to the base of the sandbox, consistent with previous analogue experiment results of Schreurs (2003). Some of these faults branch towards the surface in cross section (Figs. 3.5B, 3.6). The entire region of granular material over the stretchable material is darker grey in tone and the faults within it are lighter compared to the region of localised deformation (c.f., Figs. 3.5A and B). This reflects the degree of localisation and the amount of bulk dilation across both regions. In the region of localised simple shear, almost all of the deformation and associated dilation is concentrated on the faults so they have a very dark appearance. In the region of distributed simple shear, the granular material dilates across a much wider area that accommodates deformation, giving this region a dark grey tone. Since there is less displacement and dilation on each individual fault in the region of distributed simple shear, they have lighter tones compared to faults in the region of localised simple shear.

3.5. Discussion

3.5.1. Comparison of fault development in regions of distributed and localised simple shear

The laboratory experiments presented here show that fault development processes are different in regions undergoing distributed versus localised simple shear. In regions of distributed simple shear in the upper crust, deformation localises to form a sub-parallel array of approximately equally spaced strike-slip faults (Fig. 3.5B, 3.6). These sub-parallel arrays of independent strike-slip faults appear to nucleate in the upper crust and propagate vertically to sub-vertically downwards towards the zone of basal distributed simple shear. These faults develop sequentially across the region of distributed simple shear with a spacing that is likely controlled by the thickness of the deforming layer (e.g. Zuza et al., 2017; Yang et al., 2019). Where distributed simple shear occurs as a basal boundary condition there is no primary fault present for these secondary faults to merge with at depth, unlike faults that develop in regions of localised simple shear. Faults that develop in regions of localised simple shear appear to nucleate on the lower discontinuity and propagate upwards and outwards as helicoidal shear zones. Secondary faults appear to branch upwards and outwards from primary faults (Fig 3.5A, 3.6).

In map view strike-slip faults that form in regions of distributed simple shear propagate laterally and can eventually intersect the primary transform fault. These secondary faults therefore have an abutting relationship with the primary transform fault and create a map pattern which is self-similar to a branching fault pattern that can develop in regions of localised simple shear, despite having a different process of development (Peacock et al., 2017).

The branching fault networks which develop where localised simple shear is the basal boundary condition have a width that is approximately equal to or less than the depth to the branching point of the primary fault (3.2B,C, 3.5A, 3.6). The fault networks which develop where distributed simple shear is the basal boundary condition, develop across regions where the width of the basal distributed simple shear is much wider than the thickness of the brittle upper crust (3.2A, 3.5B, 3.6). These results highlight the importance of consideration of scale when interpreting the development of faults that appear to have a branching fault pattern.

3.5.2. Comparison to case studies

Results of the analogue experiments indicate the process of development of strike-slip fault systems like the southern SAFS and MFS is different to that of the Sciacca and Vienna Basin faults. Experimental faults formed over regions of distributed simple shear (Figs. 3.5B, 3.6) are consistent with interpreted cross sections of geophysical data across the MFS (Fig. 2A) (Wannamaker et al., 2009; Eberhart-Phillips and Bannister, 2010). Therefore, both the MFS and similar scale southern SAFS are inferred to have developed within large-scale regions of distributed upper-crustal deformation. Faults that develop within regions of localised upper crustal simple shear (Figs. 3.5A, 3.6) are consistent with cross sections of the Sciacca and Vienna Basin faults (Figs. 3.2B, C) (Beidinger and Decker, 2011; Fedorik et al., 2018, 2019). The Sciacca Fault and the Vienna Basin Fault are smaller scale positive and negative flower structures in the zones of localised deformation.

The results of the analogue experiments suggest the major faults of the MFS and southern SAFS develop sequentially over the region of distributed simple shear and propagate laterally towards the primary transform fault, consistent with previous interpretations (Scholz et al., 2010; Vermeer et al., 2021). The relationship between these secondary faults and the primary transform fault is therefore abutting, which does not conform to the definition of the word ‘splay’. Whereas our results indicate that the branching fault networks of the Sciacca Fault and the Vienna Basin Fault form by branching from the primary fault and therefore conform to the definition of ‘splay’. The true relationship of the major faults within the MFS, as determined by our analogue modelling results, are shown in Table 3.1.

Some of the faults that form within regions of distributed simple shear develop ‘tertiary’ branching (Figs. 3.5B, 3.6). These coalesce with secondary faults at depth in a similar manner to faults that develop over the region of localised simple shear. These smaller scale branching faults are consistent with true

splay faults and are similar to branching faults in nature, such as the Elliott Fault, which appears to splay from the Clarence Fault in the MFS (Figs. 3.1B, 3.7; Table 3.1).

3.5.3. To splay or not to splay?

Splay faults are inferred to form by branching from a primary fault. Faults that develop within regions of distributed simple shear in the upper crust do not fit this formation mechanism. We propose that only faults that branch from a primary fault should be classified as splay faults, in agreement with the most widely accepted mode of development of a splay fault and the definition of the word 'splay'. Therefore, faults formed in regions of localised simple shear, such as fault networks associated with the termination of the Sciacca Fault, and the Lasse Fault segment of the Vienna Basin Fault, are true splay faults. Whereas faults that develop within regions of distributed upper crustal simple shear, such as the MFS and southern SAFS should not be deemed to be splay faults. As an example, the true relationship and intersection of the Marlborough Fault System faults are listed in Table 3.1.

Fault	Relationship	Intersection	Branch at depth?
Alpine/Wairau	Primary	Primary	N/A
Awatere	Secondary	Abutting	No
Clarence	Secondary	Abutting	No
Elliott	Tertiary	Splay	Yes
Hope	Secondary	Abutting	No

Table 3.1. The true relationship and intersection of the faults of the Marlborough Fault System based on their inferred method of development from analogue model results.

3.5.4. Application to a 3D interpretation of the MFS

Geological reasoning refers to the process and techniques applied to make interpretations of geological objects (Frodeman, 1995; Bond et al., 2015). Geological interpretations are made by combining knowledge, experience and observations, including 3D geometries, map patterns and geological histories (Bond et al., 2007a, 2011). The knowledge of the expected process of development of fault networks with branching fault surface geometries has implications for building geological interpretations (Bond et al., 2007b; Grose et al., 2020, 2021). Figure 3.7 shows a 3D geological model of the fault surfaces in the MFS built using LoopStructural (Grose et al., 2020, 2021). (Rotatable 3D versions are available in Appendix A). Using LoopStructural, fault relationships can be specified to be either 1) overprinting, 2) abutting or 3) splaying. Therefore an understanding of the process of the development is critical for creating an accurate 3D model of the MFS, highlighting the importance of a consistent definition of the term 'splay fault'.

The fault surfaces in Figure 3.7 were interpolated using an implicit modelling approach starting with the surface fault geometries and existing structural data available from GNS (© GNS Science 2016).

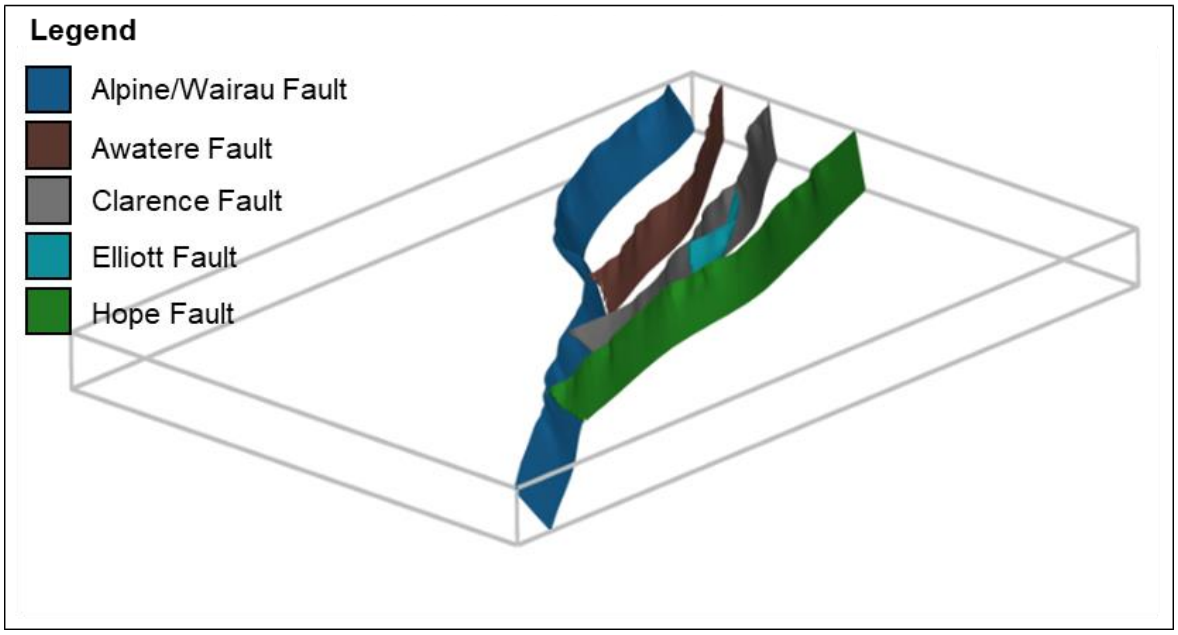

Figure 3.7. 3D model of the Marlborough Fault System (MFS) developed using LoopStructural (see Appendix A for online interactive version). The 3D model used fault surface geological and structural data from GNS (© GNS Science 2016) and then applies geological reasoning based on an inferred process of development determined from Experiments 1 and 2. Fault intersections and relationship following those outlined in Table 1. The inferred process of development is basal distributed simple shear and so the secondary MFS faults have an abutting relationship with the primary Alpine/Wairau Fault.

The faults were given the intersection relationship shown in Table 3.1, based on the expected intersection relationship determined from the analogue modelling results. Therefore, the major MFS faults have an abutting relationship with the primary Alpine/Wairau Fault and do not coalesce at depth. These faults have not been interpreted to have propagated away from the primary Alpine Fault. Rather they are assumed to have form some distance away from the Alpine Fault to subsequently approach and intersect it, in a similar manner to the distributed simple shear experiments presented here. The smaller Elliott faults is interpreted as a 'tertiary' fault which splays from the Clarence Fault and therefore is shown to branch from the Clarence Fault at depth.

3.6. Conclusion

Laboratory experiments indicate that fault networks that develop in the upper crust within regions of distributed simple shear, such as the ~ 100 km scale MFS and the southern SAFS, form as secondary, non-interacting, sub-parallel, vertical fault arrays, which propagate downward from the surface. Where these faults propagate laterally to approach and intersect a primary transform fault, the surface fault geometry appears similar to smaller scale splay faults, which from by branching upward from a primary

fault in experiments with localised upper crustal simple shear. We therefore propose that use of the term splay fault be restricted to describe synthetic faults that form by branching from a primary fault at an acute angle. This study highlights the importance of consideration of scale when interpreting fault networks. Namely, that splay faults tend to occur in strike-slip systems where the width of the (localised) deformation zone is approximately equal to its thickness (cf., Figs. 3.2B,C and 3.5A). When upper-crustal strike-slip deformation is distributed across a region that is much wider than the thickness of the brittle crust, equally-spaced, vertical, non-interacting faults propagate from the surface downwards (Figs. 3.5B, 3.6). These secondary faults propagate laterally and can eventually intersect a primary transform fault, with which they have an abutting, rather than splaying, relationship (Figs. 3.1A,B).

Chapter 4

Sandbox experiments explain migration of the Marlborough Fault System, New Zealand

Abstract

Hundreds of kilometres of strike-slip displacement are accommodated at the intersections of continental transform faults and convergent plate boundaries, within broad intervening 'transition zones' (Wilson, 1965; Legg et al., 2004). Such transition zones are at risk of cascading and / or multi-fault earthquakes with moment magnitudes (Mw) greater than earthquakes that remain confined on their associated transform faults, yet how deformation localises and migrates across transition zones remains poorly understood (Bilich et al., 2004; Wilson et al., 2004). The unusually complex 2016 Mw 7.8 Kaikoura earthquake is associated with the ongoing development of the Marlborough Fault System (MFS), a 200 km wide transition zone in South Island, New Zealand between the continental transform Alpine Fault and the Hikurangi subduction zone (Hamling et al., 2017). Here we show that the development of the MFS and the migration of localised high strain zones across this transition zone can be explained by simulating the tectonic boundary conditions of South Island in scaled laboratory sandbox experiments. We demonstrate that the MFS developed sequentially southward as four equally spaced crustal scale shear bands, each localising from zones of diffuse shear strain that migrate southward over time. We attribute the initiation and complex rupture pattern of the Kaikoura earthquake to a region of diffuse faulting in the southernmost part of the transition zone where localisation is still ongoing to form the next major fault in the system.

4.1. Introduction

The NE-trending dextral transpressive Alpine Fault accommodates most of the ~ 40 mm/yr oblique convergence between the Australian and Pacific Plate across central South Island, New Zealand (Altamimi et al., 2012; Beavan et al., 2016). In North Island, the bulk of this plate motion is accommodated by oblique subduction of the Pacific Plate under the Australian Plate along the Hikurangi margin (Nicol and Beavan, 2003). The Hikurangi margin extends offshore of northeast South Island and terminates against the continental Chatham Rise (Fig. 4.1), where subduction rates are negligible (Wallace et al., 2012). Quaternary slip rates show that the Marlborough Fault System (MFS)

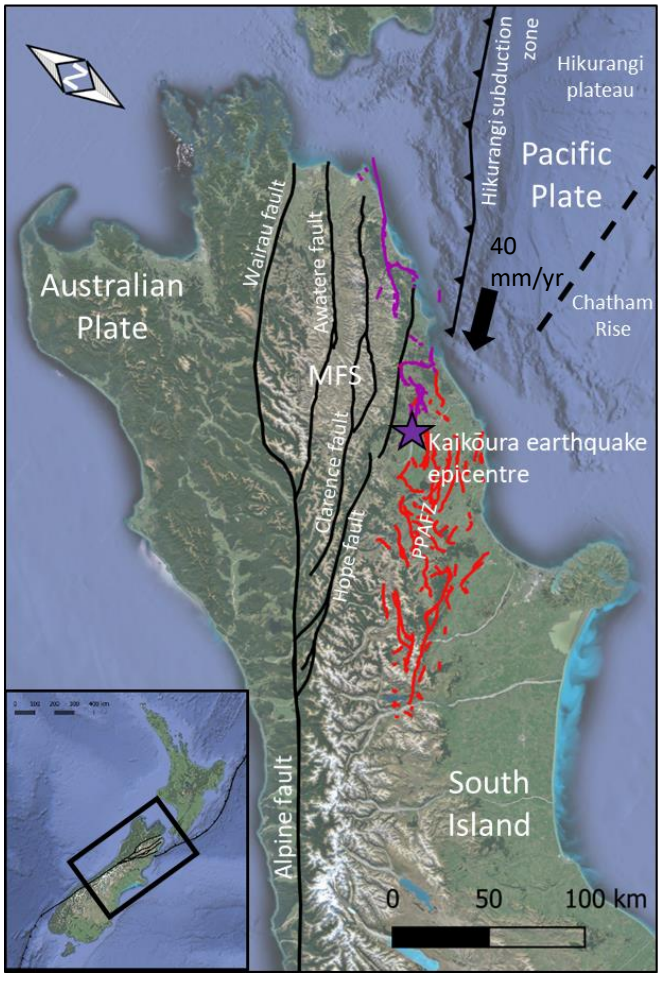

Figure 4.1. Tectonic setting of northeast South Island. Major, crustal scale faults are shown in black (MFS=Marlborough Fault System). The Kaikoura earthquake ruptures are shown in purple. The PPAFZ (Porters Pass to Amberley Fault System), a zone of smaller scale diffuse faulting is shown in red. Fault data © GNS Science 2016

(Fig. 4.1) comprises a series of four equally spaced, dextral strike-slip faults, that accommodate the bulk of the plate motion in northeast South Island (Wallace et al., 2007). The MFS developed sequentially southward across the transition zone between the Alpine Fault and Hikurangi margin (Browne, 1992; Little and Jones, 1998; Langridge and Berryman, 2005) and strikes sub-parallel to the oblique convergent plate motion vector. The MFS is inferred to split from the Alpine Fault, which offsets basement terranes dextrally by 480 km but is hypothesised to have accommodated at least 700

km of dextral strike-slip deformation (Little and Jones, 1998; Lamb et al., 2016). Estimates of the collective dextral displacement in the MFS are ~ 200 km, with ~ 140 km accounted for by the Wairau Fault, a continuation of the Alpine Fault plus 55 – 65 km of cumulative displacement recorded by the other major faults (Little and Jones, 1998). The northernmost faults (the Wairau, Awatere and Clarence faults) have a slip rate of 4 – 8 mm/yr, while the Alpine and Hope faults record Quaternary slip rates of 18 – 30 mm/yr (Van Dissen and Yeats, 1991; Litchfield et al., 2014). Seismic and resistivity profiles indicate that the lower crust of the MFS deforms by distributed strain and that the surface faults extend to a depth of no more than 15 km (Wilson et al., 2004; Wannamaker et al., 2009; Eberhart-Phillips and Bannister, 2010).

Palaeomagnetic data from the sedimentary bedrock within the transition zone record between 100° and 140° clockwise rotation since ca. 20 Ma. The bulk of this rotation occurred between 20 Ma and 10 Ma and is ascribed to the rotation of the Hikurangi subduction zone about its termination point with the Chatham Rise. At ca. 10 Ma the Hikurangi subduction zone and Alpine Fault had attained their present day orientation and there has been minimal rotation recorded in northeast South Island since this time (up to 20 ° is constrained to have occurred at the very northeast edge of the MFS) (Little and Roberts, 1997; Hall et al., 2004; Lamb, 2011; Randall et al., 2011).

Subvertical bedding in the Cretaceous subduction-accretion complex basement rocks of the MFS strikes consistently NNE, suggesting that deformation in the MFS must be accommodated entirely along the faults (Wallace et al., 2012). Consequently, it is generally accepted that the MFS consists of numerous crustal scale fault blocks that are bounded by relict accretionary complex thrusts. It is hypothesised that these blocks underwent vertical axis rotation during the rotation of the Hikurangi margin, until 10 Ma when the pre-existing faults attained orientations favourable for reactivation. These faults are thought to have reactivated sequentially southward from ca. 6 Ma to form the present-day MFS (Little and Roberts, 1997; Hall et al., 2004; Lamb, 2011; Randall et al., 2011).

The MFS is undergoing active deformation and is considered to be one of the highest earthquake hazard zones in New Zealand (Berryman et al., 2018). However, the epicentre of the Mw 7.8 Kaikoura earthquake, which shook New Zealand on 14th November 2016, occurred 20 km south of the MFS in the relatively low strain rate Porters Pass to Amberley Fault Zone (PPAFZ). The PPAFZ (Fig. 4.1) is a zone of diffuse faulting and the hypothesised location of an incipient fifth MFS fault (Cowan et al., 1996). The 2016 Kaikoura earthquake is recognised to have the most complex rupture pattern observed in modern history, comprising 21 different fault segments with a wide array of orientations and displacement kinematics (Hamling et al., 2017; Berryman et al., 2018). Gaps of up to 15 km occurred between some ruptures, including ruptures on faults that had not been previously identified. Surface ruptures associated with the 2016 Kaikoura earthquake subsequently propagated northeast into the high strain rate MFS, bypassing the Hope Fault, concentrating on NNW-trending thrust faults between the

major MFS faults. The influence of the subducted slab on the initiation of the earthquake rupture propagation is highly debated (Hamling et al., 2017; Lamb et al., 2018; Ulrich et al., 2019).

4.2 Significance

Considering the PPAFZ as an incipient fifth fault in the MFS contradicts the proposed tectonic development model for the MFS because the wide, diffuse nature of faulting in the PPAFZ negates the presence of rigid crustal blocks and the reactivation of intra-block pre-existing crustal scale weaknesses. The PPAFZ also does not split from or connect to the Alpine Fault. The complexity of the 2016 Kaikoura earthquake, and the occurrence of its epicentre within the low strain rate PPAFZ highlights the need for a better understanding of how deformation migrates and localises across the transition zone in South Island, New Zealand, and how, where, and why each major fault in the MFS developed.

The development of the MFS has yet to be investigated using numerical or laboratory analogue experiments. Here, we use a three-dimensional laboratory analogue modelling approach to simulate the present-day simple shear conditions of the transition zone between the Alpine Fault and the Hikurangi subduction zone. Analogue modelling is an excellent tool for this type of investigation because we can monitor the evolution and development of structures, and quantify changes in surface strain through time using Digital Image Correlation (DIC) (Adam et al., 2005).

4.3 Methods

Our analogue 'sandbox' apparatus comprises a 20 cm x 40 cm x 4 cm box with a central discontinuity, which allows one side of the box to move horizontally relative to the other side (Schrank et al., 2008) (Fig. 4.2). A linear actuator pushes one half of the box at a constant velocity to create dextral strike-slip motion. Figure 4.2A shows the analogue sandbox without any modification and 4.2B shows a photograph of the sandbox while an experiment is being conducted, where the linear actuator has pushed one half of the sandbox, causing displacement of the sand. Without modification, deformation of an upper crustal analogue becomes localised over the central discontinuity at the base of the box.

The basal boundary conditions of the MFS are outlined in Figure 4.3A, B and C. The Alpine Fault is shown to deform by localised deformation (when considering as a transform fault on a tectonic scale), while the MFS is shown to be subject to distributed simple shear. To create a region of distributed simple shear in the analogue model, we modified the base of the box by taping a 7 cm x 14 cm piece of four-way stretchable elastic material to the base in a position analogous to the 100 x 200 km transition zone in northeast South Island (Fig. 4.3A, D). During shear displacement of the box, this elastic material deforms by distributed simple shear (Fig. 4.3E, F), analogous to the deformation of the lower

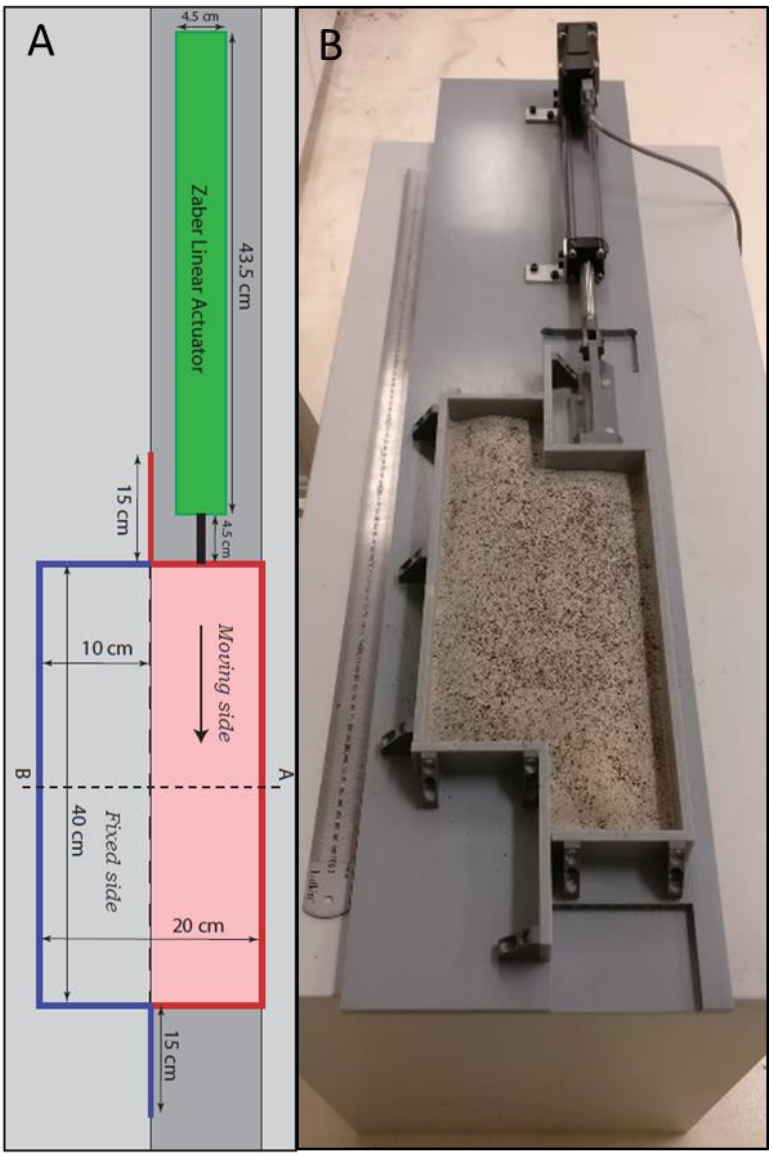

Figure 4.2. Analogue modelling apparatus aka 'the sandbox' used to conduct experiments for this investigation. **A.** Schematic diagram of the Sandbox. **B.** Photograph of the sandbox after the moving side has pushed 6 cm by the linear actuator (From Chapter 1 in this thesis).

crust beneath the MFS. The granular material above this stretchable material is therefore subjected to the effects of distributed simple shear as an underlying boundary condition. The remainder of the granular material is above the unmodified shear box, and so deforms by localised deformation over the central discontinuity, analogous to current deformation along the Alpine Fault. In our experiment we do not use a ductile lower crustal analogue because the stretchable material deforms by distributed simple shear and is sufficient to provide a boundary condition that simulates distributed simple shear in the lower crust.

The sandbox is filled with 2.5 cm of a sand and ceramic Envirospheres® mix (ratio 60:40), which have homogeneous grain size distributions and a density of 960 kg/m^3. As explained in detail in Chapter 1, Molnar et al., (2017) used a Hubbert-type shear box to determine an internal friction angle of angle < 38° and a cohesion value of ~9 Pa for this material. This granular material is therefore an appropriate analogue for the brittle, Mohr Coulomb behaviour the upper crust (Byerlee, 1978; Davy and Cobbold,

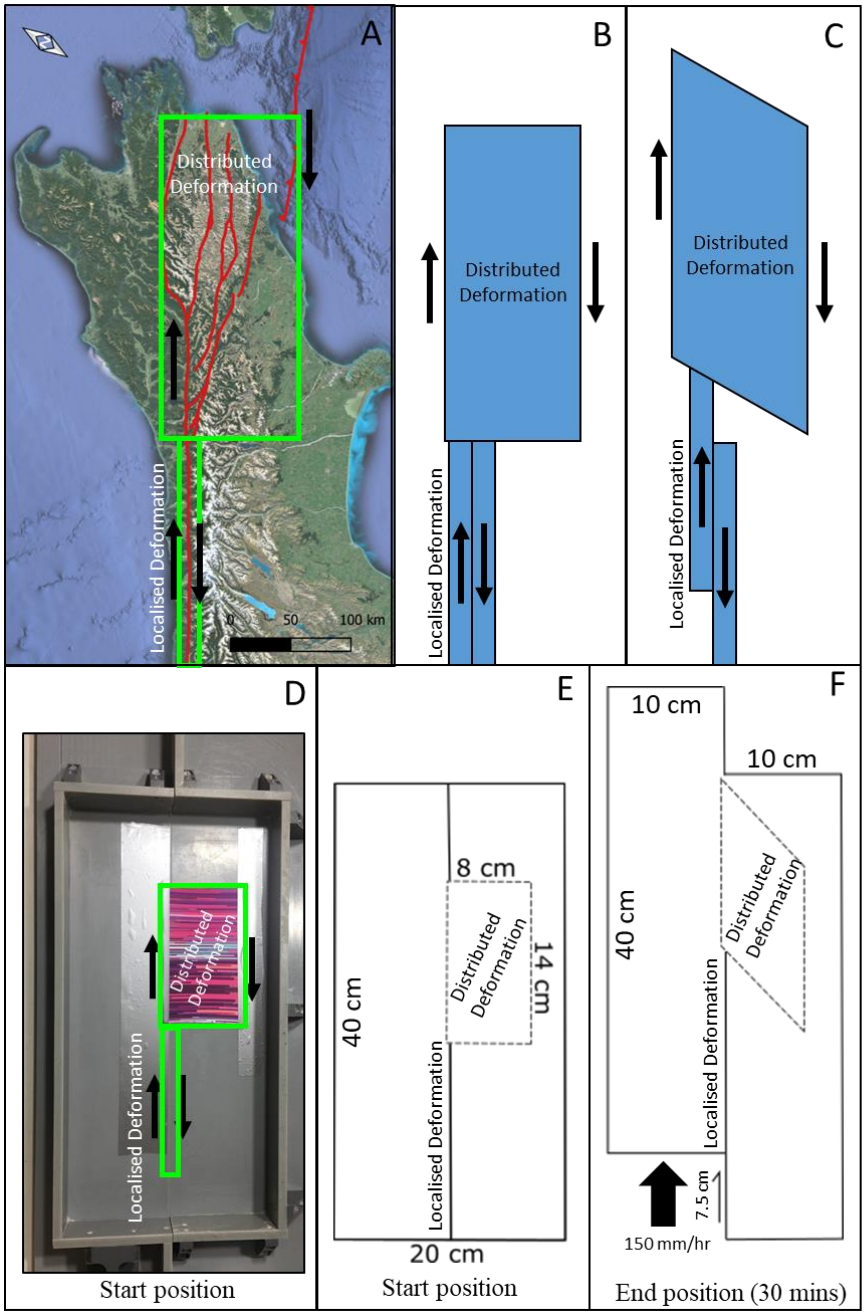

Figure 4.3. The strike-slip boundary condition of the South Island, New Zealand and the analogue model experiment. **A**, **B** and **C** outline the ongoing strike-slip deformation in South Island. The Alpine Fault is subject to localised simple shear while the transition zone, where the Marlborough Fault System has developed, is subject to distributed simple shear as a basal boundary condition. This is simulated in our analogue model, as shown in **D**, **E** and **F**.

1991; Schellart, 2000). Consistent with the experiments in Chapter 1, the granular material was sieved into the sandbox from a height of 10 cm and once in the sandbox was not manipulated in any way to avoid localised compaction of grains.

The sandbox was deformed at a constant velocity of 150 mm/hr and was displacement 75 mm over 30 minutes. The amount of displacement reflects the limit of stretch of the stretchable material. The limit of stretch did not affect the experiment outcome as a mature fault system had developed over the region

where the stretchable material was taped after 30 mm displacement of the sandbox. The results presented in this investigation are shown up to 30 mm of displacement, as no more faults developed after this time (See Appendix A for a full set of images from this experiment). Scaling for the experiment follows Chapter 1 of this thesis.

A Nikon D7500 digital camera captured top view images of the experiment surface at fixed 30 second intervals during deformation of the sandbox. We use Digital Image Correlation (DIC) analyse the 2D surface deformation in the experiments (Adam et al., 2005), which is explained in detail in Chapter 1. Results are presented as incremental shear strain maps of the surface of the analogue models, which are determined from DIC analysis. Incremental shear strain is the calculated 'instantaneous' strain from the tracked changes in particle locations between two images along an XY axis where X is parallel to the direction of shear strain (Ramsay and Graham, 1970; Ramsay, 1980; Schrank et al., 2008).

4.4. Results

Figure 4.4 shows the incremental shear strain across the surface of the model at 5 mm displacement intervals. The development of structures in the region of localised simple shear follows that documented by many studies (Dooley and Schreurs, 2012). The first structures to develop after 3.75 mm of displacement in the experiment are Riedel shears in the area of localised simple shear of the shear box (Fig. 4.4B, 5 mm displacement). These Riedel shears have a maximum orientation of 18 °

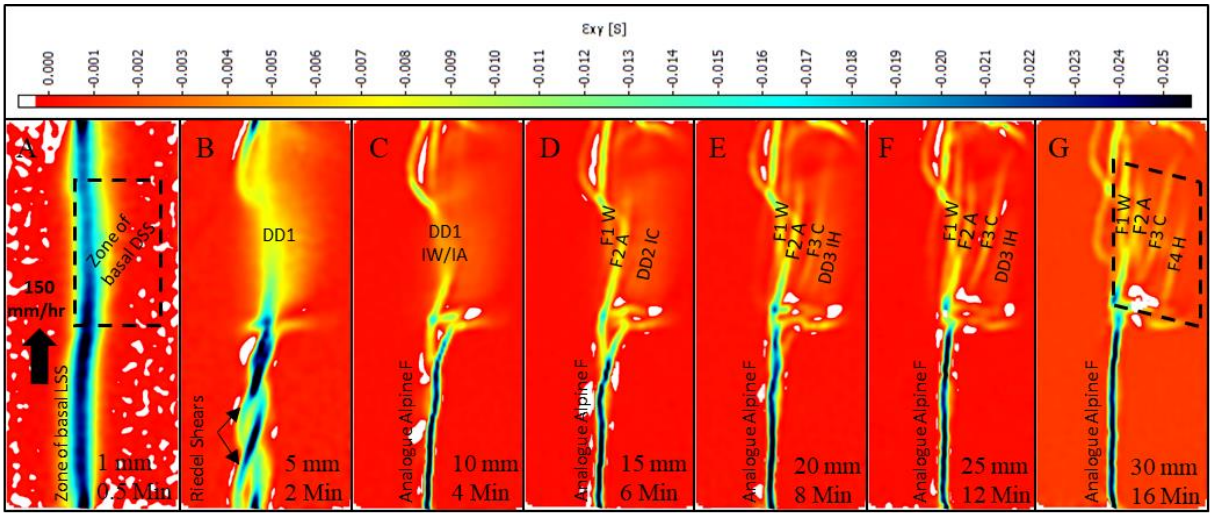

Figure 4.4. The shear strain across the surface of the analogue experiment at 5 mm displacement intervals, determined from Digital Image Correlation (DIC). A – G show incremental shear strain maps of the surface of the analogue experiment, with blue indicating high shear strain and red low shear strain. The dashed box in A and G indicates the position of the stretchable fabric at the base creating a basal boundary condition of distributed simple shear (DSS) in that region. The rest of the sandbox is subject to localised simple shear (LSS) as the basal boundary condition from the central discontinuity at the base of the sandbox. The region of distributed simple shear (DSS) is labelled as follows: DD = Diffuse deformation. F = Fault. I = Incipient, followed by a number which reflects the order of formation and the MFS analogue: W = Wairau Fault, A = Awatere Fault, C = Clarence Fault, H = Hope Fault

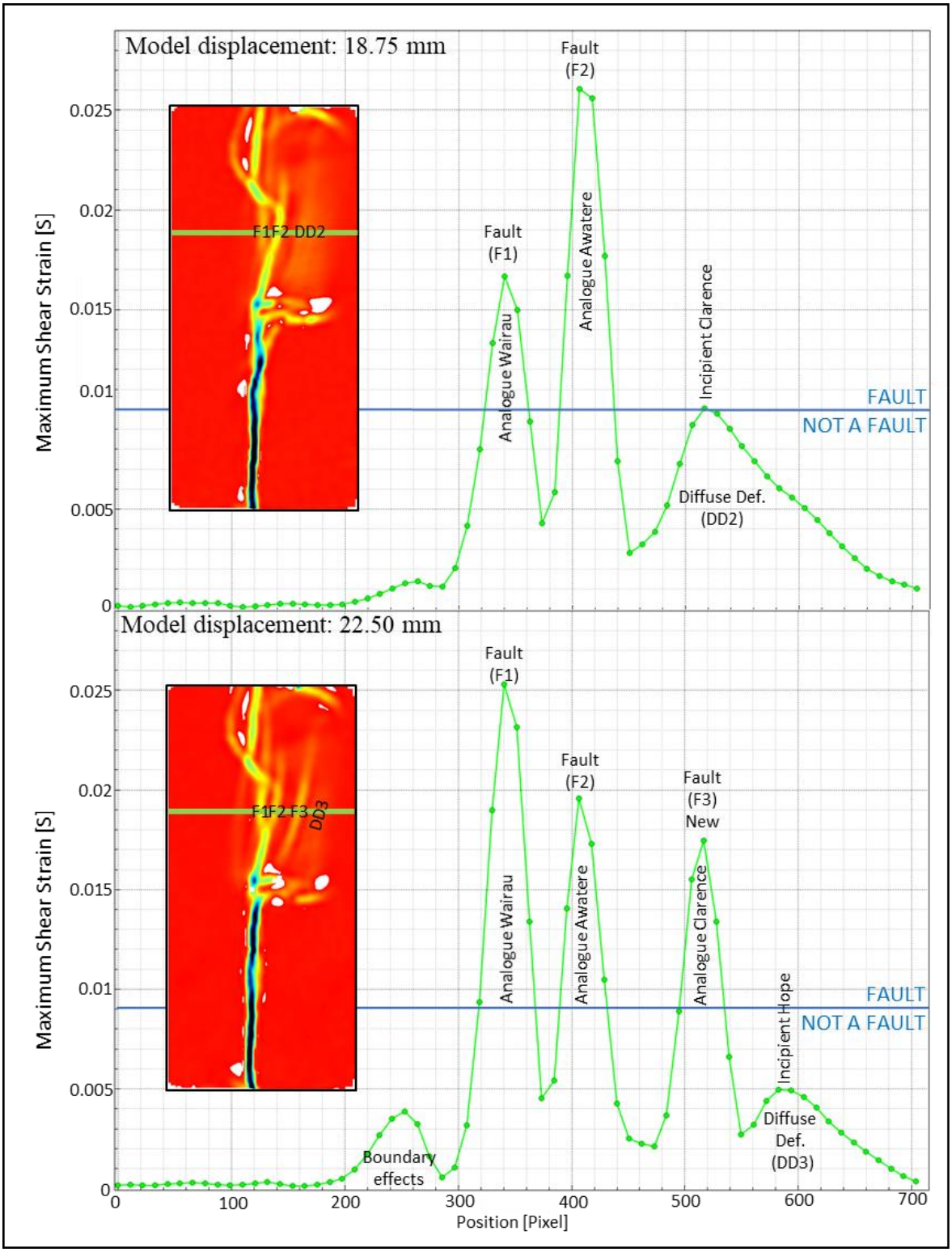

Figure 4.5. The maximum shear strain across the green line within the DIC map at 18.75 mm and 22.5 mm displacement of the sandbox. This shows the maximum shear strain across the region of sand which is subject to distributed simple shear as the basal boundary condition. F = Fault, DD = Diffuse Deformation. The MFS analogue is labelled on the graph. Boundary effects are explained in section 4.9. The graphs show a region of diffuse deformation (DD2) at 18.75 mm sandbox displacement, which localises to form a fault by 22.5 mm sandbox displacement, and a region of diffuse deformation shifts away from the centre of the box. The blue line dictates the maximum shear strain at which we consider a fault to have formed.

clockwise relative to the central discontinuity, with a horizontal spacing of ~ 20 mm between them. After 8.5 mm of displacement, deformation in the region of localised simple shear is entirely centred on a single fault located over the central discontinuity (Fig. 4.4C, 10 mm displacement), and it remains this way for the remainder of the experiment.

Faults require greater displacement of the sandbox to develop in the region of distributed simple shear compared to the region of localised simple shear. Initially the sand in the region of distributed simple shear deforms by diffuse deformation (Fig. 4.4B), which becomes increasingly localised towards the centre of the box (Fig. 4.4C) leading to the development of the first faults at 12.5 mm displacement (Fig. 4.4D, 15 mm displacement). Two further faults form progressively across the region of distributed simple shear towards the edge of the sandbox, at 20 mm displacement and 27 mm displacement, respectively (Fig. 4.4E, Fig. 4.4G). These faults do not splay from or connect with the older faults that formed closer to the centre of the sandbox. Both emerge from a region of diffuse deformation that localises to form a fault. Figure 4.5 shows the maximum shear strain across the region of distributed deformation for chosen DIC maps at 18.75 mm and 22.5 mm displacement of the sandbox. These graphs show the formation of the third major fault (F3), from the region of diffuse deformation (DD2), and the subsequent region of deformation developing (DD3), which forms the fourth major fault. The faults that develop over the region of distributed deformation are equally spaced, with a fault perpendicular, horizontal spacing of ~ 20 mm and they are oriented 18° clockwise relative to the central discontinuity, consistent with previous analogue experiments that investigate distributed progressive simple shear (Schreurs, 2003).

4.5. Experimental artefacts and limitations

As explained in Section 4.8, the experiment is limited by the elasticity of the stretchable material, which cannot deform infinitely. This effect is avoided in the experiment by limiting the displacement of the sandbox so that the stretch limit of the material is not reached.

Artefacts develop at the ends of each experiment, which are associated with the vertical side boundaries and corners of the sandbox. The boundary effects are outside the region of interest in the analogue model and do not influence the experiment results.

There are a number of structural artefacts that develop during the experiment, which are associated with the transition of the basal boundary conditions from localised simple shear with no sandbox modification, to distributed simple shear above the stretchable material. These artefacts include large pull apart and pop up structures, corresponding to releasing and restraining bends at either end of the stretchable fabric where the transition from localised to distributed deformation occurs. These features increase in size with increasing displacement of the sandbox. In nature, the basal boundary condition is ductile and has a contributing factor to the size of structures that develop because the lower crust can

flow and respond isostatically to crustal thickening and thinning. However, in our analogue experiment, the basal boundary condition is rigid so the scale of the edge effects of the transition zone are significantly enhanced and grow to a size that has no equivalent in nature. We therefore consider these features as artefacts and restrict our analyses to the central part of the stretchable over the region, which is not influence by edge effects.

Our analogue model experiment is limited to strike-slip deformation only. While the dominant mode of deformation in South Island is strike-slip deformation, there is also a component of transpression. This includes the uplift of the Southern Alps along the Alpine Fault, where the Pacific Plate is being thrust over the Australian Plate (Norris and Cooper, 1995), and the uplift of the Seaward and Inland Kaikoura ranges in the MFS (Van Dissen and Yeats, 1991; Little and Jones, 1998; Nicol and Van Dissen, 2002; Collett et al., 2019). Uplift over the Alpine Fault is partitioned onto small thrust segments and the strike slip to uplift ratio is 10:1 (Norris and Cooper, 1995). Uplift in the MFS is limited to the Seaward and Inland Kaikoura ranges in the eastern part of the transition zone and is hypothesised to be the result of compression in the overriding plate caused by congestion of the Hikurangi Plateau in the Hikurangi subduction zone at its termination point (Willis, 2017). The Hope and Clarence faults are proposed to accommodate some of the uplift due to a 15° change in strike of the faults in this region, which makes accommodation by uplift favourable (Lamb, 1988; Collett et al., 2019). The rest of the uplift is accommodated on NNE-SSW trending thrust faults. Despite this region of uplift in the MFS, the bulk of the MFS deforms by strike-slip deformation. The Hope Faults has a horizontal:vertical slip ratio of 33:1 (Khajavi et al., 2018), and the MFS faults are proposed to have developed as dextral strike-slip faults in their present day regime (Collett et al., 2019). Therefore, although there are some transpression elements in nature, the strike-slip component is dominant, and we consider the strike-slip analogue experiment models a representative simulation for this dominant component of deformation in northeast South Island, New Zealand.

Our analogue model does show some topographic variation through the development of strike-slip faults, as seen in nature. For example, there is also some uplift associated with the restraining bend of the Wairau Fault, a feature that our analogue model also simulates.

4.6. Discussion

Between 25 mm and 30 mm displacement in the experiment (Fig 4.4F and 4.4G), the fault pattern is strikingly similar to northeast South Island (Fig. 4.1). The single fault that developed over the central discontinuity at the base of the sandbox, in the region of localised simple shear, is analogous to the Alpine Fault, being oriented parallel to the main direction of strike-slip motion, and accommodating the bulk of the deformation in that region. The faults that developed over the region of distributed simple shear are analogous to the major faults of the MFS, being equally spaced and oriented ~18°

clockwise relative to the principle direction of strike-slip motion. We consider the formation of the faults in the experiment up to this stage of finite displacement to be a reasonable analogue for the development of the MFS. The experiment also shows sequential development of faults over time, consistent with the proposed southward development of the MFS.

Our experiment suggests that the development of the MFS may be a consequence of increasing simple shear that was distributed within a ~ 100 x 200 km wide transition zone between the northeast propagating Alpine Fault and the southwest migrating Hikurangi subduction zone. Distributed deformation between the two plate boundaries likely initiated around 10 Ma, once the Hikurangi subduction zone had rotated sufficiently to align with the Alpine Fault (Little and Roberts, 1997; Hall et al., 2004; Lamb, 2011; Randall et al., 2011). As summarised in Table 4.1, if we scale our experiment to consider that distributed deformation initiated at 10 Ma, then our experiment suggests that the first faults would have initiated at ca. 5.84 Ma, consistent with the proposed initiation of the Wairau and Awatere faults (Little and Jones, 1998; Ghisetti, 2021). The next fault would have initiated at ca. 3.4 Ma, consistent with the Clarence Fault (Browne, 1992), and the next at ca. 0.91 Ma, close to the proposed age of the Hope Fault (Langridge and Berryman, 2005).

Fault:	**Development in model (mm)**	**Scaled age development (Ma)**	**Analogous to:**	**Proposed age of development (Ma)**
F1	12.5 mm	5.84 Ma	Wairau Fault	~ post 10 Ma
F2	12.5 mm	5.84 Ma	Awatere Fault	~ 6.2 – 5.5 Ma
F3	20 mm	3.4 Ma	Clarence Fault	~ 3 Ma
F4	27 mm	0.91 Ma	Hope Fault	~ 2 – 1 Ma

Table 4.1 Summary of the development of each fault in the region of distributed simple shear in the analogue model experiment, its subsequent scaled age within Marlborough Fault System when considering distributed simple shear to have initiated at 10 Ma, and comparison to proposed ages of fault development from literature. Sources of fault ages (in the order they appear in literature are: Ghisetti (2021); Little and Jones (1998); Browne (1992); Langridge and Berryman (2005).

After the initiation of distributed deformation at ca. 10 Ma, and prior to the development of the Wairau and Awatere faults, our experiment indicates that deformation was accommodated by diffuse shear across the transition zone (Fig. 4.4B-C), which became increasingly localised to form the Wairau and Awatere faults (Fig. 4.4C-D). As these faults developed, the region of diffuse deformation shifted southward (Fig. 4.4D-E), and eventually localised to form the Clarence Fault (Fig. 4.4E), and then the Hope Fault (Fig. 4.4G). The discrepancy between the displacement on the Alpine Fault and the MFS

(Little and Jones, 1998; Lamb et al., 2016) in the last 10 Myrs can therefore be attributed to accumulation of diffuse regional deformation prior to the development of each fault in the MFS. The formation of faults in this manner highlights the slip rate variability of the faults through time (Fig 4.4, 4.5), consistent with interpretation of slip rates through time in the MFS (Khajavi et al., 2018).

The presence of the PPAFZ south of the Hope Fault is consistent with development of each fault from a zone of diffuse deformation that then localises to form a major fault, consistent with the fault pattern evolution in the transition zone of our experiment. We therefore suggest that, with continued distributed deformation, the PPAFZ will form the next major fault in the MFS (Cowan et al., 1996). Once each fault develops in the region of distributed simple shear in the experiment, it remains active for the remainder of the experiment and deformation becomes concentrated on these faults, with minimal deformation occurring between them, which is again consistent with the observed mode of deformation in the present day MFS (Randall et al., 2011; Wallace et al., 2012).

The consistency of the experimental results with present day northeast South Island suggests that the MFS need not have developed by the reactivation of pre-existing faults in the upper crust as previously hypothesised (Little and Roberts, 1997; Hall et al., 2004; Lamb, 2011; Randall et al., 2011), and negates the requirement for individual upper crustal fault blocks floating on the ductile lower crust.

The structures that develop over the region of distributed simple shear in the analogue model presented here are separate structures to the fault that develops over the region of localised simple shear. This includes F1 and F2, the analogue Wairau and Awatere Faults in Figure 4.4, which are shown to link to the analogue Alpine Fault after 20 mm of displacement, consistent with their appearance in nature. The Wairau Fault, despite appearing as a continuation of the present-day Alpine Fault can therefore be interpreted to have initiated as a separate structure, consistent with the tectonic reconstruction by Ghisetti (2021). The subsequent faults, which form progressively away from the centre of the box in the region of distributed simple shear, do not splay, or split from the fault in the region of localised simple shear. Following their initiation, these faults propagate outwards towards the edges of the region of distributed simple shear, including towards the region of localised simple shear. Formation of faults in this manner causes slip rate variability on the fault, an aspect that is well documented along the Hope Fault (Khajavi et al., 2018). Based on these observations, we interpret that the Clarence and Hope faults formed separately within the transition zone and then propagated back towards the Alpine Fault, which is consistent with data from the MFS (Rattenbury et al., 2006; Litchfield et al., 2014). The Clarence Fault trace has not been mapped to join the Alpine Fault, and any such relationship is only inferred on published geological maps. Furthermore, the Hope Fault has been shown to be propagating back towards the Alpine Fault, rather than emerging from it (Vermeer et al., 2021). The PPAFZ, is also currently forming independently of Alpine Fault as the incipient fifth fault in the MFS.

Figure 4.5 shows how the maximum shear strain changes across the region of distributed deformation, as shear strain localises to form the next fault in the system. Each new fault takes around 5 mm of displacement to develop in the experiment. By upscaling to nature, this suggests that each fault in the MFS develops over a ~ 1.6 Myr interval. Figure 4.5 shows the localisation of a zone of diffuse shear caused by migration of strain across the model. During this localisation process there is no pre-existing crustal scale fault to accommodate deformation across this zone, as the sand is homogeneous. Figure 4.5B shows the increase in maximum shear strain localises on the newly developed fault as strain continues to migrate across the model. We suggest that the PPAFZ is undergoing the same localisation process and increase in shear strain due to the southward migration of strain across the transition zone, and that currently there is no crustal scale fault to accommodate deformation across this zone. The increase in shear strain in the PPAFZ without the presence of a significant plate boundary fault to break may explain the initiation and complex rupture pattern of the Kaikoura earthquake to the south of the Hope Fault. While our model suggests earthquake initiation could have occurred from the ongoing development of strike-slip faults across the transition zone, it cannot explain the propagation of earthquake ruptures onto the thrust faults within the MFS. These thrust faults are linked to localised transpression and uplift of the Seaward and Inland Kaikoura ranges caused by congestion of the subducting slab. Our model is limited to strike-slip deformation and so we cannot model this transpression element.

4.7. Conclusions

Our analogue experiment successfully replicates the southward migration of shear strain across the transition zone between the Alpine Fault and Hikurangi subduction zone in northeast South Island, due to distributed shear strain in the lower crust between the two plate boundaries (Wilson et al., 2004; Wannamaker et al., 2009; Eberhart-Phillips and Bannister, 2010). This southward migration of shear strain forms regions of diffuse deformation in the upper crust that subsequently localise to form the major faults of the MFS. The experimental results confirm the southward development of the faults in the MFS, and predict that the PPAFZ will localise further and form the next major fault in the system (Cowan et al., 1996; Little and Jones, 1998; Wallace et al., 2012). The experiment shows that the PPAFZ is undergoing a significant increase in maximum shear strain, and that there is currently no major crustal scale fault underlying the PPAFZ available to accommodate this strain. This may explain the initiation and complexity of the 2016 Kaikoura earthquake ruptures to the south of the MFS, suggesting that earthquakes of a similar nature will occur in the region in the future.

Chapter 5

A new interpretation for the structural development of the Marlborough Fault System, New Zealand, from 20 Ma to present day

Abstract

The results of recent analogue modelling experiments are used to propose a new hypothesis for the development of the Marlborough Fault System that satisfies the existing palaeomagnetic and structural data. We show how a palaeomagnetically constrained ~ 90 ° clockwise rotation of northeast South Island between 20 Ma and 10 Ma and a change in strike of basement fabrics can be explained by flexural slip about a hinge located to the south of the present-day Hope Fault, above the southern termination of the Hikurangi subduction zone. In contrast to previous studies, inherited NNE-SSW trending structures in the basement rocks of NE South Island were oriented unfavourably for reactivation after the 20 Ma to 10 Ma rotation period, hence relic faults are unlikely to have contributed significantly to the development of the MFS. A second hinge zone emerged in the northeast of the region, which accommodated a further ~ 30 ° of clockwise rotation over the last 10 Ma, linked to the development of a transpression in the system, as proposed by previous studies.

5.1. Introduction

The Marlborough Fault System (MFS) is located in the transition zone between the Pacific and Australian plates in north-eastern South Island, New Zealand. Here, the plate boundary transitions from subduction of the Pacific Plate along the Hikurangi trough east of North Island, to continental collision along the oblique dextral Alpine Fault on South Island (Rattenbury et al., 2006; Walters et al., 2006) (Fig. 5.1). Hundreds of kilometres of strike-slip displacement are accommodated by the MFS and its associated faults across this transition zone (Wilson, 1965; Legg et al., 2004; Wallace et al., 2012). How the MFS developed remains an open topic for discussion and multiple hypotheses have been proposed for its development (Little and Roberts, 1997; Townsend, 2001; Hall et al., 2004; Wilson et al., 2004; Wood and Stagpoole, 2007; Wannamaker et al., 2009; Randall et al., 2011; Ghisetti, 2021). Two 'end member' hypotheses for the development of the MFS are referred to as the 'flexed telephone book' model and the 'floating block' model (Little and Roberts, 1997; Hall et al., 2004). In the 'flexed telephone book' model, rotation of NE South Island was accommodated via a migrating hinge located in the northeast of the Marlborough region (Fig. 5.1) (Little and Roberts, 1997). In the 'floating block' model, the same rotation was accommodated by vertical axis rotations of crustal scale fault blocks (Hall et al., 2004). However, a combination of these hypotheses is generally accepted to explain the development of the MFS (Lamb, 2011; Randall et al., 2011). In the context of the rotational history of NE South Island, it has also been proposed that nucleation of the present-day faults of the MFS occurred by reactivation of pre-existing faults that were inherited from the Cretaceous history of the Marlborough region as the accretionary complex of a Gondwanan subduction zone. Alternatively, the results of recent laboratory analogue experiments (Chapter 2, 3 and 4) suggest that the fault pattern of the MFS may have developed during brittle upper crustal deformation over a ductile lower crust deforming by large-scale distributed deformation, without the need for reactivation of older pre-existing crustal weaknesses.

Here, a critical appraisal of existing hypotheses for the development of the MFS combined with existing palaeomagnetic and structural data and the findings of recent analogue modelling are used to develop a new framework for the development of the MFS.

5.2. Background

5.2.1. Marlborough Fault System

The MFS is undergoing active deformation and is one of the highest earthquake hazard zones in New Zealand (Berryman et al., 2018). The MFS consists of four large, active, oblique strike-slip faults (Figs. 5.1 & 5.2). From north to south these are the Wairau Fault (a continuation of the Alpine Fault), Awatere Fault, Clarence Fault and Hope Fault. These four dextral faults strike sub-parallel to the Australian – Pacific relative plate motion vector (Wallace et al., 2012). The local scale mode of deformation is essentially distributed simple shear sub-parallel to the Wairau Fault, with an average plate motion of 41

mm/yr (Hall et al., 2004; Wilson et al., 2004; Wannamaker et al., 2009; Eberhart-Phillips and Bannister, 2010; Wallace et al., 2012).

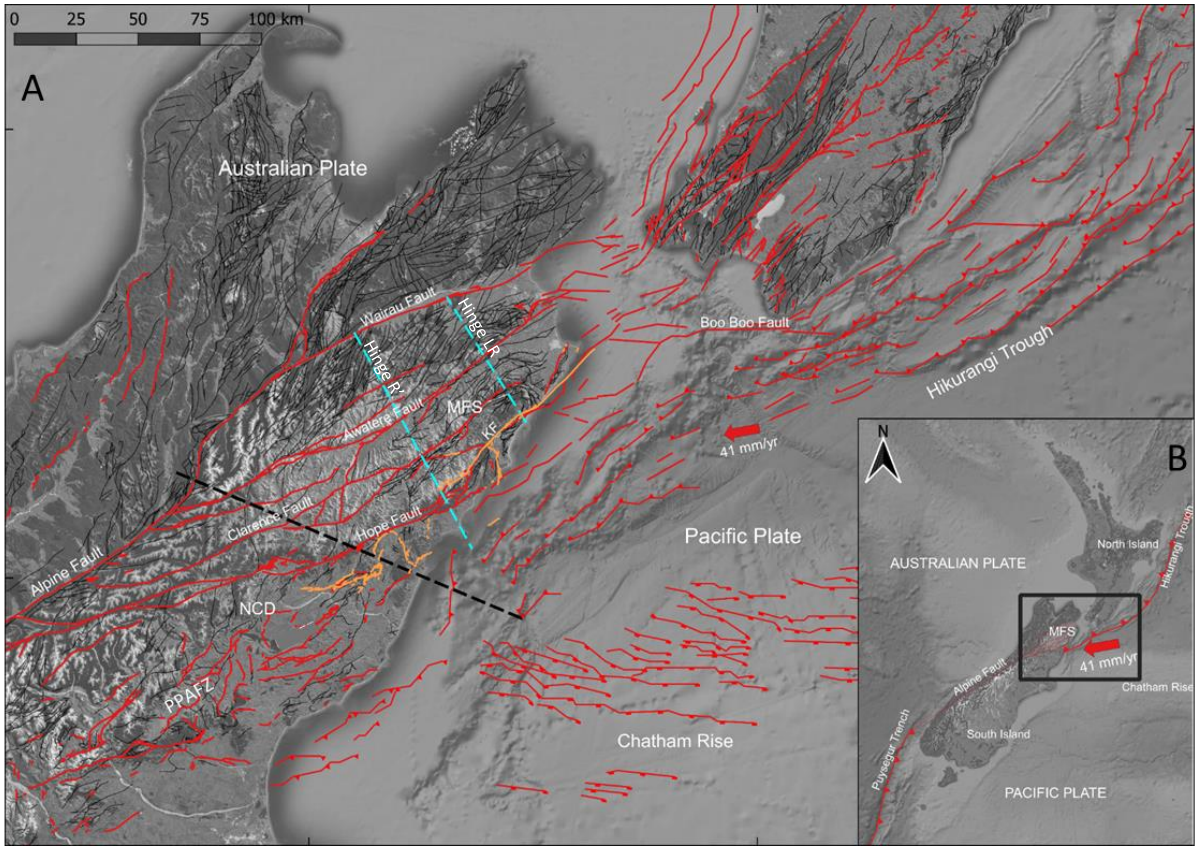

Figure 5.1. A. Tectonic setting of northeast South Island. Active faults are shown in red, inactive faults are shown in black (fault data © GNS Science 2016 and from Wallace *et al.* 2012). The Kaikoura earthquake ruptures are shown in orange. The thick black dashed line is surface projection of the approximation of the edge of the subducted slab according to Randall et al. (2011). The blue dashed lines are proposed hinge lines for the axis of rotation within the MFS. Hinge LR is the hinge line for the rotation proposed by Little and Roberts (1997). Hinge R' is the hinge line proposed by Randall et al. (2011), marking their proposed change in location between small km scale fault blocks to the south and larger 10 km scale fault blocks to the north. MFS=Marlborough Fault System. NCD=North Canterbury Tectonic Domain. KF=Kekerengu Fault. PPAFZ=Porters Pass to Amberley Fault Zone. **B.** The tectonic setting of New Zealand. Box indicates location of Figure 5.1.A.

As summarized by Wallace et al., (2012), there is a general southward decrease in age in the MFS: the Awatere Fault initiated at ca. 5.5 – 6.2 Ma (Little and Jones, 1998), the Clarence Fault at ca. 3 Ma (Browne, 1992) and the Hope Fault at 1 – 2 Ma (Langridge and Berryman, 2005). There are many smaller faults within the fault blocks bounded by these four larger faults (Fig. 5.1). The southernmost faults accommodate most of the current deformation and the Hope Fault records the highest Quaternary slip rate in the region at 20 - 25 mm/yr (Van Dissen and Yeats, 1991). Slip rates in the MFS decrease northward, being 4-8 mm/yr on the Clarence Fault, 5-10 mm/yr on the Awatere Fault, to 4-6 mm/yr on the Wairau Fault (Van Dissen and Yeats, 1991). These faults account for almost all of the current relative plate motion in northeast South Island; GPS data show that the present day rotation within the MFS is negligible (Hall et al., 2004; Wallace et al., 2012).

To the south of the Hope Fault is the North Canterbury tectonic domain (NCD), which has a relatively low average strain rate compared to the MFS (Figs. 5.1 & 5.2). The NCD contains a zone of diffuse transpressional faulting called the Porters Pass to Amberley Fault Zone (PPAFZ; Fig. 5.1). The PPAFZ may be currently developing into a fifth through-going fault in the system (Cowan et al., 1996).

5.2.2. Geology of the MFS

The Mesozoic Torlesse composite terrane, comprising the Rakaia and Pahau terranes and the Esk Head melange belt, makes up the basement (and most of the outcropping geology) of the NCD and MFS (Rattenbury et al., 2006) (Fig. 5.2A, which shows a geological map consistent with the Kaikoura QMAP area from Rattenbury et al. (2006)). This composite terrane is composed of indurated quartzo-feldspathic sedimentary rocks, commonly termed greywacke. Although no crystalline basement is recognised, the Torlesse composite terrane makes up the basement of a younger sequence of c. 108 – 95 Ma sedimentary 'cover' rocks (Reay and Pye, 1993; Rattenbury et al., 2006; Willis, 2017; Gardiner and Hall, 2021; Gardiner et al., 2022). The 2016 Kaikoura earthquake fault ruptures developed within basement rocks of the Pahau terrane.

The Pahau terrane is composed of indurated grey quartzo-feldspathic sandstones and mudstones (Fig. 3), which are thought to represent clastic detritus recycled from the older Rakaia terrane (MacKinnon, 1983). The depositional environment of these sedimentary rocks has been interpreted as marginal marine fan-deltas and/or deep-water submarine fans (Reay and Pye, 1993; Bassett and Orlowski, 2004). Conglomerate lenses and large tectonic melange zones are common throughout the Pahau terrane (Rattenbury et al., 2006). Rattenbury et al., (2006) characterise the Pahau terrane as consisting of imbricate thrust slices and/or recumbent folds of largely middle Cretaceous rocks, locally interleaved with tectonic melange that contains rocks as old as the late Triassic (Fig. 5.3).

The deposition of the sedimentary basement rocks occurred from the Late Jurassic to Early Cretaceous, when New Zealand was in the overriding plate of the East Gondwana subduction zone. Trench advance accreted the Rakaia terrane as an accretionary complex over a period of 10-15 Myrs as part of the Rangitata I orogeny. The collision of the Hikurangi Plateau at 105 Ma caused localised shortening and accretion of the Pahau terrane into a forearc basin as part of the Rangitata II orogeny (Willis, 2017). The Esk Head melange belt separates the Pahau and Rakaia terranes, and is often used as a structural marker to visualise the horizontal offsets on the MFS faults (Fig. 5.2A). The Esk Head Belt melange belt consists of a deformed mix of the Rakaia and Pahau terranes and its boundary with the Pahau terrane is gradual over several kilometres, and is characterised by shear fabrics (Hall et al., 2004; Rattenbury et al., 2006).

Deposition of clastic and carbonate sedimentary cover rocks occurred between the Late Cretaceous and the Eocene. Local tectonics through this time involved slab break off followed by a passive margin setting (Gardiner and Hall, 2021; Gardiner et al., 2022), associated with the regional-scale rifting,

continental break up and sea floor spreading during the opening of the Tasman Sea. Deposition of post-Eocene cover rocks is associated with the Kaikoura Orogeny and the development of the modern-day plate boundary (Reay and Pye, 1993; Rattenbury et al., 2006; Willis, 2017). Sedimentary cover rocks crop out sparsely across the MFS region and are generally exposed adjacent to the major MFS faults (Fig. 5.2A).

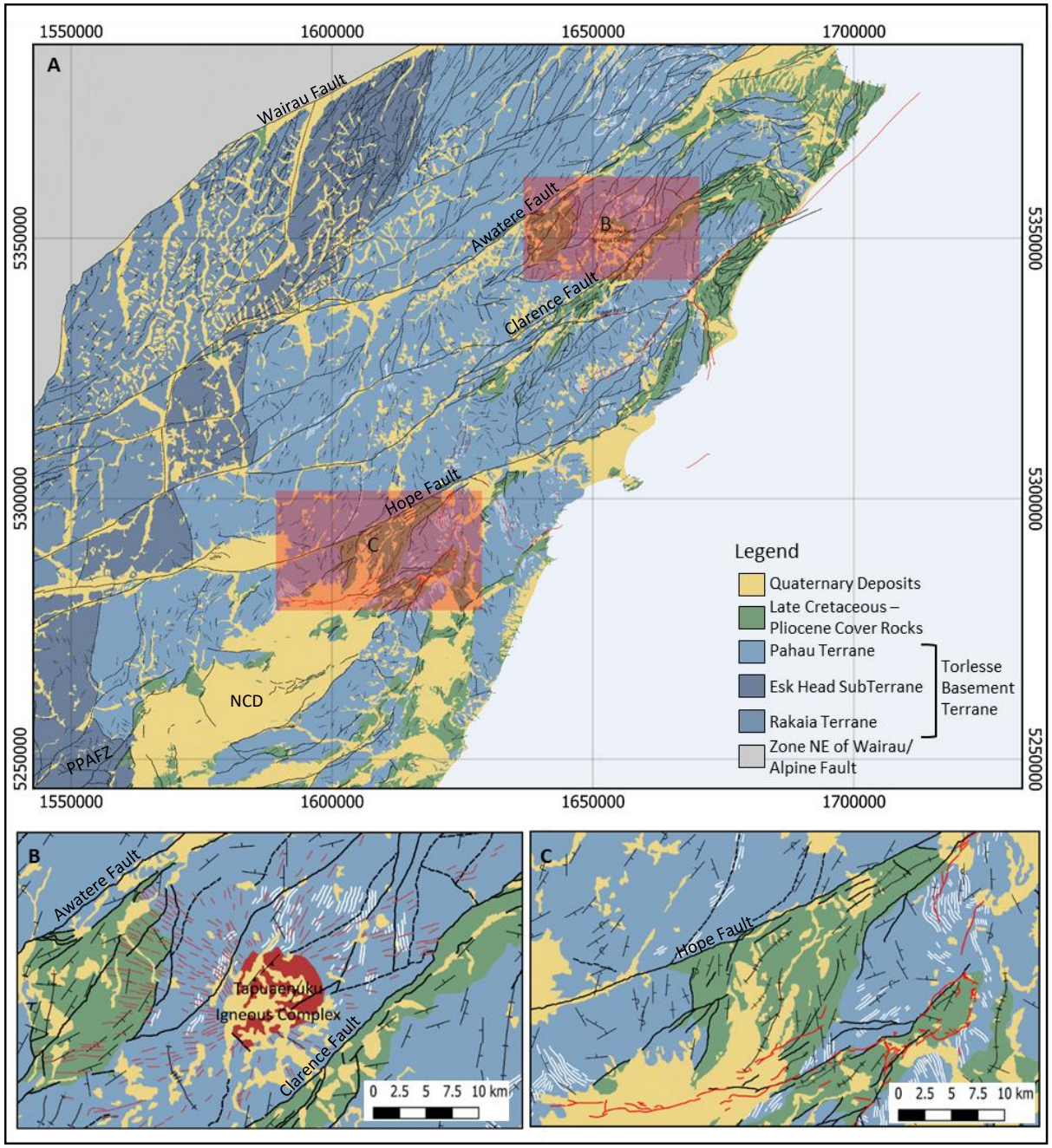

Figure 5.2. A. Simplified geological map of the Marlborough Fault System, divided into basement and cover rock and Quaternary rocks (adapted from GNS Shapefile Data © GNS Science 2016). The area northwest of the Wairau Fault is greyed out. Pink boxes indicate locations of B and C. NCD: North Canterbury Tectonic Domain. PPAFZ: Porters Pass to Amberley Fault Zone **B.** The Tapuaenuku igneous complex (red) in the northeast MFS remains undeformed between the Awatere and Clarence faults, indicating minimal internal strain between the major faults. **C.** Folds within the cover rocks appear 'dragged' by the Hope Fault, indicating internal strain within the NCD. Faults in red indicate faults that ruptured during the 2016 Kaikoura earthquake.

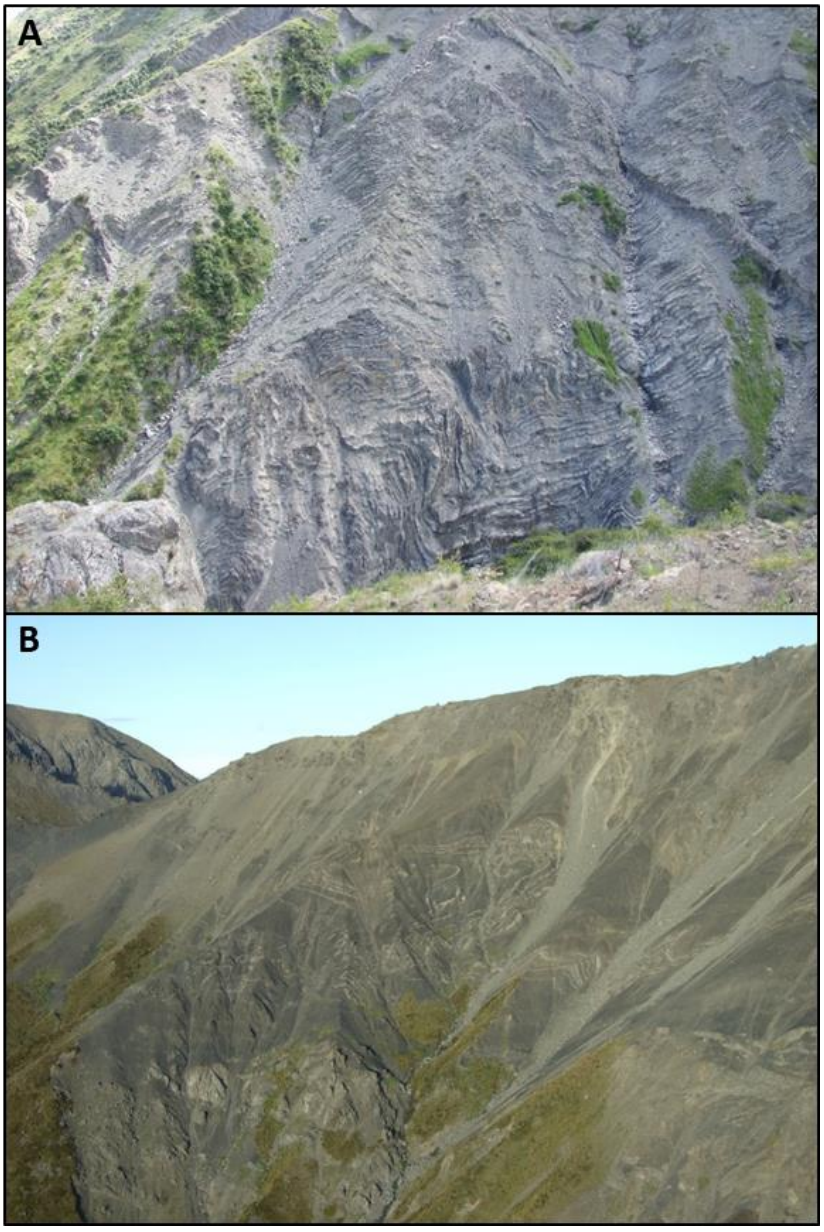

Figure 5.3. The Pahau Terrane, part of the Torlesse basement terrane is the dominant outcropping geology within the MFS and NCD. This basement terrane consists of turbidites that were deformed in an accretionary complex from the Gondwanan subduction zone in the Cretaceous. **A.** Photo taken of facing North from the Clarence Valley, of a section of the Inland Kaikoura Range, showing folded turbidites within the Pahau Terrane. **B** Photo taken facing SE within the Clarence Valley, of a section of the Seaward Kaikoura Range, showing recumbent folds within the Pahau Terrane.

5.2.3. Accommodating plate motion

Plate reconstructions indicate ~800 km relative dextral strike-slip offset between the Australian and Pacific Plates, across New Zealand, since 45 Ma (Stock and Molnar, 1987; Sutherland, 1995; Little and Jones, 1998). The dextral offset of basement terranes across the Alpine Fault is 460 km, indicating that it has accommodated just over half of this relative plate motion since its initiation at ~25 Ma. More recently, Lamb et al. (2016) proposed that prior to the initiation of the Alpine Fault as a dextral strike-slip fault, there was > 225 km of sinistral displacement across Zealandia, which has been subsequently

reversed by the Alpine Fault. Lamb et al. (2016) therefore argue that the Alpine Fault has a cumulative offset of around 700 km, accommodating close to the entire dextral strike-slip displacement of New Zealand across central South Island.

Hall et al. (2004) proposed a total dextral displacement of 273 ± 52 km across the major MFS faults, calculated from a kinematic model of deformation of elongate fault blocks. Most other estimates of the cumulative strike-slip displacement across all of the major faults of the MFS are slightly less than 200 km, these estimates are calculated from the offset of the Esk Head Subterrane (Fig. 5.2A) (Little and Roberts, 1997; Little and Jones, 1998). The Wairau Fault accounts for ~140 km of this ~200 km dextral displacement (Little and Roberts, 1997; Little and Jones, 1998), and the cumulative displacement along the other major faults is 55 – 65 km. Individual dextral offsets on the other major faults are ~ 7 – 16 km on the Awatere Fault , <18 km on the Clarence-Kekerengu-Fidget faults (Little and Jones, 1998), ~20 km on the Hope Fault (Van Dissen and Yeats, 1991) and ~2 km on the Porters Pass to Amberley Fault zone south of the Hope Fault (Cowan et al., 1996).

GPS horizontal velocity data do not provide strong evidence for rotation and diffuse deformation within the present-day MFS (Wallace et al., 2007, 2012). The basement fabric and smaller faults within the MFS have a remarkably consistent trend. Features such as the Cretaceous Tapuaenuku igneous complex and the associated radiating dyke swarm, located between the Awatere and Clarence faults (Fig. 5.2B), appear undeformed. These observations suggest that there has been little penetrative deformation within the blocks between the MFS faults since the emplacement of the Tapuaenuku igneous complex. This implies that all of the deformation within the MFS at the current level of exposure must be localised along faults, with almost no internal strain between them. These observations compliment GPS horizontal velocity measurements across the MFS (Wallace et al., 2012), which indicate deformation within fault block interiors are unlikely to be detectable within the GPS measurement uncertainty. Conversely, in the NCD the basement fabric and faults have variable orientations, and a large syncline has been rotated or dragged into the PPAFZ (Fig. 5.2C), which indicates that internal deformation has accumulated within the block south of the Hope Fault. This is also consistent with Wallace et al.'s (2012) fault block interpretation, in which a more diffuse zone of faulting such as the PPAFZ has been proposed south of the Hope Fault.

Mid-crustal seismicity is distributed across the MFS rather than being limited to discrete fault zone at the surface (Eberhart-Phillips and Bannister, 2010). This is thought to reflect widening of shear zones and large-scale distributed deformation at depth (Wannamaker et al., 2009; Eberhart-Phillips and Bannister, 2010).

5.3. Data Analysis

5.3.1. Palaeomagnetic data

The palaeomagnetic data used in this investigation (Fig. 5.4A) is taken from Lamb, (2011) and Randall et al., (2011), who present new and compiled palaeomagnetic rotations measured in samples collected from volcanics and sedimentary cover rocks from the MFS and NCD. The principle techniques of deriving palaeomagnetic rotation data are described by Butler (1992). Randall et al. (2011) explain in the detail the method of palaeomagnetic data collection, processing and analysis for those measurements within the Marlborough region, which are summarised by Lamb (2011). The principle problem with palaeomagnetic data collection from the Marlborough region is the dominance of sedimentary rocks, which have very weak natural remnant magnetisms. The sedimentary rocks with a high enough remnant magnetism for measurement were the micritic limestones, mudstones and siltstones within the cover rocks of the MFS (Lamb, 2011; Randall et al., 2011). However, these sedimentary rocks still gave an 80% failure rate in the presence of a primary magnetisation. To alleviate this problem, hundreds of measurements were taken within the same stratigraphic units within close proximity (Lamb, 2011). Natural remnant magnetisms were stronger within the igneous rocks of the MFS. The palaeomagnetic data from within the MFS is therefore limited to the sedimentary cover rocks and igneous rocks. The tectonic rotations determined from the paleaomagnetic data are summarised in Figure 5.4A. These rotations are relative to the Pacific Plate, which is essentially the same as true north for the Neogene (Lamb, 2011). Figure 5.4A differentiates rotations that occurred before and after 10 Ma. This distinction has been made because 10 Ma represents the approximate time when the Hikurangi subduction zone and Alpine Fault begin to interact, leading to distributed deformation and the subsequent the development of the MFS. Hence, < 10 Ma old palaeomagnetic data records rotation that occurred during the development of the MFS, whereas older data represents rotations prior to the development of the MFS (in its present day strike-slip regime).

Pre-10 Ma palaeomagetic data records rotations between 51° and 146°. Paleopole rotations > 88° are limited to the eastern MFS and are associated with a series of thrust sheets within the cover rocks between the Clarence and Hope faults, which rotate with the strike of bedding by up to 180°. Clockwise palaeomagnetic rotations within this area range from 97° to 146°, averaging ~120°. In other parts of the MFS, >10 Ma rotations generally decrease southwards, with minimal values in the NCD. Close to the Hope Fault >10 Ma rotations range from 51° to 54° and within the central MFS they are between 21° and 88°.

Significant post-10 Ma palaeomagnetic data is confined to the north-eastern edge of the MFS, northeast of Little and Roberts' (1997) hinge (Fig. 5.4A). Here paleopoles record an approximately consistent clockwise rotation between 20° and 35° (with one outlier at 44°) that coincides spatially with a 'kink' and change in orientation of bedding and faulting within the MFS. Outside of this hinge zone <10 M palaeomagnetic data indicates negligible rotation.

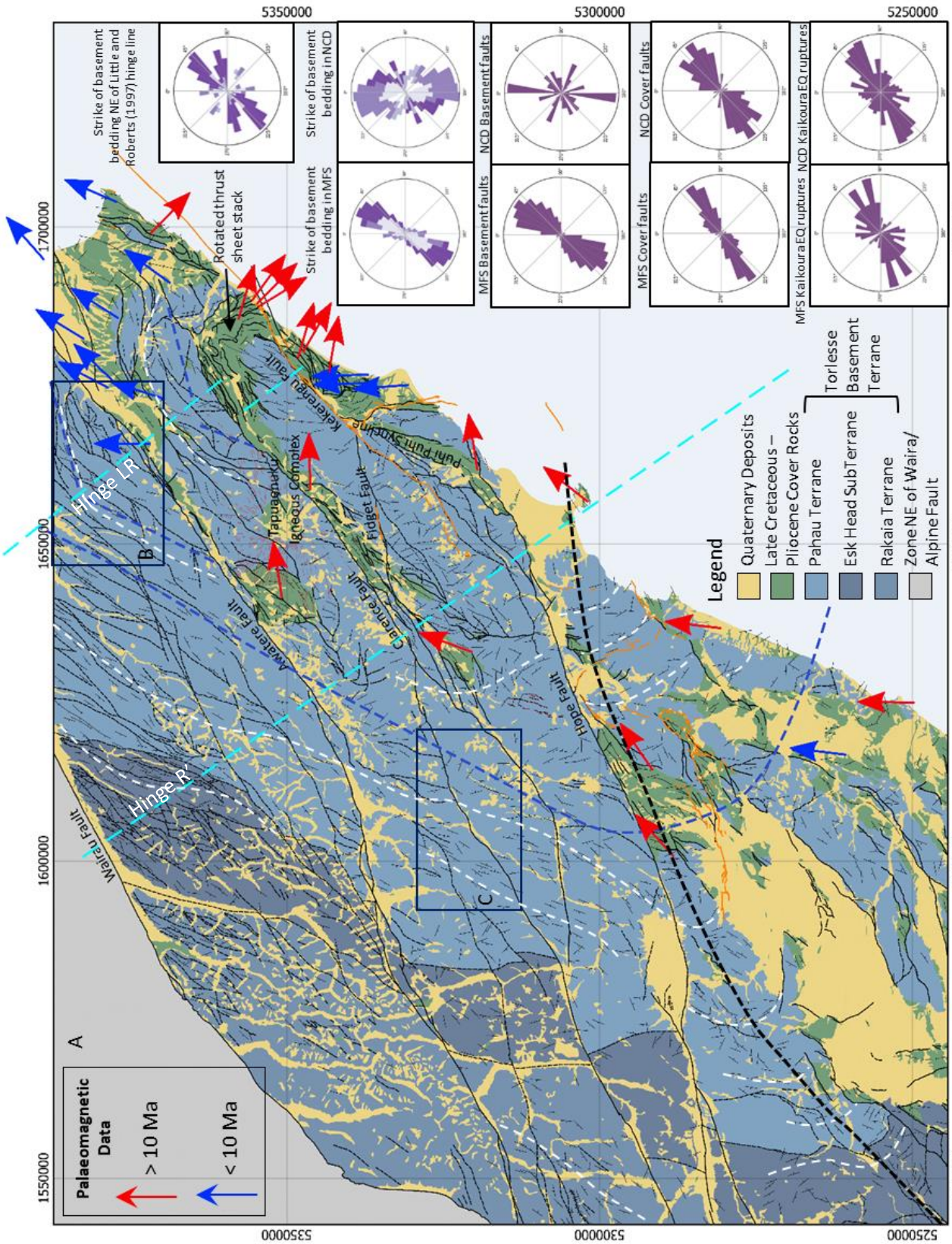

Figure 5.4. See next page for continued figure and figure description

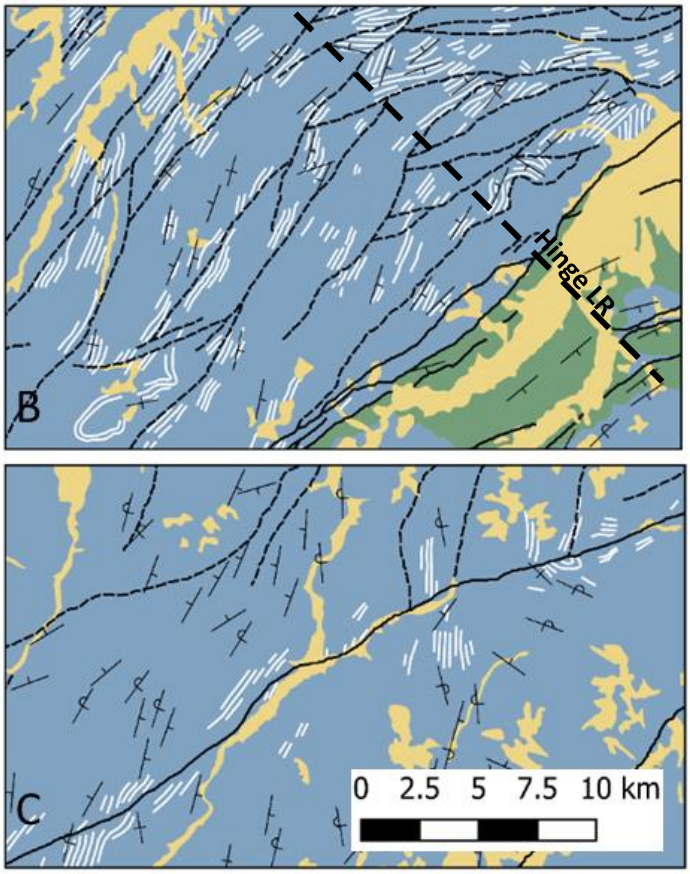

Figure 5.4 A. A simplified geological map of the MFS with arrows representing palaeomagnetic rotations from Randall et al. (2011) and Lamb et al. (2011). The blue dashed lines are proposed hinge lines for the axis of rotation within the MFS. Hinge LR is the hinge line for the rotation proposed by Little and Roberts (1997). Hinge R' is the hinge line proposed by Randall et al. (2011), marking their proposed change in location between small km scale fault blocks to the south and larger 10 km scale fault blocks to the north. The dark blue dashed line represents the general change in strike of bedding in basement rocks from Hall et al. (2004). The white dashed lines are generalised bedding form lines within the MFS basement rocks. Faults are shown in black, with dashed lines representing faults within the basement and solid lines representing faults associated with cover rocks, including the MFS faults. The Kaikoura earthquake ruptures are shown in orange. Rose diagrams at right plot strikes of bedding and faults in basement and cover rocks of the MFS and NCD, north and south of the Hope Fault, respectively. **B.** Detail of the northern part of the MFS showing consistent strike of the bedding and basement faults and a distinct 'kink' in their orientations in the northeast. **C.** The Clarence Fault crosscuts bedding form lines and the faults within the basement rocks in the central MFS.

5.3.2. Structural data

Publicly available, Geological and Nuclear Sciences (GNS) shapefiles (© GNS Science 2016) were used to constrict the geological maps presented in Figures 5.2 and 5.4. Analyses of generally steeply dipping bedding and fault strike orientations within the MFS and NCD were carried out using form lines and by generating rose diagrams from data sets provided by GNS (Fig. 5.4A). Faults were subdivided into older faults (i.e., faults that occur in the basement rocks) and younger faults (i.e., faults that are in or are linked to the cover rocks).

Figure 5.4A shows that bedding within the MFS strikes in a remarkably consistent NNE – SSW direction and that older faults within the basement rocks are oriented parallel to it.

A number of faults occur within the basement rocks between the major MFS faults, particularly between the Wairau and Awatere faults (Figure 5.4A). These faults are straight and appear to interconnect with each other. These older faults parallel the strike of bedding in the basement (Fig. 5.4A and Fig.5.4B). Faults that are labelled as active in the GNS dataset tend to be oriented similarly to the major ENE-WNW trending MFS faults and they mostly crosscut the bedding form lines of the basement (Fig. 5.4C).

Bedding strikes and fault trends kink and rotate at least ~25° clockwise in the northeast portion of the MFS, consistent with palaeomagnetic data for this area (Figs. 5.4A and 5.4B). Bedding and fault orientations rotate significantly in the eastern section of the map where there is a stack of deformed thrust sheets, as labelled on Figure 5.4. Following the cover rocks constrained between the Clarence Fault and Hope Fault, the strike of the bedding and the thrust sheet orientations rotate up to 180 ° in this region (Fig. 5.4). This area corresponds with the ~120 ° clockwise palaeomagnetic rotations identified in the previous section.

Bedding orientations within the NCD are much more variable compared to the MFS (Fig. 5.4A). Rose diagrams for the NCD show larger spread in the strike of the bedding with a mean NNW – SSE trend, which is ~40° clockwise from the strike of the bedding in the basement rocks of the MFS. Bedding form lines in basement rocks indicate a ~90° clockwise rotation in the MFS relative to the NCD (Fig. 5.4A). The general south to north increase in the amount of rotation indicated by paleopoles that are older than 10 Ma is consistent with the observed change in orientation of bedding in the basement.

Faults within the NCD basement rocks also have a much wider array of orientations compared to those within the MFS and tend to follow basement bedding form lines (Fig.5.4A). In general, the active faults within the NCD have similar orientation to the MFS faults.

5.4. Review of current tectonic models

Some interpretations of the MFS do not consider vertical axis rotation within the system (King, 2000; Wood and Stagpoole, 2007; Ghisetti, 2021). Although previous palaeomagnetic studies comprised data restricted to the northeast margin of South Island (Little and Roberts, 1997), the work by King (2000) was published prior to the publication of palaeomagnetic data within the central MFS (Hall et al., 2004). The rotation in King's (2000) tectonic model is confined to the North Island, which is consistent with Wood and Stagpoole (2007) who suggested that the required rotation was accommodated by the deformation along the East coast of North Island, rather than the MFS. Ghisetti's (2021) proposed interpretation of the tectonic development of South Island was developed following the plate tectonic template of Zealandia from Müller et al., (2019), which in turn follows plate tectonic models of King, 2000, and Wood and Stagpoole (2007). Since Ghisetti's (2021) model is confined to the period since 10 Ma, the rotation that occurred prior to this time is outside the scope of her study and therefore not considered in her model of tectonic development of South Island.

Wood and Stagpoole (2007) showed the development of the MFS by faulting along the edges of crustal blocks over the last 8 Ma, which is consistent with the interpretations of Hall et al. (2004), Lamb (2011) and Randall et al. (2011). King (2000) suggested that the 'proto' MFS faults developed as strike-slip faults as early as 21 Ma to connect the Alpine Fault to the Hikurangi subduction zone, following evidence presented by Audru and Delteil, (1998) for strike-slip faulting in southern Marlborough in the early Miocene. Ghisetti (2021) interpreted the 'proto' MFS faults as normal faults located in NE South Island, consistent with present-day faulting within the Chatham Rise.

Where paleomagnetic rotations within the MFS are considered for tectonic reconstructions of New Zealand, rotation is generally hypothesised to have occurred by either: 1) rotation about a migrating hinge that was coincident with the termination of the Hikurangi subduction margin against the Chatham Rise (Little and Roberts, 1997). 2) rigid block rotation (Hall et al., 2004), or 3) a combination of these hypotheses (Lamb, 2011; Randall et al., 2011; Wallace et al., 2012). The main hypotheses for the location of this hinge and how rotation is accommodated within the MFS are summarised below (Fig 5.5). Both Hall et al (2004), and Randall et al (2011) used the observed clockwise change in orientation of the basement fabric from the NCD into the MFS to support hypothesis for rigid block rotation between 20 Ma and 8 Ma.

The bulk rotation of NE South Island is generally considered to be both caused and controlled by the anticlockwise rotation and subsequent slab rollback of the Hikurangi subduction zone about its termination point, which occurred as an oroclinal event between 20 Ma and 10 Ma (Little and Roberts, 1997; Lamb, 2011; Randall et al., 2011; Willis, 2017). At 20 Ma propagation of the Hikurangi subduction zone had reached the Hikurangi Plateau and the Chatham Rise causing subduction to terminate and initiating the anticlockwise rotation and slab rollback, as demonstrated in the numerical models by Willis (2017) and the more general numerical models of orocline formation by Moresi et al. (2014).

In the existing literature, rotation is often described to occur around a 'hinge' line. This hinge line is not a vertical point but rather a horizontal line on a map that differentiates domains that have rotated by differing amounts. For consistency, we continue to refer to such lines as hinge lines throughout this chapter. The hinge line facilities rotation about a vertical axis point, which in the case of rotation in the MFS, is associated with the Hikurangi subduction zone and its termination, as described below.

5.4.1. Flexed Telephone Book Model (Little and Roberts, 1997)

Little and Roberts (1997) proposed that the ~100° clockwise vertical axis rotation within the MFS occurred about two hinges associated with two crustal boundaries near the east coast of Marlborough since 20 Ma (Figs. 5.4A, 5.5A). The hinges developed southwestward with ~50° rotation occurring on the northeast hinge from 20 – 4 Ma, and a further ~30 – 50° rotation after 4 Ma about a hinge further to the southwest (Figs 5.1, 5.4A). In this model, MFS contained pre-existing faults that reactivated from

~ 8 Ma once they were rotated into a favourable orientation (Fig. 5.5A). The bulk of the MFS remained undeformed during this time, while the northeastern edges accommodated the rotation, generating the hinge line (Fig. 5.5A). The axis of rotation shifted southwestward, following the propagation of the Hikurangi subduction zone, creating a migrating hinge with faults bent around it, akin to a 'flexed telephone book.' It should be noted that the palaeomagnetic data available in 1997 was constrained to the NE corner of the MFS and is perhaps why there is no interpreted rotation for the central MFS. Little and Roberts (1997) attributed rotation greater than ~100° (recorded by palaeomagnetic data near Kekerengu associated with the thrust sheets labelled in Fig. 5.4A) to local shear zone effects, and concluded that such large rotations are not representative of northeast South Island as a whole.

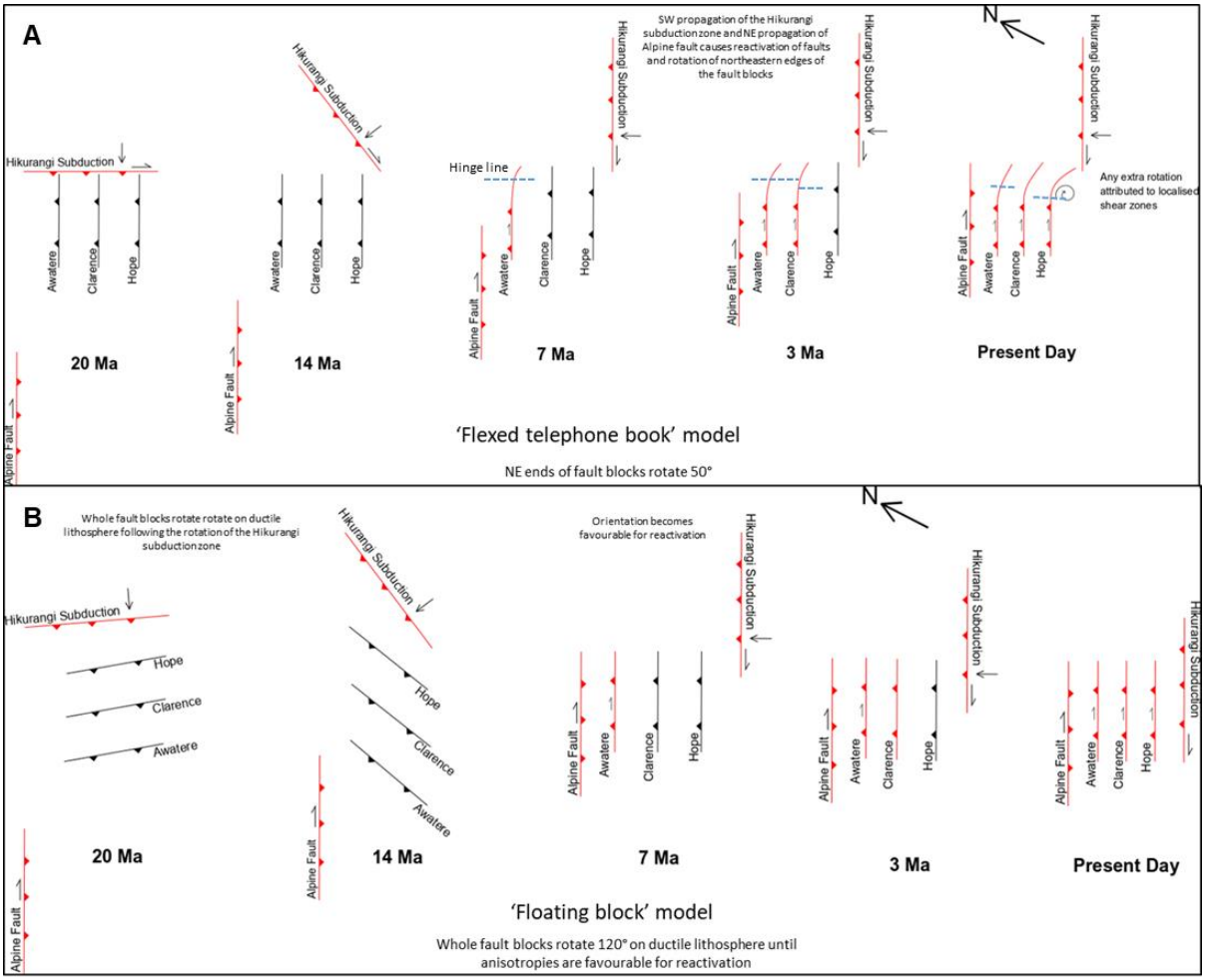

Figure 5.5. Schematic diagrams illustrating two hypotheses for the evolution of the Marlborough Fault System. **A.** In the 'flexed telephone book' model (Little and Roberts, 1997), pre-existing weaknesses reactivate sequentially southward. As the migration of the Hikurangi subduction zone margin continues southwards, rotation occurs in the northeastern edges of the MFS about a crustal scale hinge. **B.** In the 'floating block' model (Hall et al. 2004), pre-existing weaknesses oriented 080° to the relative plate motion rotate with the propagation of the Alpine Fault and Hikurangi subduction zone. As the pre-existing weaknesses become sub-parallel with the relative plate motion vector, they reactivate sequentially southward.

5.4.2. Floating Block Model (Hall et al., 2004)

Hall et al. (2004) combined palaeomagnetic rotations along with the change in orientation of basement trend to determine that there has been ~100° clockwise rotation within the MFS since 50 Ma. The

majority of this rotation occurred between 25 – 8 Ma, contemporaneously with the motion on the Alpine Fault during this time period. Hall et al. (2004) concluded that the palaeomagnetic data indicates rotation of rigid crustal blocks with no evidence for faulting or shearing internally within these blocks. They account for this rigid block rotation via a 'floating block' model (Fig. 5.5B) in which rigid crustal blocks are bounded by pre-existing, accretionary upper crustal scale thrust faults overlying a deformable ductile lower crust. In order to match the required distributed finite shear strain in the lower crust, Hall et al. (2004) estimated that the entire upper crust of the MFS must have rotated ~100° as rigid elongate fault-bounded blocks. At 8 Ma the pre-existing thrust faults became favourably aligned for reactivation, which occured sequentially southward to form the MFS.

A further ~30° clockwise rotation has occurred on the block edges since 8 Ma. Hall et al. (2004) account for this by the northeastern fault block edges becoming more equidimensional due to the southwest propagation of the Hikurangi subduction zone.

5.4.3. Combination model (Randall et al., 2011)

Randall et al. (2011) present the most recent palaeomagnetic data and combine this with previous palaeomagnetic data to interpret ~130° of clockwise rotation since 20 Ma. They hypothesised that the MFS originated as pre-existing, northwest trending thrust faults, inherited from the earlier Cretaceous accretionary complex, which rotated ~80° in the central MFS, in a manner similar to the 'floating block' model, until their orientation became favourable for reactivation. The faults reactivated sequentially southward to form the present-day northeast trending strike-slip faults of the MFS. Randall et al. (2011) estimated that a further 40 – 50° of clockwise rotation occurred in the northeast MFS due to higher shear strains arising from the southwestward migrating subduction zone but did not attribute this rotation to a change in fault block shape, suggesting this rotation was more similar to the 'flexed telephone book' model. Randall et al. (2011) estimated that the rotated elongate fault blocks in the central MFS are 50 x 10 km in size, while crustal blocks in the southern MFS are on a scale of 1 – 10 km. The line indicated in Figures 5.1 and 5.4A marks the change from small blocks in southern Marlborough to elongate blocks in the central MFS.

5.4.4. Insights from numerical and analogue modelling

Following numerical geodynamic experiments of orocline development by Moresi et al. (2014), Willis (2017) presented numerical models with tectonic boundary conditions similar to those of northeast South Island at 20 Ma. These models reproduce similar rotations of the subduction zone and associated accretionary complex that are consistent with palaeomagnetic data (Little and Roberts, 1997; Hall et al., 2004; Lamb, 2011; Randall et al., 2011). However, unlike previous interpretations, the crust in the numerical models deforms by toroidal flow around the rotating subduction zone, rather than via the rotation of rigid crustal blocks.

Analogue laboratory experiments (Chapters 2, 3 and 4) have been used to investigate the development of transition zones at the termination of continental transform faults, where the 'connecting' plate boundary is 'misaligned', with particular focus on the development of the MFS (Chapter 4) (Fig. 5.6).

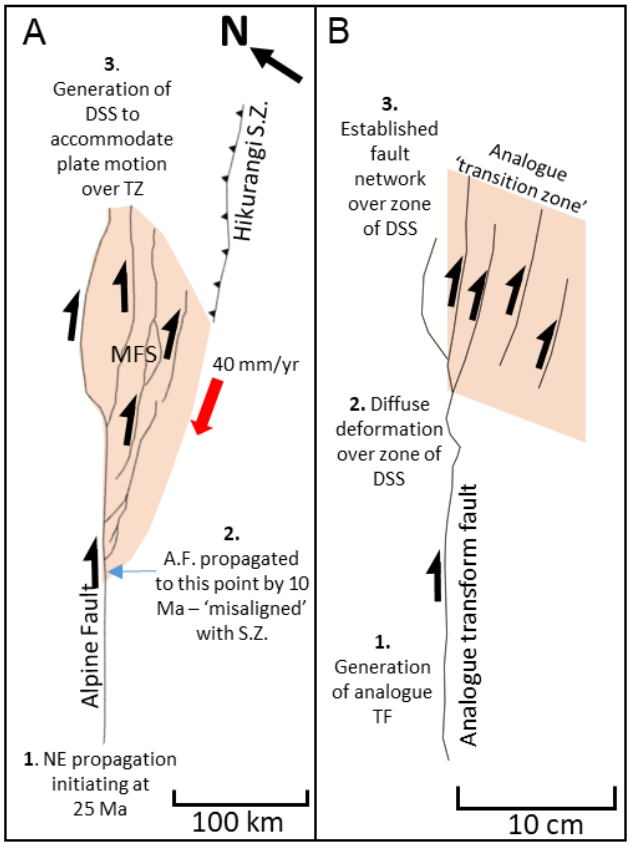

Figure 5.6. A. Fault outlines of the major faults in NE South Island New Zealand, illustrating the MFS has developed across a transition zone where the two major plate boundaries are misaligned. The fault outlines have been rotated for comparison with the analogue experiment. (Fault geometries © GNS Science 2016) **B.** The traced fault outline of a 'transition zone' analogue experiment at 30 mm displacement of a modified analogue shear box**.** The analogue experiment is simulating a transition zone with a basal boundary condition of distributed deformation in a position analogous to the transition zone of the MFS, and an upper crustal analogue is subject to deformation by these basal boundary conditions. The region of proposed distributed shear is highlighted in orange each for each example. Red arrow indicates direction of plate motion. DSS = Distributed Simple Shear. TZ = Transition Zone. SZ = Subduction Zone. TF = Transform Fault. (Modified from Chapter 2).

The results suggest that the MFS has a fault pattern that is consistent with other plate boundary transition zones across the globe, such as the southern termination of the San Andreas Fault and the western termination of the North Anatolian Fault (Chapter 2). The fault pattern that develops in the analogue model with basal boundary conditions analogous to the plate boundary transition zone in NE South Island, appears strikingly similar to the present day MFS (Fig. 5.6). Therefore, we consider the development of the faults within this analogue model to be a reasonable analogue for the development of the MFS faults. Results from the analogue experiments demonstrate that this fault pattern develops as a result of brittle upper crustal deformation above a lower crust deforming by distributed simple shear, consistent with interpretations from geophysical data of the MFS (Wannamaker et al., 2009; Eberhart-

Phillips and Bannister, 2010) (Chapter 1 and 4). When viewed in an orientation consistent with South Island, the experimental faults develop sequentially southward across the region of distributed simple shear from zones of diffuse shear strain that localise to form through going faults (Fig. 5.7). These faults develop as crustal-scale Riedel shears (Schreurs, 2003) that are equally spaced and oriented ~18 ° clockwise relative to the direction of strike-slip plate motion. The experimental results are consistent with Yang et al., (2019) and Zuza et al., (2017), who show that fault spacing is controlled by brittle-layer thickness, viscous lower crust thickness, the strength contrast between active faults and surrounding intact blocks, and lower crust viscosity.

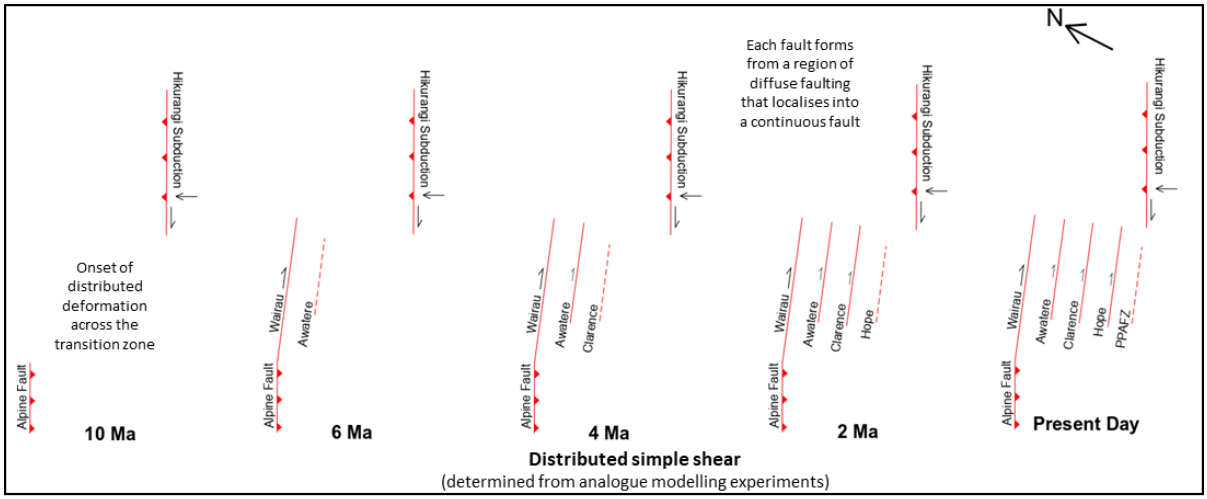

Figure 5.7. Schematic diagrams showing hypothesis of development of the MFS based on analogue modelling results. Distributed simple shear within the transition zone between the Alpine Faults and the Hikurangi subduction zone results in sequential north to south nucleation of the MFS faults.

In contrast to the previous hypotheses for development of the MFS summarised above, the analogue experiments indicate that fault systems analogous to the MFS can develop without reactivation of pre-existing crustal scale weaknesses (Fig. 5.7). It is important to note that the analogue experiment reported here and in Chapters 2-4 only intended to model the development of the MFS since 10 Ma, which is the approximate time of initiation of distributed simple shear across the transition zone between the Alpine Fault and the Hikurangi subduction zone. The experiments are not designed to investigate how rotation and associated deformation was accommodated before 10 Ma.

5.5. Discussion

5.5.1. Comparison of existing hypotheses for the development of the MFS

Most of hypotheses reviewed above for the development of the MFS involve the sequential reactivation of pre-existing crustal scale weaknesses (Little and Roberts, 1997; King, 2000; Hall et al., 2004; Wood and Stagpoole, 2007; Randall et al., 2011; Ghisetti, 2021). However, recent analogue modelling

(Chapters 2, 3, and 4) suggest it is possible to form faults with the orientations and spatial patterns observed across the MFS, without the need for reactivation of pre-existing weaknesses.

The ~ 100° clockwise rotation of northeast South Island between 20 Ma and 10 Ma, prior to the development of the MFS, must be accommodated with minimal penetrative deformation of the upper crust. Hence, the generally accepted hypothesis for this rotation is via vertical axis rotation of rigid crustal blocks (Hall et al., 2004; Lamb, 2011; Randall et al., 2011). However, because complex fault arrays are required to accommodate vertical axis rotations of separate crustal blocks, it would be unlikely to preserve the remarkably consistent strike of basement structures across the MFS region. Furthermore, such rotations would create geometric space problems between fault blocks that should be accommodated by additional intra-block deformation.

5.5.2. Interpretation of existing data

20 – 10 Ma: Accommodation of 90° clockwise vertical axis rotation

The consistency between the palaeomagnetic and structural data suggests that the bend in the basement to the south of the Hope Fault is due to relative rotation between the NCD and the MFS, consistent with previous interpretations (Hall et al., 2004). This change in bedding strike orientation occurs slightly south of the Hope Fault and thus is accounts for the wider range of basement strikes in the NCD compared to the MFS. This rotation is also consistent with the mapped change in orientation of the Esk Head Subterrane going from the NCD into the MFS (Fig. 5.4A).

The Torlesse terrane consists of a folded and faulted accretionary stack of turbidites deformed in the East Gondwanan subduction zone in Late Jurassic to Early Cretaceous time (Willis, 2017). During this accretionary history, bedding, faults and fold hinges within the Torlesse terrane would have been oriented broadly perpendicular to the maximum shortening direction, and therefore sub-parallel to the trace of the subduction zone. Although there is some m- to km variation of accretionary structure orientation (e.g., Fig. 5.3) due to smaller scale deformation, the strike of bedding and faults are very consistent strike throughout the basement rocks of the NCD and MFS. The rotation of bedding and fault orientations within the MFS relative to the NCD must therefore reflect rotation of the region as a whole, along with the rotation of the Hikurangi subduction zone from 20 Ma to 10 Ma.

This change in orientation of basement structure occurs slightly south of the Hope Fault (Fig. 5). We propose that this location represents the approximate hinge of the palaeomagnetically constrained ~90 ° rotation that occurred prior to 10 Ma. This hinge line (Fig. 5.4A) has been drawn by linking the points of maximum curvature on the bends in basement bedding form lines and differentiates a domain in the NCD that shows no rotation, with the domain in the MFS that shows 90° clockwise rotation. The point of maximum curvature and location of the hinge line therefore shows 45° rotation. The proposed hinge line connects with the termination of the Hikurangi subduction zone and Chatham Rise, providing further evidence that rotation about this hinge is coeval and coaxial with the rotation of the Hikurangi

subduction zone. The Hikurangi subduction zone propagated southward to reach its current termination at 20 Ma (Willis, 2017). Randal et al. (2011) propose that the lithosphere in southern Marlborough has remained largely 'warm' and weak because it is further away from the cooling effects of subduction, whereas the lithosphere in northern Marlborough has remained relatively 'cool' since it has been located above a downgoing slab since subduction initiated in the Miocene. Therefore, the lithosphere south of the Hope Fault in southern Marlborough is likely to have lower bulk strength, and thus is capable of accumulating more internal deformation. In contrast, the area over the subducted slab will have higher bulk strength due to a steeper geotherm. A change the relative bulk strength of the crust between the NCD and MFS due to the initiation of subduction at 20 Ma could have facilitated the observed ~90° rotation. If present day slab termination is rotated anticlockwise to its likely position at 20 Ma (e.g. Fig. 5.8), the resulting location corresponds reasonably well with hinge of rotation proposed in Figure 5.4.

Rotation about this hinge line would allow the higher bulk strength proto-MFS region to rotate without accumulating significant internal strain, as indicated by the undeformed nature of the radiating dyke swarm around the Tapuaenuku Igneous Complex (Fig. 5.2B). The relatively lower bulk strength of the NCD may explains the higher amounts of internal deformation such as the region folding of cover rocks south of the Hope Fault (Fig. 5.2C).

The form lines appear to accommodate rotation around this hinge via flexural slip. Rotation being accommodated in this manner does not reflect rotation of individual, rigid crustal faults blocks, as proposed by (Hall et al., 2004; Lamb, 2011; Randall et al., 2011) and does not leave any geometric space problems. Perhaps the only effects of accommodation of rotation via flexural slip around a hinge could be elongation of bedding and associated structural features within the MFS, similar to the limbs of a fold. This could perhaps be an additional contributor to the extremely consistent bedding strike and the elongate faults in the northern MFS.

To summarise this interpretation: we propose the 90° clockwise rotation, which occurred between 20 – 10 Ma, is accommodated by flexural slip around a rotating hinge line located to the south of the present day Hope Fault (Fig 5.4A & 5.8A-C). The hinge line connects to the termination point of the Hikurangi subduction zone and underwent vertical axis rotation about this termination point, coeval and coaxial with the rotation of the subduction zone between 20 – 10 Ma. We propose the hinge was generated due to a change in bulk strength in the crust overlying the subducted slab. Rotation via flexural slip about this hinge describes adequately the rotations shown by the palaeomagnetic and structural data, allowing the bulk proto-MFS to rotate without internal deformation.

10 Ma to present: Development of the MFS

The major MFS faults developed in an orientation consistent with Riedel shears associated with distributed progressive simple shear with a shear plane parallel to the relative plate motion vector for South Island (Chapters 2, 4) (Schreurs, 2003). These faults are also oriented 20° clockwise relative to

the trend of both bedding and older faults in the MFS basement rocks, which they crosscut (Figs. 5.4A,C), and they offset the Esk Head Subterrane dextrally (Hall et al., 2004; Rattenbury et al., 2006). The consistent NNE-SSW trending structural features in the basement are inherited weaknesses from the Gondwanan subduction-accretion complex in which the basement rocks formed. This evidence suggests that the MFS faults may not be inherited accretionary structures and suggests that the MFS could have formed in its present orientation without reactivation of pre-existing crustal-scale weaknesses.

Analogue modelling results show the development of each fault from a region of diffuse faulting, consistent with hypotheses that the PPAFZ is an incipient fifth fault in the system (Cowan et al., 1996). The structural data in Figure 5.4A shows that this diffuse faulting within the NCD has a wider range of orientations than the MFS faults. The diffuse nature of the faulting with a wider array of orientations suggests there is no major pre-existing crustal scale fault in this region to reactivate and form the next major fault in the system. If there were a crustal scale weakness, we would expect the faulting to be localised on this weakness.

The array of orientations within the PPAFZ has been attributed to use of the previously structured crust to grow and evolve (Quigley et al., 2019). However, the basement structures that are suggested to influence to growth of the PPAFZ are on a much smaller scale than the hypothesised crustal scale pre-existing weaknesses. Smaller scale structures within the basement likely have an influence on the locations and propagation of the smaller scale faults in the zone of diffuse faulting, prior to the localisation of this zone of diffuse faulting into a continuous crustal scale fault, which overprints basement structures.

To summarise this interpretation: At 10 Ma the Alpine Fault and Hikurangi subduction zone were close enough to interact but sufficiently misaligned, which caused distributed simple shear to occur across the transition zone between the major plate boundary faults. The MFS developed sequentially southward as crustal scale Riedel shears, to accommodate the basal distributed simple shear occurring across the transition zone (Fig. 5.8C-H). Each fault developed from a zone of diffuse deformation, which localised to form a continuous crustal scale fault. The development of small-scale faults across the zone of diffuse deformation may be influenced by small-scale basement structures, however with continued deformation the tectonic regime prevails and the crustal scale strike-slip fault develops, which overprints the existing structures.

10 Ma – Present: Accommodation of 30° clockwise vertical axis rotation in NE Marlborough

The ~120° rotations in the eastern MFS, recorded by pre 10 Ma rocks, are associated with thrust sheets with strikes that rotate in orientation by up to ~180°. The rocks perhaps record this extreme rotation because they incorporate both the rotation prior to 10 Ma (of ~ 90 °) and the subsequent rotation of the northeast portion of the MFS in the last 10 Myrs (~ 20 ° - 30 °). Hence, these rotations are northeast of

the hinge line proposed by (Little and Roberts, 1997). We propose these rotations occurred via flexural slip around the hinge line proposed by (Little and Roberts, 1997) (Fig.5.4A,B & Fig.5.8C-H). This extra rotation is likely associated with ongoing compression and subsequent toroidal flow of the overriding plate from the subduction zone, and the hinge therefore likely rotated about a vertical axis constrained by the subduction zone (Fig 5.8).

5.6. An alternative interpretation for the structural development of the MFS

A series of schematic diagrams are presented in Figure 5.8 that illustrate proposed new reconstructions of NE South Island and the development of the MFS from 20 Ma to the present. These reconstructions are based on the synthesis of palaeomagnetic and structural data reviewed above and the analogue modelling results presented in Chapters 2-4.

5.6.1. Building the schematic reconstruction

The schematic reconstructions (Figure 5.8) were made using a combination QGIS and InkScape. The present-day outline of New Zealand was traced from Google Earth imagery and the major faults were added from GNS fault data (© GNS Science 2016) using the Geotrace plugin in QGIS (Thiele et al., 2017). This map was then imported into Inkscape and the Hikurangi subduction zone and Chatham Rise were added from Randall et al. (2011). The geological units were simplified and added from GNS shapefile data.

Key aspects of the reconstruction or retrodeformation from the present day back to 20 Ma were carried out by conforming to the following 'rules' (from Section 5.5.2):

From 0 Ma to 10 Ma: The Esk Head Subterrane is gradually restored as each major MFS fault is removed at ~ 2 Ma intervals. Each 2 Ma interval also incurs a 5° anticlockwise rotation about the northeast hinge proposed by (Little and Roberts, 1997) of structures northeast of this hinge, including the small section of the North Island that is included in the diagrams (Fig 5.8C-H). This axis for this rotation is the point where the proposed hinge intersects the Hikurangi subduction zone. A total of 30° anticlockwise rotation is therefore removed from 0 Ma to 10 Ma. North Island also rotates anticlockwise 30 ° over this 10 Ma period and ~140 km of dextral slip is restored on the Wairau Fault over the same interval.

From 10 Ma to 20 Ma: The Hikurangi subduction zone, the hinge line to the south of the present-day Hope Fault and everything to the north of that hinge line in the 10 Ma schematic, are rotated 90 ° anticlockwise from their position at 10 Ma (this also corresponds to their present-day locations). The vertical axis for this rotation is coincident with the southern termination of the Hikurangi subduction zone against the Chatham Rise. For simplicity and assuming steady-state conditions, we apply a 45° anticlockwise between each of 10 to 15 Ma and 15 to 20 Ma. The same rotations are also applied to

bedding form lines north of the hinge line, while bedding to the south does not rotate. This is achieved by rotating the entire system about the termination of the Hikurangi subduction zone and then bending the form lines where they cross the hinge line to restore the rotation to the south/east of the hinge line.

It should be noted that this reconstruction applies only to the MFS and NCD in South Island. The southern edge of the North Island has been added to Figure 5.8 to show the continuation of the Esk Head Subterrane into North Island and its offset by the Wairau Fault. We have purposely not attempted to restore specific details in the development of North Island, such as the offset of the North Island Shear Belt or extension within the Havre Trough. Likewise, specific details of the structural development of the Alpine Fault in northern South Island have also been omitted.

5.6.2. Structural history of NE South Island from 20 Ma to present

20 – 10 Ma

The propagation of active subduction along the Hikurangi subduction zone reaches the continental Chatham Rise by 20 Ma where the subduction zone terminates. The position of the subduction zone at 20 Ma shown in Figure 5.8A is consistent with other reconstructions (King, 2000; Wood and Stagpoole, 2007; Lamb, 2011; Randall et al., 2011). The Torlesse terrane sits south of the Chatham Rise and its internal structures parallel the Cretaceous Gondwanan subduction-accretionary complex (MacKinnon, 1983; Reay and Pye, 1993; Bassett and Orlowski, 2004; Rattenbury et al., 2006; Willis, 2017). The Alpine Fault, which initiated at 25 Ma (Lamb et al., 2016) is well established to the south but is still some distance from the Hikurangi subduction zone (and therefore is not shown in Fig. 5.8A,B) and the two plate boundaries are not connected.

Following the termination of subduction against the Chatham Rise, clockwise rotation of the Hikurangi subduction zone begins. The termination of the subducting slab creates a change in bulk strength of the overlying lithosphere (Randall et al., 2011), whereby cool strong lithosphere overlies the subducting slab, and warm weak lithosphere occurs to the south. This change in bulk strength of lithosphere creates a hinge in the overlying lithosphere that is corresponds with the lateral edge of the underlying subducting slab. Between 20 and 10 Ma this hinge and everything to its west rotates ~90° clockwise with the Hikurangi subduction zone, about its termination with the Chatham Rise (Fig 5.8A-C). This allows bulk vertical axis rotation the region that will form the MFS, without any internal deformation, allowing the Tapuaenuku igneous complex and its radiating dyke swarm to remain undeformed. The rotation of the hinge causes the Torlesse basement terrane to its west, which parallels the Chatham Rise, to be dragged in to northeast South Island. Despite being dragged into northeast South Island, the basement to the west of the hinge line does not rotate (5.8A-C), consistent the palaeomagnetic data and the structural trend of the basement rock. The proposed ~ 90 ° clockwise rotation being accommodated in this manner is consistent numerical models for the rotation of the Hikurangi subduction zone by

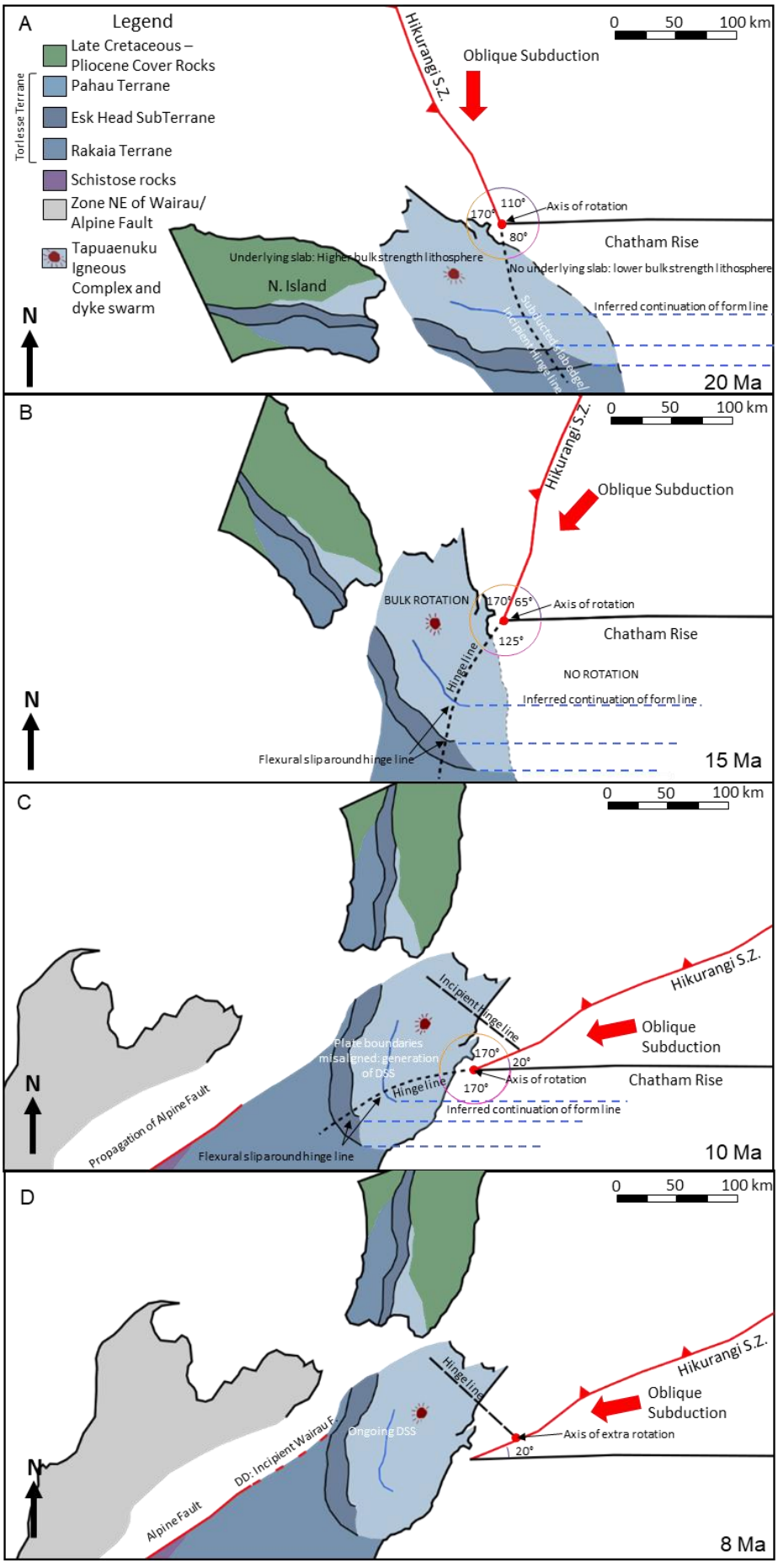
A
Legend
Late Cretaceous – Pliocene Cover Rocks
Torlesse Terrane
Pahau Terrane
Esk Head SubTerrane
Rakaia Terrane
Schistose rocks
Zone NE of Wairau/ Alpine Fault
Tapuaenuku Igneous Complex and dyke swarm
N
0 50 100 km
Hikurangi S.Z.
Oblique Subduction
110°
170°
80°
Axis of rotation
Chatham Rise
Underlying slab: Higher bulk strength lithosphere
N. Island
No underlying slab: lower bulk strength lithosphere
Inferred continuation of form line
Subducted plate edge/ Incipient Hinge line
20 Ma
B
0 50 100 km
Hikurangi S.Z.
Oblique Subduction
BULK ROTATION
170°
65°
Axis of rotation
Chatham Rise
125°
Hinge line
NO ROTATION
Inferred continuation of form line
Flexural slip around hinge line
N
15 Ma
C
0 50 100 km
Hikurangi S.Z.
Incipient Hinge line
Oblique Subduction
Plate boundaries misaligned: generation of DSS
170°
20°
Axis of rotation
Chatham Rise
Hinge line
170°
Inferred continuation of form line
Propagation of Alpine Fault
Flexural slip around hinge line
N
10 Ma
D
0 50 100 km
Hikurangi S.Z.
Hinge line
Oblique Subduction
Ongoing DSS
Axis of extra rotation
20°
DD: Incipient Wairau F.
Alpine Fault
N
8 Ma

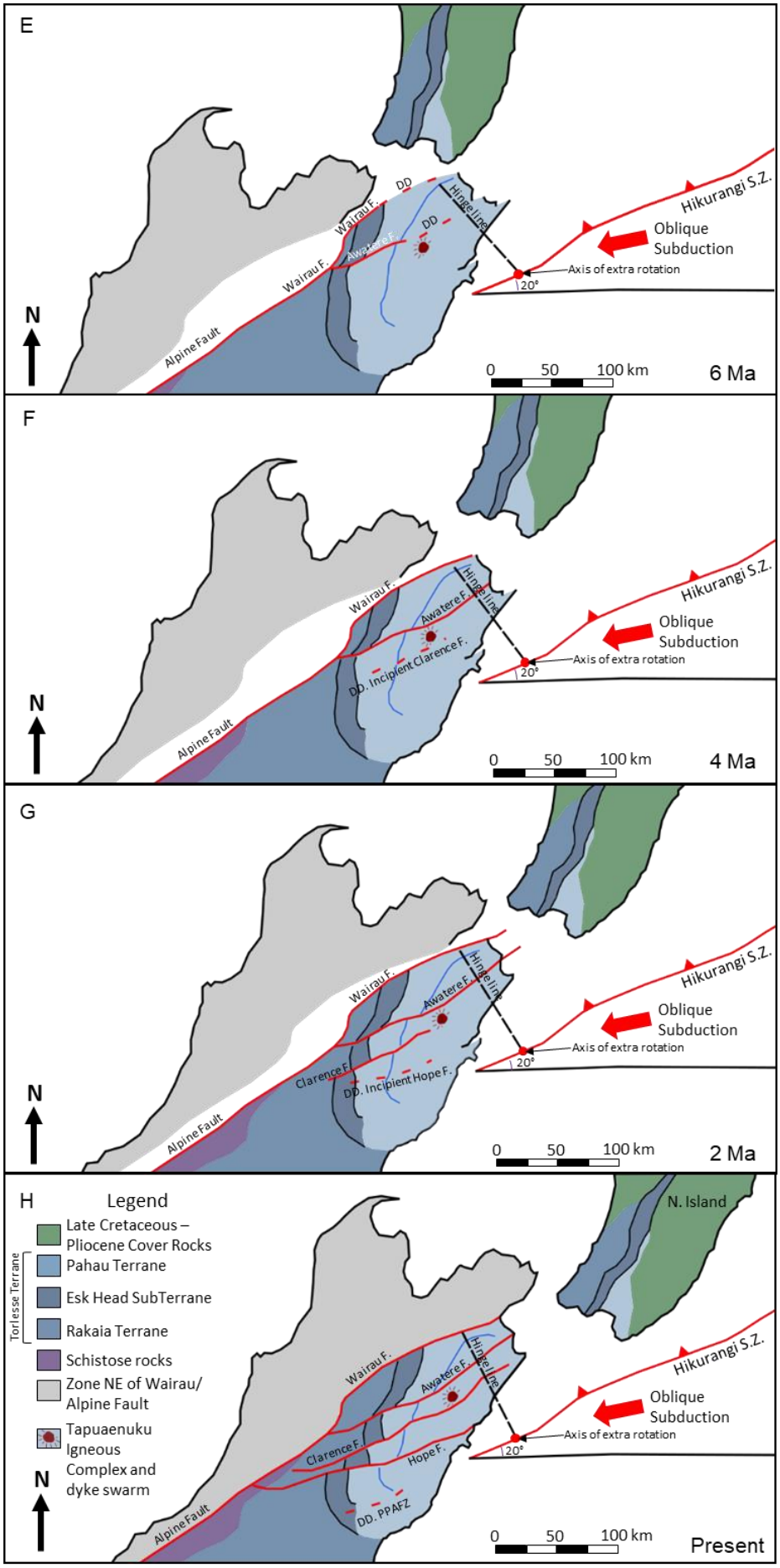
E
DD
Hinge line
Wairau F.
Awatere F.
DD
Wairau F.
Alpine Fault
Hikurangi S.Z.
Oblique Subduction
Axis of extra rotation
20°
N
0 50 100 km
6 Ma
F
Wairau F.
Hinge line
Awatere F.
DD. Incipient Clarence F.
Alpine Fault
Hikurangi S.Z.
Oblique Subduction
Axis of extra rotation
20°
N
0 50 100 km
4 Ma
G
Wairau F.
Hinge line
Awatere F.
Clarence F.
DD. Incipient Hope F.
Alpine Fault
Hikurangi S.Z.
Oblique Subduction
Axis of extra rotation
20°
N
0 50 100 km
2 Ma
H
Legend
Late Cretaceous – Pliocene Cover Rocks
Torlesse Terrane
Pahau Terrane
Esk Head SubTerrane
Rakaia Terrane
Schistose rocks
Zone NE of Wairau/ Alpine Fault
Tapuaenuku Igneous Complex and dyke swarm
N
N. Island
Wairau F.
Hinge line
Awatere F.
Clarence F.
Hope F.
DD. PPAFZ
Alpine Fault
Hikurangi S.Z.
Oblique Subduction
Axis of extra rotation
20°
0 50 100 km
Present

Figure 5.8. (Above) Schematic reconstruction of northeast South Island, New Zealand from 20 Ma to present, with simplified geological units (see legend) modified from shapefile data © GNS Science 2016. Bulk ~ 90° clockwise rotation between 20 Ma and 10 Ma occurs by flexural slip around a rotating hinge. The hinge is generated by a change in bulk strength of the lithosphere overlying the subducted slab. The hinge rotates around the termination point of the Hikurangi subduction zone, coeval with the rotation of the subduction zone. Distributed simple shear (DSS) begins at 10 Ma, causing the sequential southward development of the MFS from zones of diffuse deformation (DD) from 10 Ma to present. An extra ~ 30° clockwise rotation has occurred around a hinge in the northeast of the system since 10 Ma.

Willis, (2017) and models of congested subduction and orocline development by Moresi et al., (2014), in toroidal flow of the crust occurs around the rotating subduction zone.

10 Ma

The Alpine Fault has propagated to within ~ 200 km of the Hikirangi subduction zone (Fig. 5.8C). The locations and orientations of the Hikurangi plate margin and the Alpine Fault are sufficient to initiate distributed simple shear across the transition zone between the two plate boundaries (Wilson et al., 2004; Wannamaker et al., 2009; Eberhart-Phillips and Bannister, 2010). Accommodation of deformation by distributed deformation causes the rotation of the Hikurangi subduction zone and its associated basement and cover rocks to cease.

8 Ma

A zone of diffuse faulting develops over the region of the present day Wairau and Awatere faults, caused by distributed deformation (5.8D).

6 Ma

The Wairau and Awatere faults develop sequentially, with the bulk of the deformation being accommodated on the Wairau Fault, which develops as a continuation of the Alpine Fault (5.8E). Further south in the transition zone, a zone of diffuse faulting develops over the region of the present day Clarence Fault, where transpression also begins due to a component of compression of the overriding plate from the subduction zone. This transpression causes the northeast portion of the MFS to begin to rotate clockwise about the hinge proposed by Little and Roberts (1997).

4 Ma

The Clarence Fault initiates as a strike-slip fault (5.8F). This fault develops in the centre of the transition zone between plate boundaries and propagates outwards towards the Alpine Fault and the Hikurangi subduction zone, consistent with the fault propagation model proposed by Ghisetti (2021) and field observations by Vermeer et al. (2021). Diffuse faulting develops over the present day Hope Fault and rotation of the NE corner of the system is ongoing.

2 Ma

The Hope Fault develops in the same manner as the Clarence Fault, propagating back towards the Alpine Fault and towards the Hikurangi subduction zone from the centre of the transition zone (Fig 5.8G). The PPAFZ begins to develop to the south of the Hope Fault. Rotation of the northeast corner of the system is ongoing.

Present Day

These processes since 20 Ma lead to the present-day MFS and NCD. The MFS has developed into a series of four well-established crustal scale faults, accommodating the bulk of deformation across the transition zone between the Alpine Fault and the Hikurangi subduction zone (Fig. 5.8H). The evolution of the PPAFZ into a continuous fault is ongoing.

5.7. Conclusions

Published palaeomagetic data from northeast South Island show that the geology within the MFS underwent a clockwise ~90° rigid body rotation between 20 Ma and 10 Ma. The rotation in basement strike is also consistent with palaeomagnetic rotations in the NCD and MFS. A hinge line can be defined south of the Hope Fault that separate basement rocks to north that underwent a distinct ~90° clockwise rotation from those to the south in the NCD that did not rotate (Fig. 5.4). This proposed hinge line links with the termination of the Hikurangi subduction zone (Figs. 5.4, 5.8). We propose that this hinge line location coincides with the surface projection of the termination of the underlying slab at 20 Ma, which caused a change in bulk strength of the lithosphere from warm and weak south of the slab, to cool and strong above the slab. Rotation of the hinge line occurred about a vertical axis constrained by the subduction zone termination, and was coeval and coaxial with rotation of the subduction zone. Rotation of the overlying crust occurred by flexural slip about this hinge line, similar to how bedding bends around an axial trace of a fold. Flexural slip around this hinge line caused bulk rotation of the region of the proto-MFS without any internal strain, and no rotation to the east of the hinge line, without the requirement of pre-existing crustal scale weaknesses to accommodate vertical block rotation.

At 10 Ma, bulk vertical axis rotation of northeast South Island ceased when the Alpine Fault and Hikurangi subduction zone were close enough but suitably ‘misaligned’ to generate distributed deformation between the two plate boundaries. From 6 Ma to present day, the MFS developed sequentially southward across the transition zone, with each fault developing from a zone of diffuse deformation that developed into a continuous, crustal scale fault that crosscut bedding, pre-existing faults and terrane boundaries within the basement, without requiring the reactivation of a pre-existing crustal scale faults (Fig 5.8C-H).

Palaeomagnetic rotations within the last 10 Ma are limited to the northeast corner of the MFS, which has rotated clockwise by ~30° and occurred by flexural slip about a hinge line proposed in Little and

Roberts' (1997) ‘flexed telephone book’ model (Fig. 5.8C-H). This rotation is attributed ongoing compression in the overlying plate from the subduction zone.

The evolutionary model for the MFS proposed here combines aspects from previous hypotheses (Little and Roberts, 1997; Hall et al., 2004; Randall et al., 2011; Willis, 2017; Ghisetti, 2021) (Chapters 2 & 4) and satisfies all existing palaeomagnetic, geological and structural datasets, as well as findings from recent analogue laboratory experiments. The model is also consistent with the development of similar fault patterns at the termination of other major transform faults, including the southern termination of the San Andreas Fault and the western termination of the North Anatolian Fault.

Chapter 6

Discussion and Conclusions

6.1. Key Findings

This thesis investigates the development of fault networks that accommodate deformation across plate boundary transition zones in which a continental transform fault is 'misaligned' with its connecting plate boundary (e.g., Fig 6.1). To achieve this, a series of scaled analogue experiments were conducted to simulate the first-order strike-slip boundary conditions of continental transform faults and adjacent large transition zones. The resulting analogue models were analysed using Digital Image Correlation (DIC) and X-Ray Computed Tomography (XRCT) scanning techniques, and compared to natural examples. These results were used specifically to provide insight on the development of the Marlborough Fault System (MFS), a plate boundary transition zone located in northeast South Island, New Zealand, which has developed to accommodate deformation between the continental transform Alpine Fault and the Hikurangi Subduction Zone (Fig. 6.1). These results were combined with palaeomagnetic and structural data to propose a new, alternative hypothesis for the development of northeast South Island, New Zealand, from 20 Ma to present day.

Plate boundaries can become misaligned when the plate boundary transition develops by propagation of a transform fault towards its 'connecting' plate boundary. Examples where this occurs in nature are the southern termination of the San Andreas Fault, the northern termination of the Alpine Fault and the western termination of the North Anatolian Fault. We refer to the region where the plate boundary is 'misaligned' as a transition zone. Deformation of the ductile lower crust of these transition zones becomes distributed, rather than being localised on the plate boundary faults (Legg et al., 2004; Wilson et al., 2004; Wannamaker et al., 2009; Eberhart-Phillips and Bannister, 2010) (Fig. 6.1). The upper crustal rocks are therefore subjected to distributed simple shear as a basal boundary condition.

Our analogue experiments show that fault networks that form over regions of distributed simple shear develop as individually operating, equally spaced, crustal scale Riedel shears (Fig. 6.1). The first faults to form over the region of distributed simple shear are those closest to the primary transform fault, with each new continuous fault localising sequentially outwards within a zone of diffuse deformation. Each of these faults propagate from the surface downward to the basal boundary. These faults may also propagate laterally to eventually intersect the primary transform fault, creating a surface fault pattern similar to that of branching splay faults. However, these similar fault patterns do no form in the same manner or scale. As shown by experiments with localised strike-slip deformation above a basal velocity discontinuity and 1-10 km scale natural examples, typical branching splay faults are helicoidal in 3D and propagate upwards from single vertical basement fault to define either positive or negative flower structures. This contrasts with the 10-100 m scale of transition zone faults, which are vertical, propagate downwards from the surface and have an abutting or approaching relationship with the primary transform fault. We therefore argue that faults that develop across transition zones adjacent to continental transform faults should not be classified as splay faults.

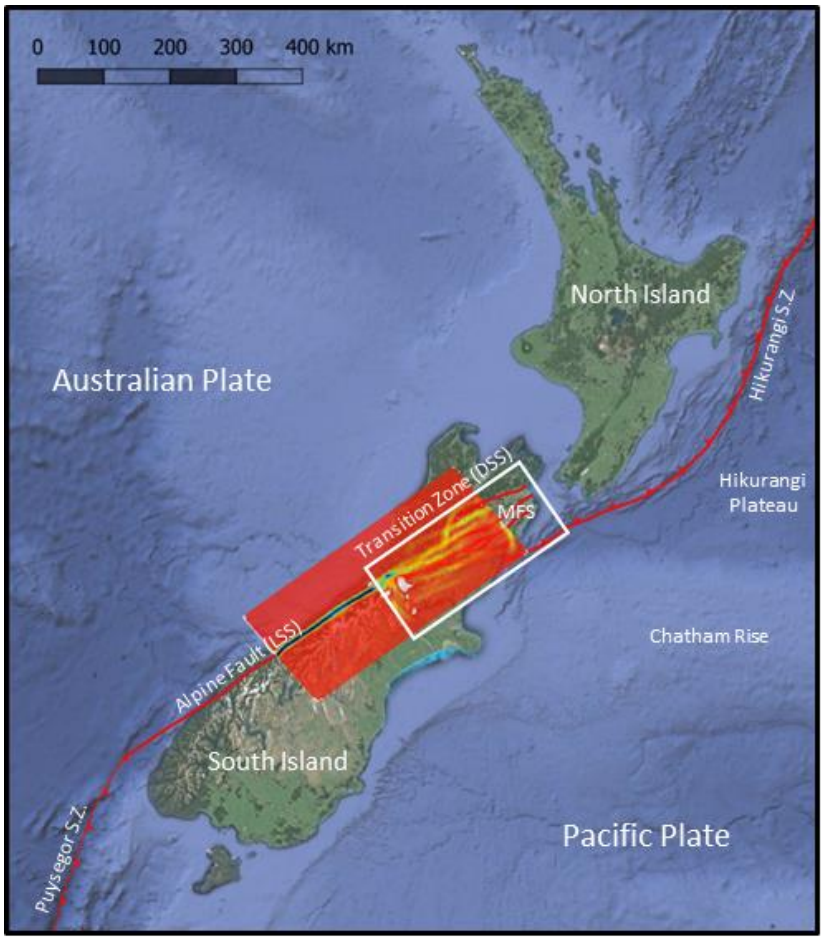

Figure 6.1. Map of New Zealand's major plate boundary faults overlain with the DIC Image of the transition analogue experiment at 30 mm displacement of the sandbox (Experiment 4, Chapter 2. Chapter 4). The transition zone between the Alpine Fault and Hikurangi Subduction Zone (S.Z.) is highlighted, this is the location where the Marlborough Fault System (MFS) has developed to accommodate plate motion. The transition zone has developed because the Alpine Fault is 'misaligned' with the Hikurangi subduction zone, which has caused a transition from localised simple shear (LSS) along the Alpine Fault to distributed simple shear (DSS) across the transition zone.

The MFS has been hypothesised to have developed by sequential reactivation of pre-existing crustal scale weaknesses from ~ 6 Ma to present day (Little and Roberts, 1997; Townsend, 2001; Hall et al., 2004; Wilson et al., 2004; Wood and Stagpoole, 2007; Wannamaker et al., 2009; Randall et al., 2011; Ghisetti, 2021). These crustal scale weaknesses are proposed to have developed as part of a subduction-accretion complex associated with a subduction zone that was active at the margin of Gondwana during the Cretaceous. However, our experimental results suggest that the development of the MFS did not require pre-existing crustal scale weaknesses to be present (Fig. 6.1). The sequential localisation of each fault from a zone of diffuse deformation is consistent with observations from the present-day Porters Pass to Amberley Fault Zone (PPAFZ), south of the MFS, which may represent an incipient fifth fault in the MFS system (Cowan et al., 1996). The timing of development of faults within the analogue experiments scales favourably with distributed simple shear developing across the transition zone at ca.

10 Ma, which is the hypothesised to be the time when the Alpine Fault and Hikurangi subduction zone began to interact (Randall et al., 2011).

Our analogue experiments indicate that the PPAFZ may be undergoing a significant increase in shear strain due to this ongoing localisation process, and speculate that this was the likely cause for the initiation of the 2016 Kaikoura earthquake. The complexity of earthquake ruptures within this region south of the Hope Fault may therefore be attributed to the absence of a major crustal scale fault in this part of the region.

Palaeomagnetic data from northeast South Island, New Zealand, indicate that the region that would later form the MFS underwent a 90° clockwise vertical axis rotation between 20 and 10 Ma (Lamb, 2011; Randall et al., 2011). This rotation is coincident and coeval with an oroclinal event, which saw the Hikurangi subduction zone rotate 90° clockwise about its termination with the Chatham Rise. Structural features such as the radiating Cretaceous Tapuaenuku dyke swarm and the remarkably consistent strike of basement structures within the region indicate that there has been minimal internal deformation of the MFS basement rocks. We propose that this rotation occurred by flexural slip about a rotating 'hinge' to the south of the present day MFS, which is defined by a distinct 90° change in strike of basement structures and connects to the southern termination of the Hikurangi subduction zone. This hinge may have been generated by a change in bulk strength of the crust overlying the subducting slab and the hinge rotation was coincident and coeval with rotation of the Hikurangi subduction zone, occurring about the southern termination of the subduction zone. Rotation around this hinge allowed bulk rotation of the proto-MFS without internal strain and without requiring the presence of pre-existing crustal scale faults to accommodate rigid block rotation.

Bulk rotation of NE South Island stopped at 10 Ma. At this time, distributed shear began to develop across the transition zone between the Alpine Fault and the Hikurangi subduction zone. We suggest that the onset of distributed simple shear caused sequential southward development of the MFS, overprinting existing structures in the basement rocks. A further 30 ° clockwise rotation has occurred in the NE corner of the MFS region since 10 Ma, which has been attributed to compression in the overriding plate from the subduction zone. This rotation occurred about a hinge line first proposed by Little and Roberts (1997) and we propose that this hinge line also accommodated rotation by flexural slip.

6.2. Suggestions for future work

The following section discusses potential future work that arises from my research project that is outside the scope for completion of this PhD thesis.

6.2.1. Analogue modelling of a transition zone: Distributed simple shear apparatus

Analogue modelling results of this thesis show that the faults that develop over the zone of distributed simple shear are much longer in length but with a similar orientation and spacing to Riedel shears that

develop over a region of localised simple shear, prior to the formation of a through-going strike-slip fault. If we assume the faults that form in the region of distributed simple shear are also Riedel shears, it would be interesting to investigate whether increased bulk displacement would result in these faults being abandoned in favour of a single fault that directly connects the plate boundaries (consistent with observed results over the region of localised deformation). Such a study is beyond the scope of this thesis due to the finite limit of stretch of the material we used at the base of the sandbox. I suggest that such an investigation would require a specially designed analogue apparatus for modelling large finite shear strains in both localised and distributed simple shear and the transition between these regimes (Fig. 6.2). This proposed new sandbox would replace the stretchable material used in this thesis to generate distributed simple shear, with a mechanical shear plate made up of rotating, extendible parallel slats (A.R. Cruden, Personal Communication 2021). Schreurs, (2003) designed a similar sandbox which simulated distributed simple shear across the entire box, however his specially designed basal plate has not been used to simulate a transition between localised and distributed simple shear in a single experiment. Such a specific apparatus would also minimise basal boundary effects in the experiments and would allow the use of a ductile lower crustal analogue beneath the upper crustal analogue. The presence of a lower crustal analogue would allow investigation into the influence of pre-existing crustal scale weaknesses over the region of distributed simple shear, following the method outlined in section 1.4.1.

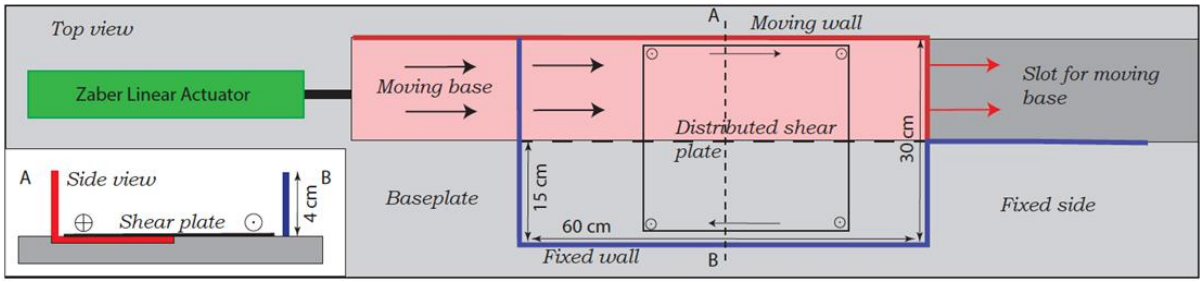

Figure 6.2. Proposed design of analogue shear zone apparatus that will be used to model a transition from localised to distributed simple shear, simulating a plate boundary 'transition zone' (A.R. Cruden, Personal Communication 2021).

6.2.2. Analogue modelling transpression and transtension

This thesis only considers the strike-slip component of transform plate boundaries and transition zones. In nature these plate boundaries have elements of transpression or transtension (despite being dominantly strike-slip). For example, the Alpine Fault is subject to transpression, which has caused the uplift of the Southern Alps, and there is an element of transpression within the MFS, which has caused the uplift of the Seaward and Inland Kaikoura ranges (Chapter 1).

Future work should incorporate transpression and transtension in analogue experiments using the recently developed *Multibox* at the Universität Hamburg. The *Multibox* has the unique capability of

imposing simultaneous horizontal shearing and transverse shortening (Fig. 6.3) (Eisermann et al., 2021). The box consists of two halves, each of which contains a computer controlled, motorised piston. One half can also be displaced laterally relative to the other half in a similar manner to the apparatus used in this thesis. Variations in transpressive or transtensional deformation regimes can be achieved by changing the relative velocities of the box halves orthogonal and parallel to the displacement direction.

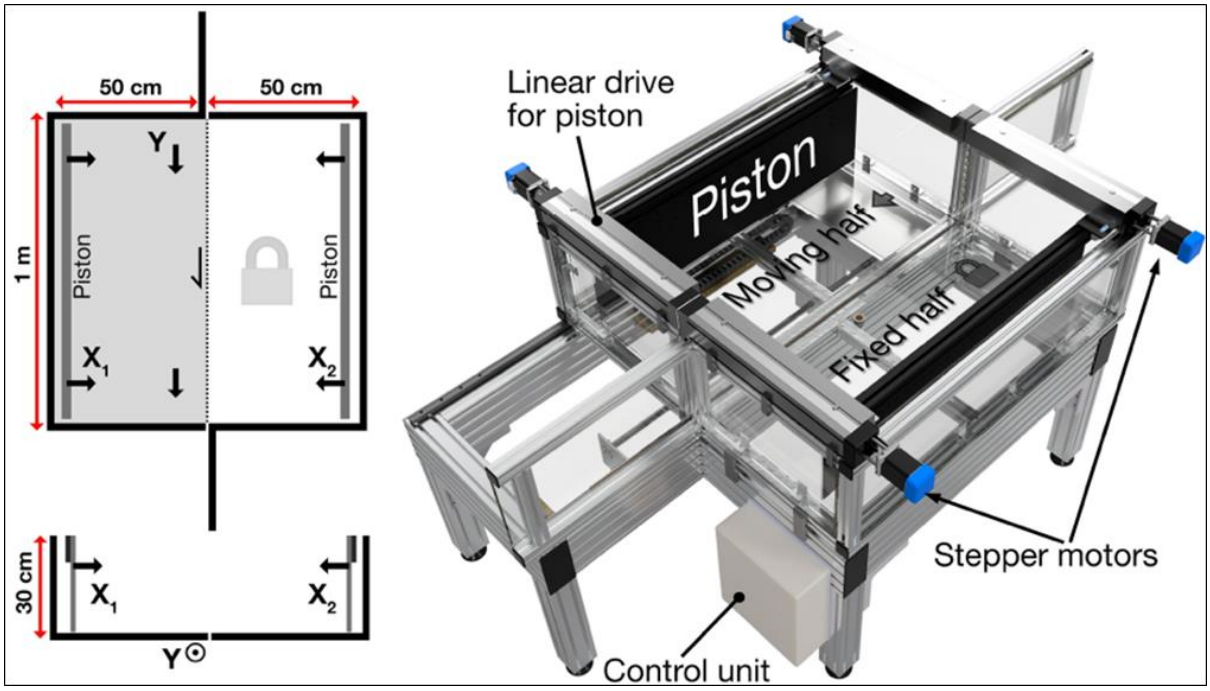

Figure 6.3. Plan view, cross section and 3D CAD rendering of the *MultiBox* apparatus at Universität Hamburg that would allow analogue modelling of transpression and transtension. (From Eisermann et al. (2021)).

6.2.3. Placing the new interpretation for the development of Northeast South Island in a broader context

Chapter 5 focused on the development of northeast South Island, New Zealand. This chapter presents a schematic sequence of diagrams for the development of northeast South Island. Future work should expand this interpretation for the whole of New Zealand.

The roles of North Island, and the regions west of the Alpine Fault and the south of the North Canterbury tectonic domain are not considered in the tectonic model presented in Chapter 5. Analysing palaeomagnetic and structural data for all of New Zealand would be the next step in expanding this interpretation.

6.3 The Kaikoura Earthquake

The 2016 Mw 7.8 Kaikoura earthquake is the most structurally complex earthquake in the modern record (Hamling et al., 2017; Shi et al., 2017; Berryman et al., 2018; Morishita et al., 2018). The 2016

Kaikoura earthquake is associated with ongoing transfer of displacement and stress across the transition zone between the Alpine Fault and Hikurangi subduction zone.

The Kaikoura Earthquake initiated in the North Canterbury Tectonic Domain (NCD). The zone of diffuse faulting in the NCD is yet to develop into a single, through-going fault that propagates from the surface to the lower crust to accommodate displacement across the transition zone, as the other major MFS faults have already done (Cowan et al., 1996).

6.3.1. Possible explanation for the complexity of the Kaikoura earthquake

Results from Chapter 4 suggest that deformation is localising in the PPAFZ and it will eventually develop into an incipient fifth fault in the MFS. This increase in shear strain in the PPAFZ, without the presence of a significant plate boundary fault, may explain the initiation and complex rupture pattern of the Kaikoura earthquake south of the Hope Fault, supporting the work by Ulrich et al. (2019).

Structural analyses of fault and bedding orientations (Chapter 5) indicate that the NCD contains a number a smaller faults with a wider array of orientations when compared to the MFS (Fig 6.4A), which may explain why surface ruptures within this region had such a complex pattern (Hamling et al., 2017; Litchfield et al., 2018; Morishita et al., 2018; Nicol et al., 2018; Williams et al., 2018). Ruptures in the basement rocks of the NCD on faults that had not been previously mapped are oriented more N-S than ruptures on known faults (Hamling et al., 2017; Shi et al., 2017) (Fig. 6.4C). These ruptures followed bedding form lines in basement rocks and likely reactivated pre-existing weaknesses. These reactivations essentially linked the 2016 Kaikoura earthquake ruptures from the region of diffuse faulting in the NCD to the MFS and may have played an important role in the transfer of displacement between these tectonic domains. The scale of these reactivated basement structures is an order of magnitude smaller than the major MFS faults. These basement structures are not crustal-scale weaknesses and will ultimately be abandoned in favour of a crustal-scale fault within the NCD consistent with that of the main MFS faults.

When the earthquake propagated into the MFS, well-established faults were available for ruptures to follow, and so the earthquake was constrained to these faults within the system (Fig. 6.4B). Ruptures occurred on the Fidget and Kekerengu faults (Kearse et al., 2018; Little et al., 2018) (Fig. 6.4C). These faults have a similar orientation to the main MFS faults and they crosscut bedding form lines in basement rocks. The Fidget and Kekerengu faults are thought to have formed to accommodate transpression within the MFS, as explained in Chapter 1.

The results from analogue experiments in Chapter 4 cannot explain the propagation of earthquake ruptures onto the thrust faults within the MFS. I suggest that the Kaikoura earthquake was the result of two different structural processes occurring within the transition zone. The earthquake epicentre and initial ruptures south of the Hope Fault were likely initiated due to a developing strike-slip regime in

the NCD. These ruptures caused a northward cascading effect into the MFS onto faults associated with transpression. This may explain the high amount of energy released on the Kekerengu Fault (Hamling et al., 2017; Berryman et al., 2018), which would have had the largest level of stored elastic strain to be release during the earthquake. Future work, including analogue modelling of transpression, could help investigate this hypothesis.

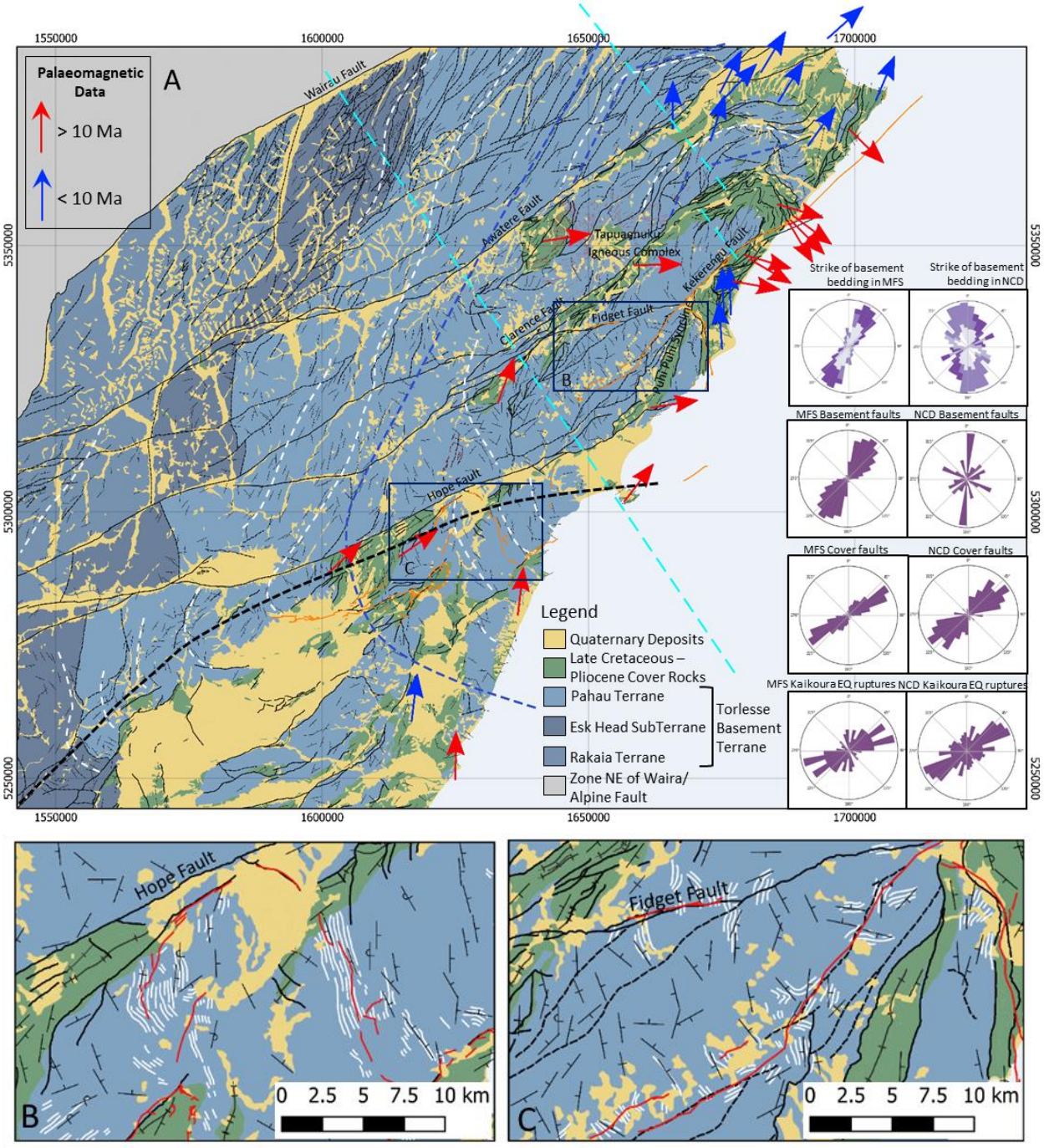

Figure 6.4. A. Simplified geological map of northeast South Island, showing the palaeomagnetic data (arrows) and structural trends of the basement rocks (dashed white and dark blue lines) within the region. (From Chapter 5, Fig. 5.4A). Bedding and fault orientations are illustrated in the rose diagrams. The boxes outline the location for B and C. **B.** Faults that ruptured during the 2016 Kaikoura earthquake in the North Canterbury Tectonic Domain (to the south of the Hope Fault), which had not been mapped prior to their rupture during the earthquake. **C.** Faults that ruptured during the Kaikoura earthquake within a section of the Marlborough Fault System.

6.4 Concluding Remarks

Continental transform faults accommodate hundreds of kilometres of strike-slip plate motion, and their role is to 'transform' plate motion between their connecting plate boundaries. Where the plate boundary connection develops by propagation of the transform fault towards the existing plate boundary, the plate boundaries can become 'misaligned'. Relative plate motion must therefore be transferred across a broad intervening transition zone between the two plate boundaries. The result of analogue experiments presented in this thesis show that faults that form within these transition zones develop in a consistent and predictable manner, related to distributed simple shear of the brittle upper crust. These faults are effectively crustal-scale Riedel shears that localise sequentially across the transition zone. The consistency between the experimental results and the present-day Marlborough Fault System in NE South Island, New Zealand (Fig. 6.1) suggests that this fault system did not require reactivation of pre-existing crustal-scale weaknesses, and that it likely developed in a similar manner to other transition zones, including the southern termination of the San Andreas Fault, and the western termination of the North Anatolian Fault.

References

Adam, J., Klinkmüller, M., Schreurs, G., Wieneke, B., 2013. Quantitative 3D strain analysis in analogue experiments simulating tectonic deformation: Integration of X-ray computed tomography and digital volume correlation techniques. Journal of Structural Geology 55, 127–149. https://doi.org/10.1016/j.jsg.2013.07.011

Adam, J., Urai, J.L., Wieneke, B., Oncken, O., Pfeiffer, K., Kukowski, N., Lohrmann, J., Hoth, S., van der Zee, W., Schmatz, J., 2005. Shear localisation and strain distribution during tectonic faulting—new insights from granular-flow experiments and high-resolution optical image correlation techniques. Journal of Structural Geology 27, 283–301.

Adams, J., 1980. Contemporary Uplift and Erosion of the Southern Alps, New Zealand. Geological Society of America Bulletin 91, 1–114.

Altamimi, Z., Métivier, L., Collilieux, X., 2012. ITRF2008 plate motion model. JOURNAL OF GEOPHYSICAL RESEARCH 117, 1–14. https://doi.org/10.1029/2011JB008930

Ando, R., Shaw, B.E., Scholz, C.H., 2009. Quantifying natural fault geometry: Statistical of splay fault angles. Bulletin of the Seismological Society of America 99, 389–395. https://doi.org/10.1785/0120080942

Audru, J.-C., Delteil, J., 1998. Evidence for early miocene wrench faulting in the Marlborough fault system, New Zealand: structural implications. Geodinamica Acta 11, 233–247. https://doi.org/https://doi.org/10.1016/S0985-3111(99)80012-6

Baker, J., Seward, D., 1996. Timing of Cretaceous extension and Miocene compression in northeast South Island, New Zealand: Constraints from Rb-Sr and fission-track dating of an igneous pluton. Tectonics (Washington, D.C.) 15, 976–983.

Barnes, P.M., 1994. Continental extension of the Pacific Plate at the southern termination of the Hikurangi subduction zone: The North Mernoo Fault Zone, offshore New Zealand. Tectonics 13, 735–754.

Barnes, P.M., De Lépinay, B.M., Collot, J.Y., Delteil, J., Audru, J.C., 1998. Strain partitioning in the transition area between oblique subduction and continental collision, Hikurangi margin, New Zealand. Tectonics 17, 534–557. https://doi.org/10.1029/98TC00974

Bassett, K.N., Orlowski, R., 2004. Pahau Terrane type locality: Fan delta in an accretionary prism trench slope basin. New Zealand Journal of Geology and Geophysics 47, 603–623.

Beavan, J., Matheson, D., Denys, P., 2004. A vertical deformation profile across the Southern Alps, New Zealand, from 3.5 years of continuous GPS data. Proceedings of the Cahiers Du Centre Europ´een de G´eodynamique et de S´eismologie Workshop: The State of GPS Vertical Positioning Precision: Separation of Earth Processes by Space Geodesy, Luxembourg 23, 111–123.

Beavan, J., Wallace, L.M., Palmer, N., Denys, P., Ellis, S., Hreinsdottir, S., Pearson, C., Denham, M., Beavan, J., Wallace, L.M., Palmer, N., Denys, P., Ellis, S., Fournier, N., Hreinsdottir, S., Pearson, C., Denham, M., Zealand, N., 2016. New Zealand GPS velocity field : 1995 – 2013. New Zealand Journal of Geology and Geophysics ISSN: 59, 5–18. https://doi.org/10.1080/00288306.2015.1112817

Beidinger, A., Decker, K., 2011. 3D geometry and kinematics of the Lassee flower structure: Implications for segmentation and seismotectonics of the Vienna Basin strike-slip fault, Austria.,

Tectonophysics. https://doi.org/10.1016/j.tecto.2010.11.006

Bennett, R.A., Friedrich, A.M., Furlong, K.P., 2004. Codependent histories of the San Andreas and San Jacinto fault zones from inversion of fault displacement rates. Geology 32, 961–964. https://doi.org/10.1130/G20806.1

Berryman, K., Hamling, I., Kaiser, A., Stahl, T., 2018. Introduction to the Special Issue on the 2016 Kaikōura Earthquake. Bulletin of the Seismological Society of America 108, 1491–1495. https://doi.org/10.1785/0120180131

Bilich, A., Frohlich, C., Mann, P., 2004. Global seismicity characteristics of subduction-to-strike-slip transitions. Journal of Geophysical Research: Solid Earth 106, 19443–19452. https://doi.org/10.1029/2000jb900309

Boiret, M., Rutledge, D.N., Gorretta, N., Ginot, Y.-M., Roger, J.-M., 2014. Welcome to Dropbox ! Journal of Pharmaceutical and Biomedical Analysis 90, 78–84.

Bond, C.E., Gibbs, A.D., Shipton, Z.K., Jones, S., 2007a. What do you think this is? "Conceptual uncertainty" In geoscience interpretation. GSA Today 17, 4–10. https://doi.org/10.1130/GSAT01711A.1

Bond, C.E., Johnson, G., Ellis, J.F., 2015. Structural model creation: the impact of data type and creative space on geological reasoning and interpretation. Geological Society Special Publication 421, 83–97.

Bond, C.E., Philo, C., Shipton, Z.K., 2011. When there isn't a right answer: Interpretation and reasoning, key skills for twenty-first century geoscience. International Journal of Science Education 33, 629–652. https://doi.org/10.1080/09500691003660364

Bond, C.E., Shipton, Z.K., Jones, R.R., Butler, R.W.H., Gibbs, A.D., 2007b. Knowledge transfer in a digital world: Field data acquisition, uncertainty, Visualization, and data management. Geosphere 3, 568–576. https://doi.org/10.1130/GES00094.1

Boutelier, D., 2016. TecPIV-A MATLAB-based application for PIV-analysis of experimental tectonics. Computers and Geosciences 89, 186–199. https://doi.org/10.1016/j.cageo.2016.02.002

Boutelier, D., Cruden, A., 2013. Slab rollback rate and trench curvature controlled by arc deformation. Geology 41, 911–914. https://doi.org/10.1130/G34338.1

Boutelier, D., Schrank, C., Regenauer-Lieb, K., 2019. 2-D finite displacements and strain from particle imaging velocimetry (PIV) analysis of tectonic analogue models with TecPIV. Solid Earth 10, 1123–1139. https://doi.org/10.5194/se-10-1123-2019

Brace, W.F., Bombolakis, E.G., 1963. A note on brittle crack growth in compression. Journal of Geophysical Research 68, 3709–3713.

Browne, G.H., 1992. The northeastern portion of the clarence fault: Tectonic implications for the late neogene evolution of marlborough, New Zealand. New Zealand Journal of Geology and Geophysics 35, 437–445. https://doi.org/10.1080/00288306.1992.9514538

Butler, R.F., 1992. PALEOMAGNETISM - MAGNETIC DOMAINS TO GEOLOGIC TERRANES. Blackwell Scientific Publishing, LONDON.

Byerlee, J., 1978. Rock friction and earthquake prediction, Contributions to current research in geophysics ; 6. Birkhäuser, Basel.

Casas, A.M., Gapais, D., Nalpas, T., Besnard, K., Román-Berdiel, T., 2001. Analogue models of transpressive systems. Journal of Structural Geology 23, 733–743. https://doi.org/10.1016/S0191-8141(00)00153-X

Christie-Blick, N., Biddle, K.T., 1985. Deformation and Basin Formation Along Strike-Slip Faults.

Collett, C.M., Duvall, A.R., Flowers, R.M., Tucker, G.E., Upton, P., 2019. The timing and style of oblique deformation within New Zealand's Kaikōura Ranges and Marlborough Fault System based on low-temperature thermochronology, Tectonics. https://doi.org/10.1029/2018TC005268

Cooke, M.L., Toeneboehn, K., Hatch, J.L., 2020. Onset of slip partitioning under oblique convergence within scaled physical experiments. Geosphere (Boulder, Colo.) 16, 875–889.

Cowan, H., Nicol, A., Tonkin, P., 1996. A comparison of historical and paleoseismicity in a newly formed fault zone and a mature fault zone, North Canterbury, New Zealand. Journal of Geophysical Research: Solid Earth 101, 6021–6036. https://doi.org/10.1029/95jb01588

Crowell, J.C., 1973. Origin of late Cenozoic basins in southern California. The American Association of Petroleum Geologists Bulletin 57, 774.

Cruden, A.R., Nasseri, M.H.B., Pysklywec, R., 2006. Surface topography and internal strain variation in wide hot orogens from three-dimensional analogue and two-dimensional numerical vice models. Geological Society Special Publication 253, 79–104.

Cunningham, W.D., Mann, P., 2007. Tectonics of strike-slip restraining and releasing bends. Geological Society Special Publication 290, 1–12. https://doi.org/10.1144/SP290.1

Davy, P., Cobbold, P.R., 1991. Experiments on shortening of a 4-layer model of the continental lithosphere. Tectonophysics 188, 1–25.

DeMets, C., Gordon, R.G., Argus, D.F., 2010. Geologically current plate motions. Geophysical Journal International 181, 1–80.

Dewey, J.F., Holdsworth, R.E., Strachan, R.A., 1998. Transpression and transtension zones. Geological Society, London, Special Publications 135, 1–14. https://doi.org/10.1144/GSL.SP.1998.135.01.01

Dickinson, W.R., Snyder, W.S., 1979a. Geometry of Subducted Slabs Related to San Andreas Transform. The Journal of Geology 87, 609–627.

Dickinson, W.R., Snyder, W.S., 1979b. Geometry of triple junctions related to San Andreas Transform. Journal of Geophysical Research: Solid Earth 84, 561–572.

Dooley, T.P., Schreurs, G., 2012. Analogue modelling of intraplate strike-slip tectonics: A review and new experimental results. Tectonophysics 574–575, 1–71. https://doi.org/10.1016/j.tecto.2012.05.030

Dorsey, R.J., Axen, G.J., Peryam, T.C., Kairouz, M.E., 2012. Initiation of the southern Elsinore fault at ~1.2 Ma: Evidence from the Fish Creek-Vallecito Basin, southern California. Tectonics 31, 1–21. https://doi.org/10.1029/2011TC003009

Eberhart-Phillips, D., Bannister, S., 2010. 3-D imaging of Marlborough, New Zealand, subducted plate and strike-slip fault systems. Geophysical Journal International 182, 73–96. https://doi.org/10.1111/j.1365-246X.2010.04621.x

Eberhart-Phillips, D., Reyners, M., 1997. Continental subduction and three-dimensional crustal structure: The northern South Island, New Zealand. Journal of Geophysical Research: Solid Earth 102, 11843–11861.

Eisermann, J.O., Göllner, P.L., Riller, U., 2021. Orogen-scale transpression accounts for GPS velocities and kinematic partitioning in the Southern Andes. Communications Earth & Environment 2, 1–10.

Fedorik, J., Toscani, G., Lodolo, E., Civile, D., Bonini, L., Seno, S., 2018. Structural analysis and Miocene-to-Present tectonic evolution of a lithospheric-scale, transcurrent lineament: The Sciacca Fault (Sicilian Channel, Central Mediterranean Sea). Tectonophysics 722, 342–355. https://doi.org/10.1016/j.tecto.2017.11.014

Fedorik, J., Zwaan, F., Schreurs, G., Toscani, G., Bonini, L., Seno, S., 2019. The interaction between strike-slip dominated fault zones and thrust belt structures : Insights from 4D analogue models. Journal of Structural Geology 122, 89–105. https://doi.org/10.1016/j.jsg.2019.02.010

Fossen, H., 2010. Structural Geology. Cambridge University Press, Leiden.

Frodeman, R., 1995. Geological reasoning; geology as an interpretive and historical science. Geological Society of America Bulletin 107, 960–968.

Furlong, K.P., Kamp, P.J.J., 2009. The lithospheric geodynamics of plate boundary transpression in New Zealand: Initiating and emplacing subduction along the Hikurangi margin, and the tectonic evolution of the Alpine Fault system. Tectonophysics 474, 449–462. https://doi.org/10.1016/j.tecto.2009.04.023

Gardiner, N.P., Hall, M., 2021. Discordant forearc deposition and volcanism preceding late-Cretaceous subduction shutdown in Marlborough, north-eastern South Island, New Zealand. Earth-Science Reviews 214, 103530.

Gardiner, N.P., Hall, M., Frears, B.T., Lovell, R.W.W., 2022. A stratigraphic record from syn to post subduction sedimentation in Marlborough, New Zealand, and implications for Gondwana breakup. Marine and Petroleum Geology 105472.

Ghisetti, F.C., 2021. Map-view restorations of the South Island, New Zealand: a reappraisal of the last 10 Myr of evolution of the Alpine and Wairau faults. New Zealand Journal of Geology and Geophysics. https://doi.org/10.1080/00288306.2021.1878243

Grose, L., Ailleres, L., Laurent, G., Caumon, G., Jessell, M., Armit, R., 2021. Realistic modelling of faults in LoopStructural 1.0. Geoscientific Model Development Discussions 1–26. https://doi.org/10.5194/gmd-2021-112

Grose, L., Ailleres, L., Laurent, G., Jessell, M., 2020. LoopStructural 1.0: Time aware geological modelling. Geoscientific Model Development Discussions 1–31. https://doi.org/10.5194/gmd-2020-336

Hall, L.S., Lamb, S.H., Niocaill, C. Mac, 2004. Cenozoic distributed rotational deformation, South Island, New Zealand. Tectonics 23. https://doi.org/10.1029/2002TC001421

Hamling, I.J., Hreinsdóttir, S., Clark, K., Elliott, J., Liang, C., Fielding, E., Litchfield, N., Villamor, P., Wallace, L., Wright, T.J., D'Anastasio, E., Bannister, S., Burbidge, D., Denys, P., Gentle, P., Howarth, J., Mueller, C., Palmer, N., Pearson, C., Power, W., Barnes, P., Barrell, D.J.A., Van Dissen, R., Langridge, R., Little, T., Nicol, A., Pettinga, J., Rowland, J., Stirling, M., 2017. Complex multifault rupture during the 2016 Mw 7.8 Kaikōura earthquake, New Zealand. Science 356. https://doi.org/10.1126/science.aam7194

Harding, T.P., 1985. Seismic characteristics and identification of negative flower structures, positive flower structures, and positive structural inversion. AAPG Bulletin 69, 582–600.

Hatem, A.E., Cooke, M.L., Toeneboehn, K., 2017. Strain localization and evolving kinematic efficiency of initiating strike-slip faults within wet kaolin experiments. Journal of Structural Geology 101, 96–108. https://doi.org/10.1016/j.jsg.2017.06.011

Henrys, S., Wech, A., Sutherland, R., Stern, T., Savage, M., Sato, H., Mochizuki, K., Iwasaki, T., Okaya, D., Seward, A., Tozer, B., Townend, J., Kurashimo, E., Iidaka, T., Ishiyama, T., 2013. SAHKE geophysical transect reveals crustal and subduction zone structure at the southern Hikurangi margin, New Zealand. Geochemistry, Geophysics, Geosystems 14, 2063–2083. https://doi.org/10.1002/ggge.20136

Hornblow, S., Quigley, M., Nicol, A., Van Dissen, R., Wang, N., 2014. Paleoseismology of the 2010 Mw 7.1 Darfield (Canterbury) earthquake source, Greendale Fault, New Zealand. Tectonophysics 637, 178–190.

Hubbert, M.K., 1937. Theory of scale models as applied to the study of geologic structures. Geological Society of America Bulletin 48, 1459–1520.

Hubert-Ferrari, A., King, G., Van Der Woerd, J., Villa, I., Altunel, E., Armijo, R., 2009. Long-term evolution of the North Anatolian Fault: New constraints from its eastern termination. Geological Society Special Publication 311, 133–154. https://doi.org/10.1144/SP311.5

Kearse, J., Little, T.A., van Dissen, R.J., Barnes, P.M., Langridge, R., Mountjoy, J., Ries, W., Villamor, P., Clark, K.J., Benson, A., Lamarche, G., Hill, M., Hemphill-Haley, M., 2018. Onshore to offshore ground-surface and seabed rupture of the Jordan–Kekerengu–Needles fault network during the 2016 Mw 7.8 Kaikōura earthquake, New Zealand. Bulletin of the Seismological Society of America 108, 1573–1595. https://doi.org/10.1785/0120170304

Keller, E.A., Gurrola, L., Tierney, T.E., 1999. Geomorphic criteria to determine direction of lateral propagation of reverse faulting and folding. Geology (Boulder) 27, 515–518.

Kendrick, K.J., Morton, D.M., Wells, S.G., Simpson, R.W., 2002. Spatial and temporal deformation along the northern San Jacinto Fault, southern California; implications for slip rates. Bulletin of the Seismological Society of America 92, 2782–2802.

Khajavi, N., Nicol, A., Quigley, M.C., Langridge, R.M., 2018. Temporal slip-rate stability and variations on the Hope Fault, New Zealand, during the late Quaternary. Tectonophysics 738–739, 112–123. https://doi.org/10.1016/j.tecto.2018.05.001

Kim, Y.S., Peacock, D.C.P., Sanderson, D.J., 2004. Fault damage zones. Journal of Structural Geology 26, 503–517. https://doi.org/10.1016/j.jsg.2003.08.002

Kim, Y.S., Sanderson, D.J., 2006. Structural similarity and variety at the tips in a wide range of strike-slip faults: A review. Terra Nova 18, 330–344. https://doi.org/10.1111/j.1365-3121.2006.00697.x

King, P.R., 2000. Tectonic reconstructions of New Zealand: 40 Ma to the Present. New Zealand Journal of Geology and Geophysics 43, 611–638. https://doi.org/10.1080/00288306.2000.9514913

Klinkmüller, M., 2011. Properties of analogue materials, experimental reproducibility and 2D/3-D deformation quantification techniques in analogue modelling of crustal-scale processes. University of Bern.

Klinkmüller, M., Schreurs, G., Rosenau, M., Kemnitz, H., 2016. Properties of granular analogue model materials: A community wide survey. Tectonophysics 684, 23–38.

Lamb, S., 2011. Cenozoic tectonic evolution of the New Zealand plate-boundary zone: A paleomagnetic perspective. Tectonophysics 509, 135–164. https://doi.org/10.1016/j.tecto.2011.06.005

Lamb, S., Arnold, R., Moore, J.D.P., 2018. Locking on a megathrust as a cause of distributed faulting and fault-jumping earthquakes. Nature Geoscience 11, 871–875.

Lamb, S., Mortimer, N., Smith, E., Turner, G., 2016. Focusing of relative plate motion at a continental transform fault: Cenozoic dextral displacement >700 km on New Zealand's Alpine Fault, reversing >225 km of Late Cretaceous sinistral motion. Geochemistry, Geophysics, Geosystems RESEARCH 17, 1197–1213. https://doi.org/10.1002/2015GC006225.Received

Lamb, S.H., 1988. Tectonic rotations about vertical axes during the last 4 Ma in part of the New Zealand plate-boundary zone. Journal of Structural Geology 10, 875–893.

Lamb, S.H., Bibby, H.M., 1989. The last 25 Ma of rotational deformation in part of the New Zealand plate-boundary zone. Journal of Structural Geology 11, 473–492. https://doi.org/https://doi.org/10.1016/0191-8141(89)90024-2

Langridge, R.M., Berryman, K.R., 2005. Morphology and slip rate of the hurunui section of the hope fault, South Island, New Zealand. New Zealand Journal of Geology and Geophysics 48, 43–57. https://doi.org/10.1080/00288306.2005.9515097

Lazar, M., Ben-Avraham, Z., Garfunkel, Z., 2012. The Red Sea - New insights from recent geophysical studies and the connection to the Dead Sea fault. Journal of African Earth Sciences 68, 96–110. https://doi.org/10.1016/j.jafrearsci.2012.04.001

Legg, M.R., Kemerling, M.J., Francis, R.D., 2004. Termination of strike-slip faults at convergence zones within continental transform boundaries: examples from the California Continental Borderland. Vertical Coupling and Decoupling in the Lithosphere. Geological Society, London, Special Publications, 227, 65–82.

Lewis, K.B., Pettinga, J.R., 1993. The emerging, imbricate frontal wedge of the Hikurangi margin. Sedimentary Basins of the World 2, South P, 225–250.

Lindsey, E.O., Fialko, Y., 2013. Geodetic slip rates in the southern San Andreas Fault system: Effects of elastic heterogeneity and fault geometry. Journal of Geophysical Research. Solid Earth 118, 689–697.

Litchfield, N.J., Van Dissen, R., Sutherland, R., Barnes, P.M., Cox, S.C., Norris, R., Beavan, R.J., Langridge, R., Villamor, P., Berryman, K., Stirling, M., Nicol, A., Nodder, S., Lamarche, G., Barrell, D.J.A., Pettinga, J.R., Little, T., Pondard, N., Mountjoy, J.J., Clark, K., 2014. A model of active faulting in New Zealand. New Zealand Journal of Geology and Geophysics 57, 32–56. https://doi.org/10.1080/00288306.2013.854256

Litchfield, N.J., Villamor, P., van Dissen, R.J., Nicol, A., Barnes, P.M., Barrell, D.J.A., Pettinga, J.R., Langridge, R.M., Little, T.A., Mountjoy, J.J., Ries, W.F., Rowland, J., Fenton, C., Stirling, M.W., Kearse, J., Berryman, K.R., Cochran, U.A., Clark, K.J., Hemphill-Haley, M., Khajavi, N., Jones, K.E., Archibald, G., Upton, P., Asher, C., Benson, A., Cox, S.C., Gasston, C., Hale, D., Hall, B., Hatem, A.E., Heron, D.W., Howarth, J., Kane, T.J., Lamarche, G., Lawson, S., Lukovic, B., McColl, S.T., Madugo, C., Manousakis, J., Noble, D., Pedley, K., Sauer, K., Stahl, T., Strong, D.T., Townsend, D.B., Toy, V., Williams, J., Woelz, S., Zinke, R., 2018. Surface rupture of multiple crustal faults in the 2016 Mw 7.8 Kaikōura, New Zealand, earthquake. Bulletin of the Seismological Society of America 108, 1496–1520. https://doi.org/10.1785/0120170300

Little, A., Jones, A., 1998. Seven million years of strike-slip and related off-fault deformation, northeastern Marlborough fault system, South Island, New Zealand. Tectonics 17, 285–302. https://doi.org/10.1029/97TC03148

Little, T.A., Cox, S., Vry, J.K., Batt, G., 2005. Variations in exhumation level and uplift rate along the oblique-slip Alpine Fault, central Southern Alps, New Zealand. Geological Society of America Bulletin 117, 707–723.

Little, T.A., Roberts, A.P., 1997. Distribution and mechanism of Neogene to present-day vertical axis rotations, Pacific-Australian Plate Boundary Zone, South Island, New Zealand. Journal of Geophysical Research: Solid Earth 102, 20447–20468. https://doi.org/10.1029/97jb01279

Little, T.A., van Dissen, R., Kearse, J., Norton, K., Benson, A., Wang, N., 2018. Kekerengu fault, New Zealand: Timing and size of late holocene surface ruptures. Bulletin of the Seismological Society of America 108, 1556–1572. https://doi.org/10.1785/0120170152

Lohrmann, J., Kukowski, N., Adam, J., Oncken, O., 2003. The impact of analogue material properties on the geometry, kinematics, and dynamics of convergent sand wedges. Journal of Structural Geology 25, 1691–1711.

MacKinnon, T.C., 1983. Origin of the Torlesse terrane and coeval rocks, South Island, New Zealand. Geological Society of America Bulletin. Geological Society of America Bulletin 94, 967–985.

Magistrale, H., Rockwell, T.K., 1996. The central and southern Elsinore fault zone, Southern California. Bulletin of the Seismological Society of America 86, 1793–1803.

Maillot, B., 2013. A sedimentation device to produce uniform sand packs. Tectonophysics 593, 85–94.

Mandl, G. (Georg), 1988. Mechanics of tectonic faulting : models and basic concepts, Developments in structural geology ; 1. Elsevier, Amsterdam.

Manighetti, I., King, G.C.P., Gaudemer, Y., Scholz, C.H., Doubre, C., 2001. Slip accumulation and lateral propagation of active normal faults in Afar. Journal of Geophysical Research: Solid Earth 106, 13667–13696.

Mann, P., 2007. Global catalogue, classification and tectonic origins of restraining- and releasing bends on active and ancient strike-slip fault systems. Geological Society, London, Special Publications 290, 13–142. https://doi.org/10.1144/SP290.2

Mann, P., Grindlay, N., Dolan, J., 1999. Penrose conference report: Subduction to strike-slip transition on plate boundaries. GSA Today July, 14–16.

McClay, K.R., 1990. Deformation mechanics in analogue models of extensional fault systems. Geological Society Special Publication 54, 445–453.

Mcgrath, A.G., 1995. Damage zone geometry around fault tips. Journal of Structural Geology 17, 1011–1024.

Mckenzie, D.P., Morgan, W.J., 1969. Evolution of Triple Junctions. Nature (London) 224, 125–133.

Merriam-Webster, n.d. Merriam-Webster.com dictionary. [WWW Document]. URL www.merriam-webster.com/dictionary/splay (accessed 12.12.21).

Mielke, P., Weinert, S., Bignall, G., Sass, I., 2016. Thermo-physical rock properties of greywacke basement rock and intrusive lavas from the Taupo Volcanic Zone, New Zealand. Journal of Volcanology and Geothermal Research 324, 179–189. https://doi.org/10.1016/j.jvolgeores.2016.06.002

Mills, G.I., Fisc, P.J., 1991. Segmentation and Thrusting Along the Offshore Newport-Inglewood-Rose Canyon Zone of Deformation. AAPG Bulletin 75.

Molnar, N.E., Cruden, A.R., Betts, P.G., 2018. Unzipping continents and the birth of microcontinents. Geology 46, 451–454. https://doi.org/10.1130/G40021.1

Molnar, N.E., Cruden, A.R., Betts, P.G., 2017. Interactions between propagating rotational rifts and linear rheological heterogeneities: Insights from three-dimensional laboratory experiments. Tectonics 36, 420–443. https://doi.org/10.1002/2016TC004447

Moresi, L., Betts, P.G., Miller, M.S., Cayley, R.A., 2014. Dynamics of continental accretion. Nature 508, 245–248. https://doi.org/10.1038/nature13033

Morishita, Y., Kobayashi, T., Fujiwara, S., Yarai, H., 2018. Complex crustal deformation of the 2016 Kaikōura, New Zealand, earthquake revealed by ALOS-2. Bulletin of the Seismological Society of America 108, 1746–1756. https://doi.org/10.1785/0120180070

Morton, D.M., Matti, J.C., 1993. Extension and contraction within an evolving divergent strike-slip fault complex: The San Andreas and San Jacinto fault zones at their convergence in southern California. In: Powell, R. E., Weldon, R. J., II, Matti, J.C. (Ed.), The San Andreas Fault System: Displacement, Palinspastic Reconstruction, and Geologic Evolution: Boulder, Colorado. Geological Society of America, 217–230.

Müller, R.D., Zahirovic, S., Williams, S.E., Cannon, J., Seton, M., Bower, D.J., Tetley, M.G., Heine, C., Le Breton, E., Liu, S., Russell, S.H.J., Yang, T., Leonard, J., Gurnis, M., 2019. A Global

Plate Model Including Lithospheric Deformation Along Major Rifts and Orogens Since the Triassic. Tectonics 38, 1884–1907. https://doi.org/10.1029/2018TC005462

Naylor, M.A., Mandl, G., Supesteijn, C.H.K., 1986. Fault geometries in basement-induced wrench faulting under different initial stress states. Journal of Structural Geology 8, 737–752. https://doi.org/10.1016/0191-8141(86)90022-2

Nicol, A., Beavan, J., 2003. Shortening of an overriding plate and its implications for slip on a subduction thrust , central Hikurangi Margin , New Zealand. Tectonics 22, 1–14. https://doi.org/10.1029/2003TC001521

Nicol, A., Khajavi, N., Pettinga, J.R., Fenton, C., Stahl, T., Bannister, S., Pedley, K., Hyland-Brook, N., Bushell, T., Hamling, I., Ristau, J., Noble, D., McColl, S.T., 2018. Preliminary geometry, displacement, and kinematics of fault ruptures in the epicentral region of the 2016 M w 7.8 Kaikōura, New Zealand, earthquake. Bulletin of the Seismological Society of America 108, 1521–1539. https://doi.org/10.1785/0120170329

Nicol, A., Van Dissen, R., 2002. Up-dip partitioning of displacement components on the oblique-slip Clarence Fault, New Zealand. Journal of Structural Geology 24, 1521–1535. https://doi.org/10.1016/S0191-8141(01)00141-9

Norris, R.J., Cooper, A.F., 1995. Origin of small-scale segmentation and transpressional thrusting along the Alpine Fault, New Zealand. Geological Society of America Bulletin 107, 231–240. https://doi.org/10.1130/0016-7606(1995)107<0231:OOSSSA>2.3.CO;2

Norris, R.J., Toy, V.G., 2014. Continental transforms: A view from the Alpine Fault. Journal of Structural Geology 64, 3–31. https://doi.org/10.1016/j.jsg.2014.03.003

Panien, M., Buiter, S.J.H., Schreurs, G., Pfiffner, O.A., 2006. Inversion of a symmetric basin: insights from a comparison between analogue and numerical experiments. Geological Society Special Publication 253, 253–270.

Peacock, D.C.P., Nixon, C.W., Rotevatn, A., Sanderson, D.J., Zuluaga, L.F., 2017. Interacting faults. Journal of Structural Geology 97, 1–22. https://doi.org/10.1016/j.jsg.2017.02.008

Peacock, D.C.P., Sanderson, D.J., 1999. Deformation history and basin-controlling faults in the Mesozoic sedimentary rocks of the Somerset coast. Proceedings of the Geologists' Association 110, 41–52.

Perrin, C., Manighetti, I., Gaudemer, Y., 2016. Off-fault tip splay networks: A genetic and generic property of faults indicative of their long-term propagation. Comptes Rendus - Geoscience 348, 52–60. https://doi.org/10.1016/j.crte.2015.05.002

Poirier, J.., 1988. Considerations on the use of analogues in deformation studies. Bulletin of the Geological Institutions of the University of Uppsala 14, 49–54.

Provost, A.S., Chéry, J., Hassani, R., 2003. 3D mechanical modeling of the GPS velocity field along the North Anatolian fault. Earth and Planetary Science Letters 209, 361–377. https://doi.org/10.1016/S0012-821X(03)00099-2

Qu, S., 2019. Characteristics and Geological Significance of Strike-slip Faults. IOP Conference Series: Earth and Environmental Science 384, 0–7. https://doi.org/10.1088/1755-1315/384/1/012162

Quigley, M.C., Jiménez, A., Duffy, B., King, T.R., 2019. Physical and Statistical Behavior of Multifault Earthquakes: Darfield Earthquake Case Study, New Zealand. Journal of Geophysical Research: Solid Earth 124, 4788–4810. https://doi.org/10.1029/2019JB017508

Ramberg, H., 1967. Gravity, deformation and the earth's crust : as studied by centrifuged models. Academic Press, London ; New York.

Ramsay, J.G., 1980. Shear zone geometry: a review. Journal of Structural Geology 2, 83–89.

Ramsay, J.G., Graham, R.H., 1970. Strain variation in shear belts. Canadian Journal of Earth Sciences 7, 786–813. https://doi.org/10.1139/e70-078

Ranalli, G., 2001. Experimental tectonics: from Sir James Hall to the present. Journal of Geodynamics 32, 65–76.

Randall, K., Lamb, S., Niocaill, C. Mac, 2011. Large tectonic rotations in a wide zone of Neogene distributed dextral shear, northeastern South Island, New Zealand. Tectonophysics 509, 165–180. https://doi.org/10.1016/j.tecto.2011.05.006

Rao, G., Lin, A., Yan, B., Jia, D., Wu, X., Ren, Z., 2011. Co-seismic Riedel shear structures produced by the 2010 M w 6.9 Yushu earthquake, central Tibetan Plateau, China. Tectonophysics 507, 86–94.

Rattenbury, M.S., Townsend, D.B., Johnston, M.R., 2006. Geology of the Kaikoura area, Institute Of Geological And Nuclear Sciences 1:250,000 Geological Map.

Reay, M.B., Pye, S.F., 1993. Geology of the Middle Clarence Valley; Volume 10 of Institute of Geological & Nuclear Sciences geological map. Institute of Geological & Nuclear Sciences, Lower Hutt.

Reber, J.E., Cooke, M.L., Dooley, T.P., 2020. What model material to use? A Review on rock analogs for structural geology and tectonics. Earth-Science Reviews 202. https://doi.org/10.1016/j.earscirev.2020.103107

Riedel, W., 1929. Zur Mechanik geologischer Brucherscheinungen. Centralblatt Für Mineralogie, Geologie Und Paläontologie 8, 354–368.

Riller, U., Cruden, A.R., Boutelier, D., Schrank, C.E., 2012. The causes of sinuous crustal-scale deformation patterns in hot orogens: Evidence from scaled analogue experiments and the southern Central Andes. Journal of Structural Geology 37, 65–74. https://doi.org/10.1016/j.jsg.2012.02.002

Rodgers, D.W., Little, T.A., 2006. World's largest coseismic strike-slip offset: The 1855 rupture of the Wairarapa Fault, New Zealand, and implications for displacement/length scaling of continental earthquakes. Journal of Geophysical Research: Solid Earth 111, 1–19. https://doi.org/10.1029/2005JB004065

Samsu, A., Cruden, A.R., Molnar, N.E., Weinberg, R.F., 2021. Inheritance of Penetrative Basement Anisotropies by Extension-Oblique Faults: Insights From Analogue Experiments. Tectonics 40, 1–19. https://doi.org/10.1029/2020TC006596

Samsu, A., Cruden, A.R., Molnar, N.E., Weinberg, R.F., 2019. Inheritance without reactivation: Insights from crustal-scale analogue experiments. PREPRINT Submitted for Publication in Tectonics.

Schellart, W.P., 2000. Shear test results for cohesion and friction coefficients for different granular materials: scaling implications for their usage in analogue modelling. Tectonophysics 324, 1–16.

Schellart, W.P., Strak, V., 2016. A review of analogue modelling of geodynamic processes: Approaches, scaling, materials and quantification, with an application to subduction experiments. Journal of Geodynamics 100, 7–32. https://doi.org/10.1016/j.jog.2016.03.009

Scholz, C.H., Ando, R., Shaw, B.E., 2010. The mechanics of first order splay faulting: The strike-slip case. Journal of Structural Geology 32, 118–126. https://doi.org/10.1016/j.jsg.2009.10.007

Scholz, C.H., Dawers, N.H., Yu, J.-., Anders, M.H., Cowie, P.A., 1993. Fault growth and fault scaling laws: Preliminary results. Journal of Geophysical Research: Solid Earth 98, 21951–21961.

Schrank, C.E., Boutelier, D.A., Cruden, A.R., 2008. The analogue shear zone: From rheology to associated geometry. Journal of Structural Geology 30, 177–193. https://doi.org/10.1016/j.jsg.2007.11.002

Schrank, C.E., Cruden, A.R., 2010. Compaction control of topography and fault network structure along strike-slip faults in sedimentary basins. Journal of Structural Geology 32, 184–191. https://doi.org/10.1016/j.jsg.2009.11.003

Schreurs, G., 2003. Fault development and interaction in distributed strike-slip shear zones: An experimental approach. Geological Society Special Publication 210, 35–52. https://doi.org/10.1144/GSL.SP.2003.210.01.03

Schreurs, G., 1994. Experiments on strike-slip faulting and block rotation. Geology 22, 567–570. https://doi.org/10.1130/0091-7613(1994)022<0567:EOSSFA>2.3.CO;2

Schreurs, G., Buiter, S.J.H., Boutelier, D., Corti, G., Costa, E., Cruden, A.R., Daniel, J.-M., Hoth, S., Koyi, H.A., Kukowski, N., Lohrmann, J., Ravaglia, A., Schlische, R.W., Withjack, M.O., Yamada, Y., Cavozzi, C., Del Ventisette, C., Brady, J.A.E., Hoffmann-Rothe, A., Mengus, J.-M., Montanari, D., Nilforoushan, F., 2006. Analogue benchmarks of shortening and extension experiments. Geological Society, London, Special Publications 253, 1–27. https://doi.org/10.1144/gsl.sp.2006.253.01.01

Schreurs, G., Colletta, B., 1998. Analogue modelling of faulting in zones of continental transpression and transtension. Geological Society, London, Special Publications 135, 59–79. https://doi.org/10.1144/gsl.sp.1998.135.01.05

Schueller, S., Davy, P., 2008. Gravity influenced brittle-ductile deformation and growth faulting in the lithosphere during collision: Results from laboratory experiments. Journal of Geophysical Research: Solid Earth 113, B12404--n/a.

Segev, A., Vladimir, L., Weinberger, R., 2014. Continental transform-rift interaction adjacent to a continental margin: The Levant case study. Earth-Science Reviews 139, 83–103.

Şengör, A.M.C., Tüysüz, O., Imren, C., Sakinç, M., Eyidoğan, H., Görür, N., Le Pichon, X., Rangin, C., 2005. The North Anatolian Fault: A new look. Annual Review of Earth and Planetary Sciences 33, 37–112. https://doi.org/10.1146/annurev.earth.32.101802.120415

Şengör, A.M.C., Zabcı, C., Natal'in, B.A., 2019. Continental transform faults: Congruence and incongruence with normal plate kinematics, Transform Plate Boundaries and Fracture Zones. https://doi.org/10.1016/B978-0-12-812064-4.00009-8

Shi, X., Wang, Y., Liu-Zeng, J., Weldon, R., Wei, S., Wang, T., Sieh, K., 2017. How complex is the 2016 Mw 7.8 Kaikoura earthquake, South Island, New Zealand? Science Bulletin 62, 309–311. https://doi.org/10.1016/j.scib.2017.01.033

Shuck, B., Van Avendonk, H., Gulick, S.P.S., Gurnis, M., Sutherland, R., Stock, J., Patel, J., Hightower, E., Saustrup, S., Hess, T., 2021. Strike-Slip Enables Subduction Initiation Beneath a Failed Rift: New Seismic Constraints From Puysegur Margin, New Zealand. Tectonics (Washington, D.C.) 40, n/a.

Simpson, C., De Paor, D.G., 1993. Strain and kinematic analysis in general shear zones. Journal of Structural Geology 15, 1–20.

Stock, J., Molnar, P., 1987. Revised history of early tertiary plate motion in the south-west Pacific. Nature 325, 495–499. https://doi.org/10.1038/325495a0

Sun, M., Yin, A., Yan, D., Ren, H., Mu, H., Zhu, L., Qiu, L., 2018. Role of pre-existing structures in controlling the Cenozoic tectonic evolution of the eastern Tibetan plateau: New insights from analogue experiments. Earth and Planetary Science Letters 491, 207–215. https://doi.org/10.1016/j.epsl.2018.03.005

Sunal, G., Korhan Erturaç, M., 2012. Estimation of the pre-North Anatolian Fault Zone pseudo-paleo-topography: A key to determining the cumulative offset of major post-collisional strike-slip faults. Geomorphology 159–160, 125–141. https://doi.org/10.1016/j.geomorph.2012.03.013

Sutherland, R., 1995. The Australia-Pacific boundary and Cenozoic plate motions in the SW Pacific: Some constraints from Geosat data. Tectonics 14, 819–831. https://doi.org/10.1029/95TC00930

Sutherland, R., Davey, F., Beavan, J., 2000. Plate boundary deformation in South Island, New Zealand, is related to inherited lithospheric structure. Earth and Planetary Science Letters 177, 141–151. https://doi.org/10.1016/S0012-821X(00)00043-1

Swanson, M.T., 2006. Late Paleozoic strike-slip faults and related vein arrays of Cape Elizabeth, Maine. Journal of Structural Geology 28, 456–473. https://doi.org/10.1016/j.jsg.2005.12.009

Sylvester, A.G., 1988. Strike-slip faults. Geological Society of America Bulletin 100, 1666–1703.

Tchalenko, J.S., 1970. Similarities between shear zones of different magnitudes. Geological Society of America Bulletin 81, 1625–1639.

Thiele, S.T., Grose, L., Samsu, A., Micklethwaite, S., Vollgger, S.A., Cruden, A.R., 2017. Rapid, semi-automatic fracture and contact mapping for point clouds, images and geophysical data. Solid Earth (Göttingen) 8, 1241–1253.

Toeneboehn, K., Cooke, M.L., Bemis, S.P., Fendick, A.M., 2018. Stereovision Combined With Particle Tracking Velocimetry Reveals Advection and Uplift Within a Restraining Bend Simulating the Denali Fault. Frontiers in Earth Science 6, 1–13. https://doi.org/10.3389/feart.2018.00152

Townsend, D.B., 2001. Neogene evolution of the Pacific - Australia plate boundary zone in NE Marlborough, South Island, New Zealand. Victoria University of Wellington.

Ueta, K., Tani, K., Kato, T., 2000. Computerized X-ray tomography analysis of three-dimensional fault geometries in basement-induced wrench faulting. Developments in Geotechnical Engineering. Elsevier B.V, 233–246.

Ulrich, T., Gabriel, A.-A., Ampuero, J.-P., Xu, W., 2019. Dynamic viability of the 2016 Mw 7.8 Kaikōura earthquake cascade on weak crustal faults. Nature Communications 10, 1213. https://doi.org/10.1038/s41467-019-09125-w

Vallage, A., Klinger, Y., Lacassin, R., Delorme, A., Geological, M.P., 2018. Geological structures control on earthquake ruptures : https://doi.org/10.1002/2016GL070418.Received

Van Dissen, R., Yeats, R.S., 1991. Hope Fault, Jordan Thrust, and uplift of the Seaward Kaikoura Range, New Zealand. Geology 19, 393–396. https://doi.org/10.1130/0091-7613(1991)019<0393:HFJTAU>2.3.CO;2

Vermeer, J.L., Quigley, M.C., Duffy, B.G., Langridge, R.M., Pettinga, J.R., 2021. Structure and kinematics of active faulting in the Hope-Kelly and Alpine Fault intersection zone, South Island, New Zealand. Tectonophysics 813. https://doi.org/10.1016/j.tecto.2021.228928

Wallace, L.M., Barnes, P., Beavan, J., Van Dissen, R., Litchfield, N., Mountjoy, J., Langridge, R., Lamarche, G., Pondard, N., 2012. The kinematics of a transition from subduction to strike-slip: An example from the central New Zealand plate boundary. Journal of Geophysical Research: Solid Earth 117. https://doi.org/10.1029/2011JB008640

Wallace, L.M., Beavan, J., McCaffrey, R., Berryman, K., Denys, P., 2007. Balancing the plate motion budget in the South Island, New Zealand using GPS, geological and seismological datas. Geophysical Journal International 168, 332–352. https://doi.org/10.1111/j.1365-246X.2006.03183.x

Wallace, L.M., Beavan, J., McCaffrey, R., Darby, D., 2004. Subduction zone coupling and tectonic

block rotations in the North Island, New Zealand. Journal of Geophysical Research: Solid Earth 109, 1–21. https://doi.org/10.1029/2004JB003241

Wallace, L.M., McCaffrey, R., Beavan, J., Ellis, S., 2005. Rapid microplate rotations and backarc rifting at the transition between collision and subduction. Geology 33, 857–860. https://doi.org/10.1130/G21834.1

Walters, R.A., Barnes, P., Goff, J.R., 2006. Locally generated tsunami along the Kaikoura coastal margin: Part 1. Fault ruptures. New Zealand Journal of Marine and Freshwater Research 40, 1–16. https://doi.org/10.1080/00288330.2006.9517399

Wannamaker, P.E., Caldwell, T.G., Jiracek, G.R., Maris, V., Hill, G.J., Ogawa, Y., Bibby, H.M., Bennie, S.L., Heise, W., 2009. Fluid and deformation regime of an advancing subduction system at Marlborough, New Zealand. Nature 460, 733–736. https://doi.org/10.1038/nature08204

Weijermars, R., 1986. Flow behaviour and physical chemistry of bouncing putties and related polymers in view of tectonic laboratory applications. Tectonophysics 124, 325–358.

Weijermars, R., Schmeling, H., 1986. Scaling of Newtonian and non-Newtonian fluid dynamics without inertia for quantitative modelling of rock flow due to gravity (including the concept of rheological similarity). Physics of the Earth and Planetary Interiors 43, 316–330.

Wellman, H.W., 1979. An uplift map for the South Island of New Zealand, and a model for the uplift of the Southern Alps. Royal Society New Zealand Bulletin 181, 13–20.

Wesnousky, S.G., 2006. Predicting the endpoints of earthquake ruptures. Nature (London) 444, 358–360.

Wilcox, R.E., Harding, T.P., Seely, D.R., 1973. Basic Wrench Tectonics. The American Association of Petroleum Geologists Bulletin 57, 74–96.

Williams, J.N., Barrell, D.J.A., Stirling, M.W., Sauer, K.M., Duke, G.C., Hao, K.X., 2018. Surface rupture of the Hundalee fault during the 2016 Mw 7.8 Kaikōura earthquake. Bulletin of the Seismological Society of America 108, 1540–1555. https://doi.org/10.1785/0120170291

Willis, D.M., 2017. Evolution of congested subduction zones, and their influence on the Cretaceous and Neogene tectonics of New Zealand. School of Earth, Atmosphere and Environment Doctor of. https://doi.org/10.3760/cma.j.issn.0366-6999.2010.15.020

Wilson, C.K., Jones, C.H., Molnar, P., Sheehan, A.F., Boyd, O.S., 2004. Distributed deformation in the lower crust and upper mantle beneath a continental strike-slip fault zone: Marlborough fault system, South Island, New Zealand. Geology 32, 837–840. https://doi.org/10.1130/G20657.1

Wilson, J.T., 1965. A NEW CLASS OF FAUL TS AND THEIR BEARING ON CONTINENTAL DRIFT. Nature 207, 343–347.

Wood, R.A., Stagpoole, V.M., 2007. Validation of tectonic reconstructions by crustal volume balance: New Zealand through the Cenozoic. Bulletin of the Geological Society of America 119, 933–943. https://doi.org/10.1130/B26018.1

Woodcock, N.H., Daly, M.C., 1986. The Role of Strike-Slip Fault Systems at Plate Boundaries [and Discussion]. Philisophical Transactions of the Royal Society of London. Series A, Mathematical and Physical Sciences 317, 13–29.

Wu, J.E., McClay, K., Whitehouse, P., Dooley, T., 2012. 4D analogue modelling of transtensional pull-apart basins, Regional Geology and Tectonics: Principles of Geologic Analysis, Volume 1. Elsevier B.V. https://doi.org/10.1016/j.marpetgeo.2008.06.007

Yang, H., Moresi, L.N., Quigley, M., 2019. Fault spacing in continental strike-slip shear zones. Earth and Planetary Science Letters 1, 115906. https://doi.org/10.1016/j.epsl.2019.115906

Yeats, R.S., Berryman, K.R., 1987. South Island, New Zealand, and transverse ranges, California: A seismotectonic comparison. Tectonics (Washington, D.C.) 6, 363–376.

Zuza, A. V, Yin, A., Lin, J., Sun, M., 2017. Spacing and strength of active continental strike-slip faults. Earth and Planetary Science Letters 457, 49–62.

Appendices

Appendix A: Digital Appendix

The Digital Appendix for this thesis has subfolders containing the following items:

Appendix 1: Supplementary data from Chapter 1

Folders 1.1, 1.2 and 1.3 contain sub-folders with the original photographs and incremental shear strain maps calculated from DIC from Experiments 1 – 3 respectively, presented in Chapter 1.

Appendix 2: Supplementary data from Chapter 2

Folders 2.1 – 2.5 contain sub-folders with the original photographs and incremental shear strain maps calculated from DIC from Experiments 1 – 5 respectively, presented in Chapter 2.

Appendix 3: Supplementary data from Chapter 3

Folders 3.1, 3.2 and 3.2 contain the XRCT scans conducted during experiments 1-3 respectively, as presented in Chapter 3.

Folder 3.4 contains the 3D model of the Marlborough Fault System as a HTML document and the python code to generate the model as a Jupyter Notebook. The code can also be downloaded from https://github.com/lachlangrose/Withers_2021_MFS

Appendix 4: Supplementary data from Chapter 4

Folders 4.1 contains sub-folders with the original photographs and incremental shear strain maps calculated from DIC from the transition experiments presented in Chapter 4.

These fileset can be downloaded via the following link: 10.26180/17209493

Appendix B

Original XRCT scan slices of Figures 3.5 and 3.6 from Chapter 3, without interpretations of fault locations. These are results from experiments 1, 2 and 3 presented in Chapter 3. The purple box shows the location of the stretchable fabric at the base of the box.

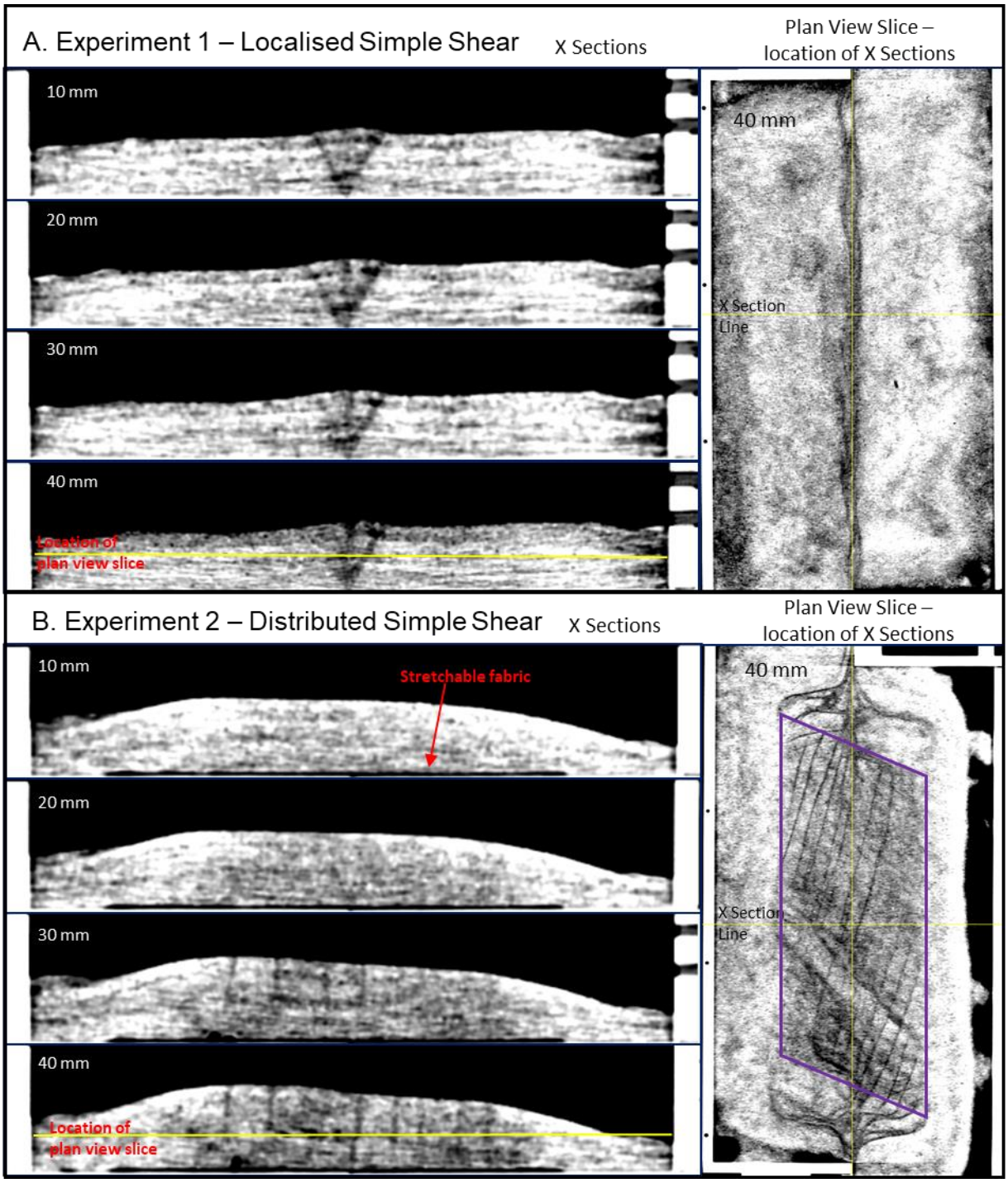

Figure 3.5, without fault interpretations

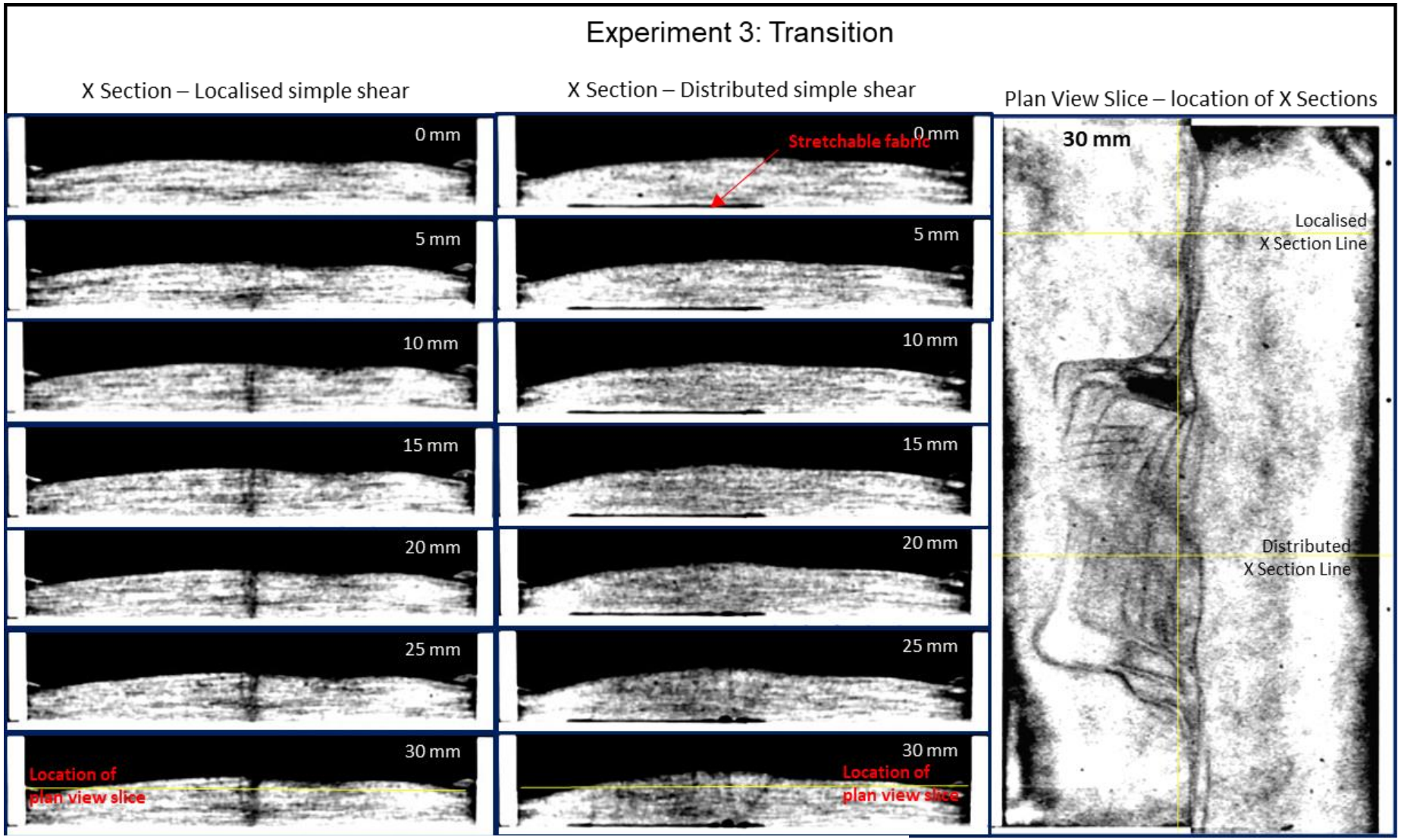

Figure 3.6, without fault interpretations